Enhanced Multicarrier Techniques for Professional Ad-Hoc and Cell-Based Communications

(EMPhAtiC)

Document Number D3.1

Training Design and Algorithms for Channel Estimation

Contractual date of delivery to the CEC:	30/11/2013
Actual date of delivery to the CEC:	18/12/2013
Project Number and Acronym:	318362 EMPhAtiC
Editor:	Eleftherios Kofidis (CTI)
Authors:	Eleftherios Kofidis (CTI), Antonios Beikos (CTI), Markku Renfors (TUT), Juha Yli-Kaakinen (TUT), Leonardo G. Baltar (TUM), Laurent Martinod (CASSIDIAN), Philippe Mége (CASSIDIAN), Luc Féty (CNAM), Didier Le Ruyet (CNAM)
Participants:	CTI, TUT, TUM, CASSIDIAN, CNAM
Workpackage:	WP3
Security:	Public(PU)
Nature:	Report
Version:	1.3
Total Number of Pages:	81

Abstract:

Channel estimation, synchronization, and equalization can be quite challenging tasks in FB-MC systems, especially under harsh propagation conditions such as those encountered in PMR systems, involving severe frequency and/or time selectivity for the physical channel. There is thus a need to revisit these problems in the present context and propose solutions that are applicable in such a reality. This report summarizes the results from such a research effort in WP3. The reported material includes theory and algorithms for an FB-MC receiver, which rely on either a preamble or scattered pilots. Simulation results are presented that validate the proposed algorithms for a variety of propagation conditions. Important remaining questions are pointed out and possible future research directions to address them are proposed.

Keywords: Channel estimation, CP-OFDM, FB-MC, FBMC/OQAM, FC-FB, FMT, LS, MAP, ML, MSE, pilots, preamble, sparse, training

Table of Contents

1. Introduction

Multicarrier modulation offers most of the key elements needed in the challenging new spectrum use scenarios, like opportunistic dynamic spectrum access, cognitive radio, and heterogeneous wireless system coexistence. Characteristic to these situations is the need to adjust the spectral characteristics of the transmitted signal, notably bandwidth and center frequency, to the available unused slots of radio spectrum. To support high data rates, it is often desirable to combine multiple non-contiguous spectrum slots in the transmission. In multicarrier systems, this can be achieved by activating only those subcarriers that are within the available frequency slots. One important example case of such fragmented spectrum use is the high data rate services to be developed for the Professional Mobile Radio (PMR), which is utilized, e.g., by safety organizations [3]. Currently, PMR supports voice and narrowband data services, based on the family of Tetra standards in Europe and many countries outside Europe, as well as APCO25 in North America.

Orthogonal frequency-division multiplexing (OFDM) is extensively utilized in modern broadband radio access systems. This is due to the simple and robust way of doing channel equalization, to its high flexibility and efficiency in allocating spectral resources to different users, as well as the ability to combining multi-antenna schemes with the core functionality [15]. However, OFDM has major limitations, in general as well as in the mentioned co-existence scenarios: spectral and power inefficiency due to the requirement for using guard intervals when transmitting, high sensitivity to frequency offsets, bad spectral containment which leads to high sensitivity to interferences from asynchronous spectral components, e.g., in fragmented spectrum use.

A more sophisticated multicarrier scheme that has been shown to constitute an attractive alternative to OFDM is offered by the filter bank (FB) based methods of waveform processing and channelization filtering [1], commonly referred to as filter bank-based multi-carrier (FB-MC) [23]. Actually, it is possible to combine both functions in filter bank based implementations:

1. The waveforms generated for transmission are spectrally well-contained and no other measures are needed to clean the unused portions of the spectrum allocated for dynamic/fragmented use.

2. The filter bank processing on the receiver side is able to suppress the interferences in the unused parts of the allocated spectrum.

Naturally, there are limitations in the reachable levels of attenuation, mostly determined by the analog RF imperfections, notably power amplifier nonlinearity on the transmitter side and nonlinearity of the active stages of the receiver chain, as well as I/Q imbalance effects on both sides [62]. These issues are beyond the scope of this report. A relatively widely studied filter bank-based waveform is FBMC/OQAM (filter bank multicarrier/ offset-QAM, more commonly known as OFDM/OQAM) [56, 24]. While reaching high spectral containment, it keeps many of the important features of OFDM. Even though FBMC/OQAM has its limitations in terms of conceptual and implementation complexity and difficulties with certain multiantenna (MIMO) transmission schemes, it has received increasing interest in the mentioned challenging spectrum use scenarios. MIMO FB-MC becomes more tractable when Filtered MultiTone (FMT) is adopted [23]. FMT has also received a lot of attention as a possible FB-MC solution [22] mainly due to its simplicity. It is however (at least in its basic form) much less spectrally efficient than FBMC/OQAM.

The gains from replacing OFDM by FB-MC may come however at the cost of losing the simplicity of common receiver functions, including channel synchronization, estimation, and

equalization. These can be quite challenging tasks in FB-MC systems, especially under realistic propagation conditions (including those encountered in PMR systems) involving severe frequency and/or time selectivity for the physical channel. For example, high mobile speeds necessitate the use of a relatively small number of subcarriers in an FB-MC system, in order to cope with the Doppler spread effects [28]. This in turn implies that the subchannels are no longer well described by a frequency flat model, as the one usually adopted in (most of) the FBMC/OQAM channel estimation schemes so far (see, e.g., [41] for a review). Although such an assumption (along with more restricting requirements on the coherence bandwith of the channel) greatly simplifies the channel estimation task in such systems, effectively translating the problem to an OFDM-like one, it typically leads to severe error floors at medium to high SNR values when it is not sufficiently accurate [41]. The reason for this is that the subchannel model inaccuracy manifests itself at such weak noise regimes as the residual intrinsic interference prevails over noise. It is thus a necessity to re-visit channel estimation in such FB-MC systems through the development of more accurate schemes that will not rely on invalid simplifying assumptions. Moreover, additional information such as the color of the noise at the demodulator output must be incorporated in the estimator in order to optimize its performance. In addition to adopting more powerful estimation techniques, the training design problem needs to be studied in the light of these increased requirements. Longer training sequences for coping with frequency selective subchannels may have to be designed or shorter ones that will be easier to use in fast fading scenarios while ensuring high estimation accuracy. The increase in the cost of channel estimation implied by the frequency and/or time selectivity of the subchannels can also be tackled through the exploitation of possible sparsity features found in the channel. With sufficiently sparse channels, such as the ones commonly encountered in wireless communications and especially PMR scenarios, increased estimation performance, possibly with significantly less training resources, can be achieved via appropriate modifications to the estimation schemes developed. An additional problem in designing training input and techniques specifically for FBMC/OQAM channel estimation stems from the undesired interference that the training part of the frame (preamble or isolated pilot) suffers from neighboring data symbols. This has to be appropriately addressed so as not to significantly compromise estimation performance while at the same time spending for that as few as possible of the resources available for estimating the channel, including training bandwidth and computational time.

Another important issue is the required level of synchronization between different users of the broadband system. This is important since the system is expected to support also direct mobile-to-mobile or ad-hoc networking scenarios. In OFDM-based multiple access, namely OFDMA, the relative frequency offsets should be in the order of one percent of the subcarrier spacing, or smaller, and timing offsets, combined with channel delay spreads, should be within the cyclic prefix. To reach such a level of synchronicity, relatively complicated synchronization procedures are required and all stations need to be under tight control of a base station, also in the idle mode. On the other hand, in FBMC/OQAM, different groups of subchannels can be well isolated from each other, by using a narrow guardband of just one subcarrier, and fully asynchronous operation is possible with high spectral efficiency. However, traditional FBMC/OQAM schemes have limited capability to support reception of asynchronous multiplexes of subcarriers. There is thus the need to also study these effects under the above challenging propagation conditions and come up with effective as well as simple to implement schemes of estimating these offsets and compensating for them. Again, the main focus of the literature so far has been on traditional CP-OFDM modulations and FBMC/OQAM with the flat-fading subchannel model [1].

The present document summarizes the main results from the research efforts on the above

topics. In Chapter 2, the system model for the FBMC/OQAM type of FB-MC (that will be mostly studied here) is recalled in a general setting and basic notations are stated that will be used throughout. Then, a brief account of the existing results and techniques for FBMC/OQAM channel estimation is given, with the aim of motivating the contributions that follow. Chapter 3 addresses FBMC/OQAM channel estimation based on a known preamble. Impulse response estimators are developed, for a variety of criteria and at both the subcarrier and wideband levels. Notably, the estimators developed can work for any given training sequence of any given length. One of the methods reported permits the transmission of data at the non-pilot subcarriers while training is performed, thus offering the possibility for increased bandwidth efficiency. Emphasis is then put on designing optimal short preambles, in view of their importance in practical fast fading channels. Moreover, sparsity-aware approaches are tested and their possible gains in improving estimation accuracy are assessed. In Chapter 4, the focus is on the multi-mode FB-MC system realized with the aid of fast convolution (FC-FB). Receiver tasks of channel estimation and equalization are all addressed in this context, with the aid of simple to implement techniques, and based on pilots scattered throughout the frame in accordance with LTE pilot formats. Time and frequency synchronization are also addressed, based on a short preamble. Simulation results are reported that validate the proposed schemes in scenarios of high frequency and time selectivity. In particular, channel models that describe harsh PMR scenarios and challenge the techniques developed are included in the comparisons. FMT systems are considered in Chapter 5. Flat but highly time varying subchannels are assumed here. To cope with this scenario, pilots are scattered throughout the frame (with no constraint on their configuration) and the channel responses at all time-frequency points are estimated with the aid of a (close to) Maximum A Posteriori (MAP) scheme. The algorithm enjoys low complexity and high performance, as exhibited by its application in single-tap per equalization. Conclusions are drawn in Chapter 6 and topics that need to be further studied in the near future are discussed.

2. Background

Most of this report focuses on FBMC/OQAM-based systems. It is thus necessary to re-state the basic definitions and principles underlying this type of FB-MC, and briefly recall the classical approaches to channel estimation in FBMC/OQAM by also pointing out their weak points that need to be addressed.

2.1 System Model

The (QAM or OQAM based) OFDM modulator output $s(l)$ is transmitted through a channel of length L_h, which is, as usual in block transmissions, assumed to be invariant in the duration of an OFDM symbol. At the receiver front-end, noise w is added, which is assumed white Gaussian with zero mean and variance σ^2. The noisy channel output is then given by

$$y(l) = \sum_{k=0}^{L_h-1} s(k-l)h(k) + w(l) \tag{2.1}$$

where

$$\boldsymbol{h} = \left[\begin{array}{cccc} h(0) & h(1) & \cdots & h(L_h-1) \end{array} \right]^{\mathrm{T}}$$

is the channel impulse response (CIR). For CP-OFDM, the classical configuration is assumed [63]. For FBMC/OQAM, the discrete-time signal at the output of the synthesis filter bank (SFB) is given by [56]

$$s(l) = \sum_{m=0}^{M-1} \sum_{n} d_{m,n} g_{m,n}(l), \tag{2.2}$$

where $d_{m,n}$ are *real* OQAM symbols, and

$$g_{m,n}(l) = g\left(l - n\frac{M}{2}\right) e^{\jmath \frac{2\pi}{M} m \left(l - \frac{L_g-1}{2}\right)} e^{\jmath \varphi_{m,n}},$$

with g being the *real symmetric* prototype filter impulse response (assumed here of unit energy) of length L_g, M being the *even* number of subcarriers, and $\varphi_{m,n} = \varphi_0 + \frac{\pi}{2}(m+n) \bmod \pi$, where φ_0 can be arbitrarily chosen [56]. In this report, $\varphi_{m,n}$ is defined as $(m+n)\frac{\pi}{2} - mn\pi$ as in [56]. The filter g is usually designed to have length $L_g = KM$, with K being the overlapping factor. The double subscript $(\cdot)_{m,n}$ denotes the (m,n)-th frequency-time (FT) point. Thus, m is the subcarrier index and n the FBMC/OQAM symbol time index.

The pulse g is designed so that the associated subcarrier functions $g_{m,n}$ are orthogonal in the *real* field, that is

$$\Re\left\{ \sum_{l} g_{m,n}(l) g^{\star}_{p,q}(l) \right\} = \delta_{m,p}\delta_{n,q}, \tag{2.3}$$

where $\delta_{i,j}$ is the Kronecker delta. This implies that even in the absence of channel distortion and noise, and with perfect time and frequency synchronization, there will be some intercarrier (and/or intersymbol) interference at the output of the analysis filter bank (AFB), which is purely real or imaginary (depending on the parity of the FT point) and is known as *intrinsic* interference [33]. Assuming, for the sake of the simplicity of the presentation, that the AFB processing includes a multiplication by $e^{-\jmath\varphi_{m,n}}$, the interference can be always seen as being imaginary and hence (the notation in [43] is adopted):

$$\sum_{l} g_{m,n}(l) g^{\star}_{p,q}(l) = \jmath \langle g \rangle^{p,q}_{m,n}, \tag{2.4}$$

2.2 Brief Summary of Earlier Work

Note that in the absence of a channel or other distortion, one can easily can get rid of this interference component by simply taking the real part of the received signal. However, in realistic conditions, the intrinsic interference presents a challenge to the receiver, whether it be for channel estimation or other signal processing tasks. Thus, as far as channel estimation is concerned, things are not that easy as in CP-OFDM anymore, where the output of the demodulator can be simply expressed as the product of the corresponding channel gain with the input symbol plus noise. Instead, in FBMC/OQAM, the channel frequency response (CFR) is in general complex valued (and in general not representable by a simple complex gain per subcarrier) hampering its estimation and the input signal recovery. A first step followed in existing works towards overcoming this difficulty is to make the assumption that the CIR is constant over the duration of the prototype filter [43], thus leading to subchannel CFRs that are (almost) flat. This is true for well localized g's provided $L_h \ll L_g$. Then one can express the AFB output at the pth subcarrier and qth FBMC symbol as [43]:

$$y_{p,q} = H_{p,q}d_{p,q} + \jmath \underbrace{\underbrace{\sum_{m=0}^{M-1}\sum_{n}}_{(m,n)\neq(p,q)} H_{m,n}d_{m,n}\langle g\rangle_{m,n}^{p,q}}_{I_{p,q}} + \eta_{p,q} \tag{2.5}$$

where $H_{p,q}$ is the channel frequency response (CFR) at that FT point, and $I_{p,q}$ and $\eta_{p,q}$ are the associated interference and noise components, respectively. $\eta_{p,q}$ has been shown to be stationary (in fact, also Gaussian with zero mean and variance σ^2) and correlated among subcarriers (see [65]). In most of the published methods so far, this correlation was neglected. In the present work, this will be explicitly taken into account when developing and applying the channel estimation algorithms.

A further step to come closer to the simplicity of CP-OFDM is to exploit the fact that the interference from FT points outside a neighborhood $\Omega_{p,q}$ of (p,q) (excluding (p,q) itself) is negligible while assuming that the CFR is almost constant over this FT area. One can then write (2.5) as

$$y_{p,q} \approx H_{p,q}c_{p,q} + \eta_{p,q}, \tag{2.6}$$

that is, in a CP-OFDM fashion, where

$$c_{p,q} = d_{p,q} + \jmath \underbrace{\sum_{(m,n)\in\Omega_{p,q}} d_{m,n}\langle g\rangle_{m,n}^{p,q}}_{u_{p,q}} = d_{p,q} + \jmath u_{p,q} \tag{2.7}$$

is the *virtual* transmitted symbol at (p,q), consisting of the pilot itself plus the interference coming from its immediate neighborhood:

$$u_{p,q} = \sum_{(m,n)\in\Omega_{p,q}} d_{m,n}\langle g\rangle_{m,n}^{p,q} \tag{2.8}$$

When known pilots are transmitted at that FT point and its neighborhood $\Omega_{p,q}$, the quantity in (2.7) can be approximated. This can then serve as a *pseudo-pilot* [43] to compute an estimate of the CFR at the corresponding FT point, as, for example,

$$\hat{H}_{p,q} = \frac{y_{p,q}}{c_{p,q}} \approx H_{p,q} + \frac{\eta_{p,q}}{c_{p,q}} \tag{2.9}$$

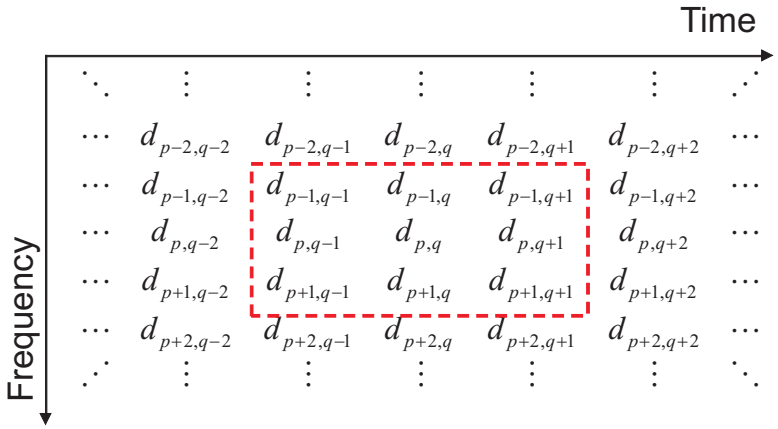

Figure 2-1: The first-order time-frequency neighborhood of FT point (p, q).

This observation underlies the so-called *Interference Approximation Method (IAM)*, originally proposed by the authors of [43].

The most common assumption for $\Omega_{p,q}$ is that, with a well time-frequency localized pulse, contributions to $I_{p,q}$ only come from the *first-order* neighborhood of (p, q), namely $\Omega_{p,q} = \{(p \pm 1, q \pm 1), (p, q \pm 1), (p \pm 1, q)\}$ (see Fig. 2-1). A special case is given by $\Omega_{p,q} = \Omega^1_{p,q} = \{(p \pm 1, q)\}$. This is used when builiding training preambles for IAM. Namely, we place nonzero pilot tones at all positions in the training FBMC symbol and zero FBMC symbols (vectors) around it. The latter are utilized as *guards* against the interference coming from unknown (control or data) samples preceding and/or following the pilot symbol. This way, the pilot symbols are kept (almost) free of unknown (and hence difficult to cope with) interference.[1] The remaining interference is then easily pre-calculated based on the knowledge of the surrounding known symbols and the filter bank employed (see [41] for explicit formulae). It is of interest to note at this point that the null FBMC symbol usually placed before the pilot symbol is in general unnecessary, in view of the already existing interframe time gaps commonly used in wireless transmissions. Hence, the preamble as a whole may last as one OFDM symbol, namely one pilot FBMC symbol followed by an all zeros one.

The above is about preambles, normally placed in the beginning of a (sub)frame. In order to be able to track channel variations in time however, pilots that are scattered throughout the payload part of the frame are also needed. Designing and placing such pilots in FBMC/OQAM is a bit more tricky. If the neighbors of (p, q) carry unknown (usually data) symbols, one cannot (directly) approximate the imaginary interference in (2.7) and hence the pilot will be contaminated by unknown interference. However, by properly choosing *one* of the neighboring symbols, say at the point (r, s), this interference can be forced to zero subject to the simplifying assumptions previously mentioned. Then the pseudo-pilot in (2.7) becomes real, equal to $d_{p,q}$. The pilot at (r, s) is then known as an *auxiliary*-pilot [33, 1].

The previous model, manifested in (2.6), has been central to the development of almost all of the channel estimation methods reported thus far. It is indeed a very convenient one in scenarios of relatively (to the size of the filter bank) low channel dispersion and has shown significant improvement over CP-OFDM especially at low to medium SNRs. The performance gain can be controlled, in preamble-based methods, through the selection of the entries of the

[1] Iterative schemes that aim at avoiding these guard symbols in order to increase bandwith efficiency have also been proposed. However, their performance is not always predictable and is in general inferior to the more classical IAM-like schemes [41].

FBMC pilot symbol. The latter, if properly designed, can lead to pseudo-pilots of maximum magnitude and hence considerable reduction of the estimation noise (cf. (2.9)). The optimal in this respect IAM scheme is known as IAM-C and involves both real and imaginary pilots (details are found in [41]). However, the underlying model assumptions fail to meet the requirements of a more dispersive environment and hence IAM methods normally exhibit performance floors at above moderate SNR values. In such regimes, the (inadequately modeled) intrinsic interference prevails over noise and the problem shows up, allowing CP-OFDM to outperform FBMC. The more dispersive the channel with respect to the FB size, the more intense this phenomenon. A more accurate subchannel model is thus needed in case M, the number of subcarriers, is not large enough with respect to the frequency selectivity of the channel [46]. This is also the case in high mobility scenarios, where M should be small, to cope with ICI from frequency dispersion [28, 25, 30]. The present report outlines results (both theoretical and experimental) from such a research direction.

Notation. Lower and upper case bold letters will be used to denote vectors and matrices, respectively. Superscripts $^{\mathrm{T}}$ and $^{\mathsf{H}}$ will respectively signify transposition and conjugate (Hermitian) transposition. Complex conjugation will be denoted by *. $\mathbf{0}_{r\times s}$ will be the all zeros matrix of dimensions $r \times s$. $\boldsymbol{I}_s$ is the sth-order identity matrix. The $r \times 1$ vector of all ones will be denoted by $\mathbf{1}_r$. Dimensions will be omitted whenever understood from the context. The diagonal matrix with the entries of the vector $\boldsymbol{x}$ on its main diagonal will be denoted by $\mathrm{diag}(\boldsymbol{x})$. $\mathrm{E}[\cdot]$, $\mathrm{tr}(\cdot)$, $\Re\{\cdot\}$ and $\Im\{\cdot\}$ stand for expectation, matrix trace, real and imaginary part, respectively. $\jmath$ will denote the imaginary unit. The sets of real and complex numbers are denoted by $\mathbb{R}$ and $\mathbb{C}$, respectively. $\otimes$ stands for the Kronecker product. The symbols $\odot$ and $\oslash$ are used to denote entry-wise multiplication and division, respectively.

3. Preamble-based FBMC/OQAM Channel Estimation

Preamble-based FBMC/OQAM channel estimation is studied in this chapter. The estimation problem is addressed in terms of both the subchannel responses and the broadband CIR. First, a *structured* approach is followed, where the knowledge of that part of the overall channel that depends on the FB is elegantly modeled and exploited to arrive at an efficient model for the system. The efficiency is meant in terms of both facilitating the development of (sub)channel estimation algorithms and also significantly reducing the required training sequence length. Notably, the scenario of transmitting data at the non-pilot subcarriers (with the aim to increase the spectral efficiency) is studied. An iterative algorithm, inspired from the Expectation Maximization ML scheme, is developed to cope with this problem. At a second stage, the CIR estimation problem is revisited with the aim of designing optimal (in the MSE sense) preambles of the shortest possible duration. This allows to further reduce the training overhead and increase the robustness of the channel estimator to time variations of the channel. Possible gains from exploiting the CIR sparsity are also investigated through simple modifications to the methods developed previously. Throughout this chapter, the channel is assumed time invariant for the duration of the preamble in each case.

3.1 Narrowband Per-subcarrier Impulse Response Estimation

3.1.1 Subcarrier Model

Assume that per-subcarrier equalizers (linear MMSE [66] or decision feedback [5, 65]) are employed. As a a consequence, a per-subcarrier estimator is sufficient for the purpose of equalizer design. In this section, we further assume that training sequences are not only employed in the subcarriers of interest, but also in their neighboring subcarriers [4, 6]. But later we will assume that only the observed subcarrier contains training. To perform the per-subcarrier channel estimation, we will model the multipath channel viewed at each subcarrier as a narrowband channel with a short impulse response and represent it at the sampling rate of the OQAM symbols, namely twice the QAM symbol rate, that is $2/T$. The subchannel model of the FBMC/OQAM system is depicted in Fig. 3-1, where the fact that no interference comes from further than the adjacent subcarriers is exploited to simplify the description. Like in [4, 6], this can be transformed to that of Fig. 3-2 to facilitate the subchannel estimation task. According to the latter mode, the signal received at subcarrier k can be arranged in an observation vector of length L_{o} and is given by

$$\mathbf{y}_k(n) = [\mathbf{X}_k(n)\mathbf{G}_{k,k} + \mathbf{X}_{k-1}(n)\mathbf{G}_{k,k-1} + \mathbf{X}_{k+1}(n)\mathbf{G}_{k,k+1}]\mathbf{h}_k + \mathbf{V}_k\mathbf{w}(l), \tag{3.1}$$

where $\mathbf{X}_k(n), \mathbf{X}_{k-1}(n), \mathbf{X}_{k+1}(n) \in \mathbb{C}^{L_{\mathsf{o}} \times L_{\mathsf{G}}}$ are Hankel matrices obtained from the training sequences of duration $L_{\mathsf{t}} = L_{\mathsf{G}} + L_{\mathsf{o}} - 1$ FBMC symbols, $\mathbf{G}_{k,k}, \mathbf{G}_{k,k-1}, \mathbf{G}_{k,k+1} \in \mathbb{C}^{L_{\mathsf{G}} \times L_{h_k}}$ are Toeplitz matrices containing the resulting filters impulse responses, $L_{\mathsf{G}} = \left\lceil \frac{2(L_g-1)}{M/2} \right\rceil + L_{h_k} - 1$

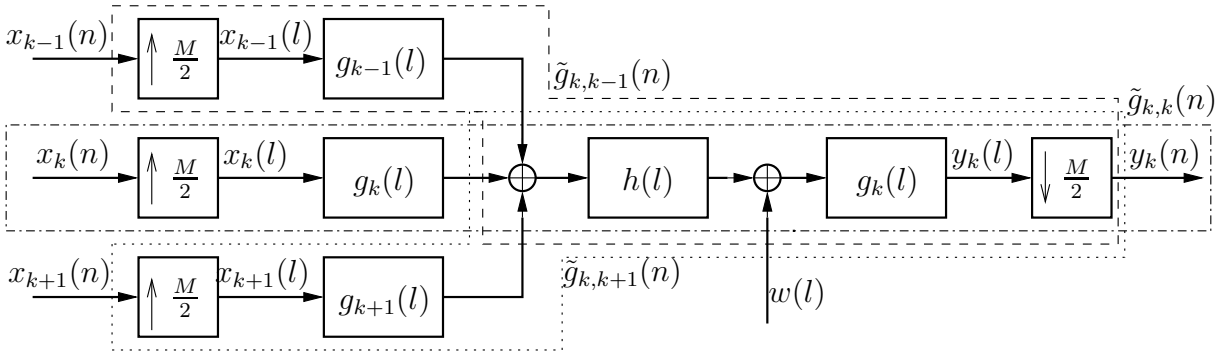

Figure 3-1: Subchannel model for the FBMC/OQAM system.

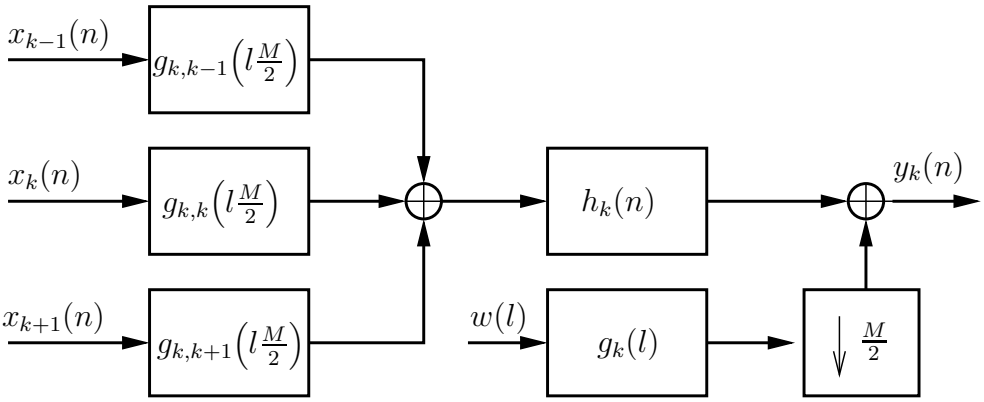

Figure 3-2: Simplified equivalent of Fig. 3-1.

is the subchannel length, and $\mathbf{h}_k \in \mathbb{C}^{L_{h_k}}$ is the kth sub-channel impulse response.

$$\mathbf{V}_k = \begin{bmatrix} g_k(0) & g_k(1) & \dots & g_k(L_g-1) & \mathbf{0}^{\mathrm{T}}_{L_\circ M/2} & \\ \mathbf{0}^{\mathrm{T}}_{M/2} & g_k(0) & g_k(1) & \dots & g_k(L_g-1) & \mathbf{0}^{\mathrm{T}}_{(L_\circ-1)M/2} \\ \mathbf{0}^{\mathrm{T}}_{M} & g_k(0) & g_k(1) & \dots & g_k(L_g-1) & \mathbf{0}^{\mathrm{T}}_{(L_\circ-2)M/2} \\ \vdots & \vdots & \vdots & \ddots & & \\ \mathbf{0}^{\mathrm{T}}_{(L_\circ-1)M/2} & g_k(0) & g_k(1) & \dots & g_k(L_g-1) & \mathbf{0}^{\mathrm{T}}_{M/2} \end{bmatrix} \in \mathbb{C}^{L_\circ \times (L_g + \lceil \frac{M}{2} L_\circ \rceil)} \tag{3.2}$$

is obtained by taking each $\frac{M}{2}$-th row of the convolution matrix constructed with the analysis filter impulse response $g_k(l)$. This is the reason why the vector $\boldsymbol{w}(l) \in \mathbb{C}^{(L_g + \lceil \frac{M}{2} L_\circ \rceil)}$, which contains white Gaussian noise (AWGN) samples with zero mean and variance σ^2, is defined at the high sampling rate M/T. Call the filtered noise $\boldsymbol{\eta}_k(n) = \mathbf{V}_k \mathbf{w}(l)$.

If we call $\mathbf{S}_k(n) = \mathbf{X}_k(n)\mathbf{G}_{k,k}$ and $\mathbf{U}_k(n) = \mathbf{X}_{k-1}(n)\mathbf{G}_{k,k-1} + \mathbf{X}_{k+1}(n)\mathbf{G}_{k,k+1}$ we get the following sub-carrier model for the sub-channel estimation

$$\mathbf{y}_k = (\mathbf{S}_k + \mathbf{U}_k)\mathbf{h}_k + \boldsymbol{\eta}_k \tag{3.3}$$

3.1.2 Per-subcarrier Least-Squares (LS)

The objective here is given by

$$\hat{\mathbf{h}}_{k,\mathsf{LS}} = \underset{\mathbf{h}_k \in \mathbb{C}^{L_{h_k}}}{\operatorname{argmin}} \|\mathbf{y}_k - (\mathbf{S}_k + \mathbf{U}_k)\mathbf{h}_k\|_2^2 \tag{3.4}$$

Applying this in our model, we get

$$\hat{\mathbf{h}}_{k,\mathsf{LS}} = [(\mathbf{S}_k + \mathbf{U}_k)^{\mathsf{H}}(\mathbf{S}_k + \mathbf{U}_k)]^{-1}(\mathbf{S}_k + \mathbf{U}_k)^{\mathsf{H}}\mathbf{y}_k \tag{3.5}$$

3.1.3 Per-subcarrier Maximum Likelihood (ML)

We can see that in the linear model of (3.3) the noise is zero mean Gaussian distributed with covariance matrix $\mathbf{C}_{\eta,k} = \sigma^2\mathbf{V}_k\mathbf{V}_k^{\mathsf{H}}$ and the observation $\mathbf{y}_k$ given $\mathbf{h}_k$ is Gaussian distributed. The Maximum Likelihood (ML) estimate of $\mathbf{h}_k$ is thus given by

$$\hat{\mathbf{h}}_{k,\mathsf{ML}} = \arg \max_{\mathbf{h}_k \in \mathbb{C}^{L_{h_k}}} p(\mathbf{y}_k|\mathbf{h}_k) = \arg \min_{\mathbf{h}_k} J(\mathbf{h}_k) \tag{3.6}$$

where

$$J(\mathbf{h}_k) = [\mathbf{y}_k - (\mathbf{S}_k + \mathbf{U}_k)\mathbf{h}_k]^{\mathsf{H}}\mathbf{C}_{\eta,k}^{-1}[\mathbf{y}_k - (\mathbf{S}_k + \mathbf{U}_k)\mathbf{h}_k] \tag{3.7}$$

Then the ML estimate of the narrowband multipath channel in each subcarrier is given by

$$\hat{\mathbf{h}}_{k,\mathsf{ML}} = [(\mathbf{S}_k + \mathbf{U}_k)^{\mathsf{H}}\mathbf{C}_{\eta,k}^{-1}(\mathbf{S}_k + \mathbf{U}_k)]^{-1}(\mathbf{S}_k + \mathbf{U}_k)^{\mathsf{H}}\mathbf{C}_{\eta,k}^{-1}\mathbf{y}_k. \tag{3.8}$$

It was shown in [4, 6] that the latter estimator works fine provided enough training is employed in the subcarriers k and $k \pm 1$. We should note that the subchannel length, L_{h_k}, is a design parameter of the estimator. It can be different for each subcarrier depending on how frequency selective the channel is for the corresponding portion of the spectrum.

3.1.4 Per-subcarrier Minimum Mean Squared Error (MMSE)

Let us now assume that the power delay profile of the sub-channel impulse response is a priori known, which then provides the covariance matrix of $\mathbf{h}_k$, here called $\mathbf{C}_{\mathbf{h}_k}$. One can then go to a MMSE estimator:

$$\hat{\mathbf{h}}_{k,\mathsf{MMSE}} = \underset{\mathbf{h}_k \in \mathbb{C}^{L_c}}{\operatorname{argmin}} \mathrm{E}\left[\|\mathbf{y}_k - (\mathbf{S}_k + \mathbf{U}_k)\mathbf{h}_k\|_2^2\right]. \tag{3.9}$$

resulting in

$$\hat{\mathbf{h}}_{k,\mathsf{MMSE}} = \mathbf{C}_{\mathbf{h}_k}(\mathbf{S}_k + \mathbf{U}_k)^{\mathsf{H}}\left[(\mathbf{S}_k + \mathbf{U}_k)\mathbf{C}_{\mathbf{h}_k}(\mathbf{S}_k + \mathbf{U}_k)^{\mathsf{H}} + \mathbf{C}_{\eta,k}\right]^{-1}\mathbf{y}_k \tag{3.10}$$

3.1.5 Per-subcarrier ML via Expectation Maximization (EM)

The entries of $\mathbf{S}_k$ in (3.3) are a result of the convolution between the training in subcarrier k and the resulting subcarrier filter. Although the resulting filter has a purely real impulse response if the prototype has a purely real impulse response, the resulting convolution with the OQAM staggered training sequence results in a complex signal. Consequently all entries of $\mathbf{S}_k$ are complex valued. In contrast, the entries of $\mathbf{U}_k$ are alternating purely real and purely

imaginary, because in addition to the OQAM data signals in subcarriers $k-1$ and $k+1$ also the impulse response between the two adjacent subcarriers has alternating real and imaginary coefficients. As a consequence, the interference term $\mathbf{u}_k$ has improper statistics [55] and if one is supposed to estimate it, a Widely Linear (WL) processing can be employed.

Now, one can rewrite the observation vector in (3.3) on each subcarrier as

$$\mathbf{y}_k = \mathbf{S}_k\mathbf{h}_k + \mathbf{H}_k\mathbf{u}_k + \boldsymbol{\eta}_k = \mathbf{S}_k\mathbf{h}_k + \mathbf{H}'_k\mathcal{O}_k\mathbf{G}_{\mathrm{u},k}\mathbf{x}_{\mathrm{u},k} + \boldsymbol{\eta}_k, \tag{3.11}$$

where now the vector $\mathbf{u}_k \in \mathbb{R}^{L_\mathrm{G}}$, or equivalently $\mathbf{x}_{\mathrm{u},k}$, in each subcarrier is unknown, $\mathbf{H}_k = \mathbf{H}'_k\mathcal{O}_k$ and $\mathbf{H}'_k$ is the convolution matrix associated to the kth subchannel impulse response, $\mathbf{h}_k$. For convenience, we define

$$\mathcal{O}_k = \begin{cases} \mathrm{diag}([1, \jmath, 1, ...]), & \text{for } k \text{ even} \\ \mathrm{diag}([\jmath, 1, \jmath, ...]), & \text{for } k \text{ odd.} \end{cases} \tag{3.12}$$

Note that in this case $\mathbf{G}_{\mathrm{u},k} \in \mathbb{R}^{L_\mathrm{G}\times 2L_\mathrm{t}}$ is a purely real matrix related to the matrices $\mathbf{G}_{k,k-1}$ and $\mathbf{G}_{k,k+1}$ in (3.1).

Although the exact values of $\mathbf{u}_k$ are unknown, its statistics can be known. Define then the interference covariance matrix as

$$\mathbf{C}_{u,k} = \frac{\sigma_d^2}{2}\mathbf{G}_{\mathrm{u},k}\mathbf{G}_{\mathrm{u},k}^\mathsf{H}, \tag{3.13}$$

where $\mathbf{x}_{\mathrm{u},k}$ was assumed to be i.i.d. and Gaussian distributed with zero mean and variance $\sigma_d^2/2$. This is usually a good approximation although $\mathbf{x}_{\mathrm{u},k}$ is composed of symbols taken from a finite constellation.

For the linear model of (3.11), the ML estimator has no closed form solution and an efficient way to implement it is to employ the iterative *expectation maximization (EM)* algorithm [47]. The EM algorithm works here as follows. Before the first iteration, a rough channel estimate is obtained that ignores the interference and only considers the training sequence in the observed subcarrier. This estimate is given by

$$\hat{\mathbf{h}}_{k,0} = (\mathbf{S}_k^\mathsf{H}\mathbf{C}_{\eta,k}^{-1}\mathbf{S}_k)^{-1}\mathbf{S}_k^\mathsf{H}\mathbf{C}_{\eta,k}^{-1}\mathbf{y}_k. \tag{3.14}$$

Then, the iterative process starts. For each iteration i, the algorithm is divided into two steps: the E-step and the M-step. In the E-step, an approximation of the ML function (here its derivative) is obtained by taking the expected value of it conditioned on the channel estimated in the iteration before and the observed sequence, as follows

$$\mathrm{E}_{\mathbf{u}|\mathbf{y},\mathbf{h}_i}\left[\frac{\partial J(\mathbf{h}_i)}{\partial \mathbf{h}_i^\mathsf{H}}\right] = \left[\mathbf{S}^\mathsf{H}\mathbf{C}_\eta^{-1}(\mathbf{S}+\mathrm{E}[\mathbf{U}]) + \mathrm{E}[\mathbf{U}]^\mathsf{H}\mathbf{C}_\eta^{-1}\mathbf{S} + \mathrm{E}[\mathbf{U}^\mathsf{H}\mathbf{C}_\eta^{-1}\mathbf{U}]\right]\mathbf{h}_i - (\mathbf{S}+\mathrm{E}[\mathbf{U}])^\mathsf{H}\mathbf{C}_\eta^{-1}\mathbf{y} \tag{3.15}$$

The result is seen to be a function of $\mathrm{E}[\mathbf{u}_k]$ and $\mathrm{E}[\mathbf{U}_k^\mathsf{H}\mathbf{C}_{\eta,k}^{-1}\mathbf{U}_k]$. $\mathrm{E}[\mathbf{u}_k] = \hat{\mathbf{u}}_{k,i}$ can be viewed as an instantaneous estimate of the interference term $\mathbf{u}_k$ in the i-th iteration.

To express the last expectation in (3.15) also in terms of the estimate $\hat{\mathbf{u}}_i$, one has first to write the matrix $\mathbf{U}_k$ as a function of vector $\mathbf{u}_k$:

$$\mathbf{U}_k = \sum_{j=1}^{L_{h_k}} \mathbf{D}_j\mathcal{O}_k\mathbf{u}_k\mathbf{e}_j^T, \tag{3.16}$$

where $\mathbf{D}_j = \begin{bmatrix} \mathbf{0}_{j-1} & \mathbf{I}_{L_\mathrm{t}} & \mathbf{0}_{L_\mathrm{o}-L_\mathrm{t}-j} \end{bmatrix}$ is a matrix that selects L_t rows of $\mathbf{u}_k$ and $\mathbf{e}_j \in \{0,1\}^{L_{h_k}}$ is a vector with one in the j-th row and the rest of its elements are zero. Then (3.16) is plugged in the expected value

$$\begin{aligned}\mathrm{E}\Big[\mathbf{U}_k^{\mathsf{H}}\mathbf{C}_{\eta,k}^{-1}\mathbf{U}_k\Big] &= \mathrm{E}\left[\sum_{l=1}^{L_{h_k}} \mathbf{e}_l \mathbf{u}_k^{\mathrm{T}} \mathcal{O}_k^{\mathsf{H}} \mathbf{D}_l^{\mathrm{T}} \mathbf{C}_{\eta,k}^{-1} \sum_{j=1}^{L_{h_k}} \mathbf{D}_j \mathcal{O}_k \mathbf{u}_k \mathbf{e}_j^{\mathrm{T}}\right] \\ &= \sum_{l=1}^{L_{h_k}} \mathbf{e}_l \sum_{j=1}^{L_{h_k}} \mathrm{E}\left[\mathbf{u}_k^{\mathrm{T}} \mathcal{O}_k^{\mathsf{H}} \mathbf{D}_l^{\mathrm{T}} \mathbf{C}_{\eta,k}^{-1} \mathbf{D}_j \mathcal{O}_k \mathbf{u}_k\right] \mathbf{e}_j^{\mathrm{T}} \\ &= \sum_{l=1}^{L_{h_k}} \mathbf{e}_l \sum_{j=1}^{L_{h_k}} \mathrm{tr}\left(\mathcal{O}_k^{\mathsf{H}} \mathbf{D}_l^{\mathrm{T}} \mathbf{C}_{\eta,k}^{-1} \mathbf{D}_j \mathcal{O}_k \mathrm{E}\Big[\mathbf{u}_k \mathbf{u}_k^{\mathrm{T}}\Big]\right) \mathbf{e}_j^{\mathrm{T}}. \end{aligned} \tag{3.17}$$

Furthermore,

$$\mathrm{E}\Big[\mathbf{u}_k \mathbf{u}_k^{\mathrm{T}}\Big] = \mathbf{C}_{\epsilon,k,i} + \mathrm{E}[\mathbf{u}_k]\mathrm{E}[\mathbf{u}_k]^{\mathrm{T}} = \mathbf{C}_{\epsilon,k,i} + \hat{\mathbf{u}}_{k,i}\hat{\mathbf{u}}_{k,i}^{\mathrm{T}}, \tag{3.18}$$

where $\mathbf{C}_{\epsilon,k,i}$ is the covariance matrix of the estimation error of $\mathbf{u}_k$ in the i-th iteration. Consequently,

$$\begin{aligned}\mathrm{E}\Big[\mathbf{U}_k^{\mathsf{H}}\mathbf{C}_{\eta,k}^{-1}\mathbf{U}_k\Big] &= \sum_{l=1}^{L_{h_k}} \mathbf{e}_l \sum_{j=1}^{L_{h_k}} \mathrm{tr}\left(\mathcal{O}_k^{\mathsf{H}} \mathbf{D}_l^{\mathrm{T}} \mathbf{C}_{\eta,k}^{-1} \mathbf{D}_j \mathcal{O}_k \mathbf{C}_{\epsilon,k,i}\right) \mathbf{e}_j^{\mathrm{T}} + \mathrm{E}[\mathbf{U}_k]^{\mathsf{H}} \mathbf{C}_{\eta,k}^{-1} \mathrm{E}[\mathbf{U}_k], \\ &= \mathbf{\Psi}_{k,i} + \mathrm{E}[\mathbf{U}_k]^{\mathsf{H}} \mathbf{C}_{\eta,k}^{-1} \mathrm{E}[\mathbf{U}_k], \end{aligned} \tag{3.19}$$

where $[\mathbf{\Psi}_{k,i}]_{j,l} = \mathrm{tr}(\mathcal{O}_{\mathbf{k}}{}^{\mathsf{H}} \mathbf{D}_j^{\mathrm{T}} \mathbf{C}_{\eta,k}^{-1} \mathbf{D}_l \mathcal{O}_k \mathbf{C}_{\epsilon,k,i})$. Finally

$$\mathrm{E}_{\mathbf{u}_k|\mathbf{y}_k,\mathbf{h}_{k,i}}\left[\frac{\partial J(\mathbf{h}_{k,i})}{\partial \mathbf{h}_{k,i}^{\mathsf{H}}}\right] = \Big((\mathbf{S}_k + \hat{\mathbf{U}}_{k,i})^{\mathsf{H}} \mathbf{C}_{\eta,k}^{-1} (\mathbf{S}_k + \hat{\mathbf{U}}_{k,i}) + \mathbf{\Psi}_{k,i}\Big) \mathbf{h}_{k,i} - (\mathbf{S}_k + \hat{\mathbf{U}}_{k,i})^{\mathsf{H}} \mathbf{C}_{\eta,k}^{-1} \mathbf{y}_k. \tag{3.20}$$

Given that an estimate of h_k and the training sequence are known, one can subtract this signal from the observation signal. Then the resulting vector can be processed with an MMSE estimator. As mentioned previously, the interference vector is composed of purely real and purely imaginary terms, and for that a WL MMSE estimator [55] can be employed, given by

$$\mathrm{E}[\mathbf{u}_{k,i}] = \hat{\mathbf{u}}_{k,i} = 2\Re\{\boldsymbol{\mathcal{W}}_k^{\mathsf{H}}(\mathbf{y}_k - \mathbf{S}_k \hat{\mathbf{h}}_{k,i})\}, \tag{3.21}$$

where

$$\boldsymbol{\mathcal{W}}_k = (\mathbf{C}_{y,k} - \mathbf{P}_{y,k}^{\mathrm{T}} \mathbf{C}_{y,k}^{-\mathrm{T}} \mathbf{P}_{y,k}^{\mathsf{H}})^{-1} (\mathbf{C}_{uy,k}^{\mathsf{H}} - \mathbf{P}_{y,k}^{\mathrm{T}} \mathbf{C}_{y,k}^{-\mathrm{T}} \mathbf{P}_{uy,k}^{\mathsf{H}}), \tag{3.22}$$

and

$$\mathbf{C}_{y,k} = \hat{\mathbf{H}}_{k,i} \mathbf{C}_{u,k} \hat{\mathbf{H}}_{k,i}^{\mathsf{H}} + \mathbf{C}_{\eta,k}, \text{ and } \mathbf{C}_{uy,k} = \mathbf{C}_{u,k} \hat{\mathbf{H}}_{k,i}^{\mathsf{H}}, \tag{3.23}$$

The pseudo-covariance matrices are given by

$$\mathbf{P}_{y,k} = \hat{\mathbf{H}}_{k,i} \mathbf{C}_{u,k} \hat{\mathbf{H}}_{k,i}^{\mathrm{T}}, \text{ and } \mathbf{P}_{uy,k} = \mathbf{C}_{u,k} \hat{\mathbf{H}}_{k,i}^{\mathrm{T}} \tag{3.24}$$

where $\hat{\mathbf{H}}_{k,i} = \hat{\mathbf{H}}'_{k,i}\mathcal{O}_k$ and $\hat{\mathbf{H}}'_{k,i}$ is a convolution matrix containing the estimated subchannel impulse response $\hat{\mathbf{h}}_{k,i}$. The corresponding error covariance matrix equals

$$\mathbf{C}_{\epsilon,k,i} = \mathbf{C}_{u,k} - 2\Re\{\boldsymbol{\mathcal{W}}_k \mathbf{C}^{\mathsf{H}}_{uy,k}\}. \tag{3.25}$$

Finally, the M-step is performed, where $J(\mathbf{h}_{k,i})$ is minimized, resulting in a new channel estimate

$$\hat{\mathbf{h}}_{k,i+1} = [(\mathbf{S}_k + \hat{\mathbf{U}}_{k,i})^{\mathsf{H}} \mathbf{C}^{-1}_{\eta,k} (\mathbf{S} + \hat{\mathbf{U}}_{k,i}] + \boldsymbol{\Psi}_{k,i})^{-1} (\mathbf{S}_k + \hat{\mathbf{U}}_{k,i})^{\mathsf{H}} \mathbf{C}^{-1}_{\eta,k} \mathbf{y}_k. \tag{3.26}$$

The estimation of $\mathbf{u}_k$ and $\mathbf{h}_k$ is then repeated N_{EM} times until convergence is achieved.

3.1.6 Simulation Results

Simulation results are reported here, from the numerical performance evaluation of the narrowband EM-based ML sub-channel estimator. ITU Veh-A channel was assumed, at a bandwidth of 10 MHz and sampling rate $M/T = 15.36$ MHz. The FBMC/OQAM system was employed with $M = 256$ subcarriers, from which 210 were occupied with training and symbols, with the rest being inactive. The resulting subcarrier spacing is 60 kHz. An RRC filter with $K = 4$ (of length $L_g = 1025$) and unit roll-off was chosen for g. With this configuration and scenario, $L_{h_k} = 5$ taps for the narrowband multipath sub-channels and $L_{\mathsf{e}} = 5$ taps for the corresponding per-subcarrier equalizers were seen to be sufficient for all subcarriers. Preamble-based channel estimation was performed, with L_{o} training observations per subcarrier. This corresponds to a training sequence of $L_{\mathsf{t}} = 19 + L_{\mathsf{o}}$ FBMC symbols. 16-QAM was adopted for FBMC/OQAM and 32-QAM for CP-OFDM. Moreover, the CP length was $L_{\mathrm{cp}} = 64$. With this combination of constellation size and CP length, the two systems achieve the same data throughput. For the training sequences, pseudorandom QPSK symbols were employed. Monte-Carlo simulations were run on 200 channel realizations for different E_{b}/N_0. For calculating the bit error rate (BER), 100 FBMC data symbols were transmitted after training.

In Fig. 3-3, the normalized MSE (NMSE) of the narrowband channel estimation as a function of E_{b}/N_0 is depicted for different observation lengths L_{o} and for different numbers of iterations N_{EM}. Also the results for the ML narrowband channel estimation with known training on the adjacent subcarriers are shown as references. We can observe a considerable loss in E_{b}/N_0 that increases with the decrease of the noise power. The resulting BER as a function of E_{b}/N_0 is shown in Fig. 3-4. The results for perfect channel state information (PCSI) are included for comparison. One can observe that for the BER the gap between the two estimation methods is not so high as the NMSE curves show. We can also note that for sufficiently many observations and iterations, quite good estimates of the subchannels can be achieved. Regarding the convergence of the algorithm, it was observed in the experiments that it practically always provides a stable solution after a certain number of iterations.

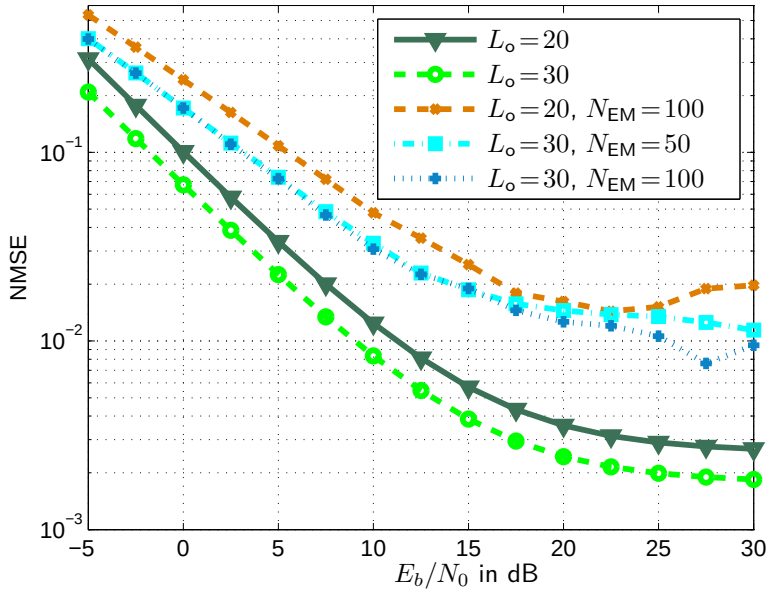

Figure 3-3: NMSE as a function of E_b/N_0 for different estimation parameters.

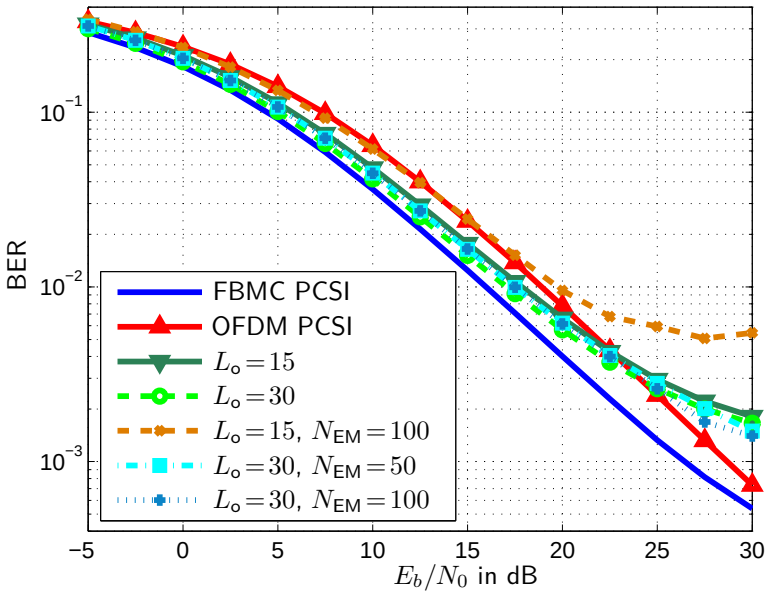

Figure 3-4: BER as a function of E_b/N_0 for different estimation parameters.

3.2 Broadband Impulse Response Estimation

The subcarrier model of Fig. 3-1 can be simplified as in Fig. 3-5 for the purpose of estimating the broadband CIR $h(l)$. The output $y_k(n)$ contains the downsampled received samples in the OQAM symbol rate and is defined as

$$y_k(n) = \tilde{g}_{k,k}(n) * x_k(n) + \tilde{g}_{k,k-1}(n) * x_{k-1}(n) + \tilde{g}_{k,k+1}(n) * x_{k+1}(n) + \eta_k(n) \tag{3.27}$$

where $*$ stands for linear convolution, and $\tilde{g}_{k,k}(n)$, $\tilde{g}_{k,k-1}(n)$ and $\tilde{g}_{k,k+1}(n)$ are the downsampled convolution of transmit filter, receive filter and frequency selective channel $h(l)$. $\eta_k(n)$ is the downsampled filtered noise. One can stack the coefficients of the impulse responses $\tilde{g}_{k,k}(n)$, $\tilde{g}_{k,k-1}(n)$ and $\tilde{g}_{k,k+1}(n)$ in vectors $\tilde{\mathbf{g}}_{k,k}$, $\tilde{\mathbf{g}}_{k,k-1}$ and $\tilde{\mathbf{g}}_{k,k+1}$. They can be represented as products of matrices $\tilde{\mathbf{G}}_{k,k}$, $\tilde{\mathbf{G}}_{k,k-1}$ and $\tilde{\mathbf{G}}_{k,k+1}$ and the CIR vector $\mathbf{h}$:

$$\tilde{\mathbf{g}}_{k,k} = \tilde{\mathbf{G}}_{k,k}\mathbf{h}, \tag{3.28}$$
$$\tilde{\mathbf{g}}_{k,k-1} = \tilde{\mathbf{G}}_{k,k-1}\mathbf{h}, \tag{3.29}$$
$$\tilde{\mathbf{g}}_{k,k+1} = \tilde{\mathbf{G}}_{k,k+1}\mathbf{h}, \tag{3.30}$$
$$\boldsymbol{\eta}_k = \mathbf{V}_k\boldsymbol{w}, \tag{3.31}$$

where

$$\tilde{\mathbf{G}}_{k,k} = \begin{bmatrix} g_{k,k}(0) & 0 & 0 & \dots \\ g_{k,k}(M/2) & g_{k,k}(M/2-1) & g_{k,k}(M/2-2) & \dots \\ g_{k,k}(M) & g_{k,k}(M-1) & g_{k,k}(M-2) & \dots \\ \vdots & \vdots & \vdots & \ddots \end{bmatrix} \in \mathbb{C}^{L_{\tilde{\mathsf{G}}} \times L_h} \tag{3.32}$$

is the result of taking each $M/2$th row of the convolution matrix of $g_{k,k}(l)$. Similarly for $\tilde{\mathbf{G}}_{k,k-1}$ and $\tilde{\mathbf{G}}_{k,k+1}$. Furthermore, $L_{\tilde{\mathsf{G}}} = \lceil (2L_g + L_h - 2)/(M/2) \rceil$.

$$\mathbf{y}_k(n) = \mathbf{X}_k(n)\tilde{\mathbf{g}}_{k,k} + \mathbf{X}_{k-1}(n)\tilde{\mathbf{g}}_{k,k-1} + \mathbf{X}_{k+1}(n)\tilde{\mathbf{g}}_{k,k+1} + \mathbf{V}_k\boldsymbol{w}(l), \tag{3.33}$$
$$= (\mathbf{X}_k(n)\tilde{\mathbf{G}}_{k,k} + \mathbf{X}_{k-1}(n)\tilde{\mathbf{G}}_{k,k-1} + \mathbf{X}_{k+1}(n)\tilde{\mathbf{G}}_{k,k+1})\mathbf{h} + \mathbf{V}_k\boldsymbol{w}(l), \tag{3.34}$$

where $\mathbf{X}_{k-1}, \mathbf{X}_k, \mathbf{X}_{k+1} \in \mathbb{C}^{L_{\mathsf{o}} \times L_{\tilde{\mathsf{G}}}}$ are Hankel matrices corresponding to $x_{k-1}(n), x_k(n)$ and $x_{k+1}(n)$, the training sequences in the subcarriers $k-1, k$ and $k+1$.

Again defining $\mathbf{S}_k(n) = \mathbf{X}_k(n)\tilde{\mathbf{G}}_{k,k}$ and $\mathbf{U}_k(n) = \mathbf{X}_{k-1}(n)\tilde{\mathbf{G}}_{k,k-1} + \mathbf{X}_{k+1}(n)\tilde{\mathbf{G}}_{k,k+1}$, we get for each observations subcarrier:

$$\mathbf{y}_k = (\mathbf{S}_k + \mathbf{U}_k)\mathbf{h} + \boldsymbol{\eta}_k. \tag{3.35}$$

Stacking M_{t} vectors with the outputs of the observations subcarriers we obtain

$$\begin{bmatrix} \mathbf{y}_0 \\ \mathbf{y}_1 \\ \vdots \\ \mathbf{y}_{M_{\mathsf{t}}-1} \end{bmatrix} = \left(\begin{bmatrix} \mathbf{S}_0 \\ \mathbf{S}_1 \\ \vdots \\ \mathbf{S}_{M_{\mathsf{t}}-1} \end{bmatrix} + \begin{bmatrix} \mathbf{U}_0 \\ \mathbf{U}_1 \\ \vdots \\ \mathbf{U}_{M_{\mathsf{t}}-1} \end{bmatrix} \right) \mathbf{h} + \begin{bmatrix} \mathbf{V}_0 \\ \mathbf{V}_1 \\ \vdots \\ \mathbf{V}_{M_{\mathsf{t}}-1} \end{bmatrix} \boldsymbol{w}, \tag{3.36}$$

$$\mathbf{y} = (\mathbf{S} + \mathbf{U})\mathbf{h} + \boldsymbol{\eta}. \tag{3.37}$$

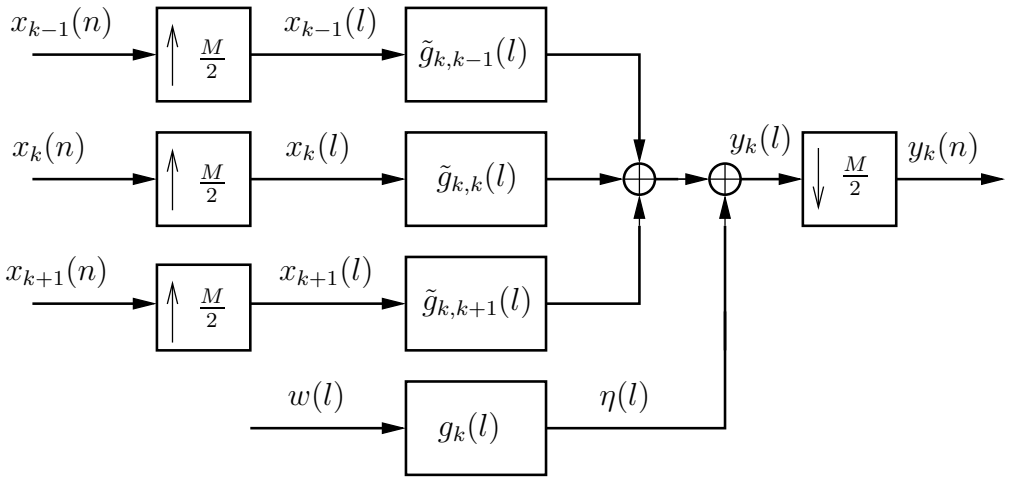

Figure 3-5: Subcarrier model for broadband channel estimation.

It should be noted that the vectors $\mathbf{y}_k$ that are collected into $\mathbf{y}$ do not need to belong to contiguous subcarriers. This means that the observations can be sparsely taken in the subcarrier domain. This allows the use of preambles that are not full in the sense that they can be frequency multiplexed with data sequences. In this way, a higher spectral efficiency is obtained by reducing the number of training symbols transmitted in the whole training block. In the simulation results, an example of this situation is presented.

3.2.1 LS Estimation

For least squares estimation,

$$\hat{\mathbf{h}}_{\mathsf{LS}} = \underset{\mathbf{h}\in\mathbb{C}^{L_h}}{\operatorname{argmin}} \|\mathbf{y} - (\mathbf{S}+\mathbf{U})\mathbf{h}\|_2^2, \tag{3.38}$$

we have the estimate

$$\hat{\mathbf{h}}_{\mathsf{LS}} = [(\mathbf{S}+\mathbf{U})^{\mathsf{H}}(\mathbf{S}+\mathbf{U})]^{-1}(\mathbf{S}+\mathbf{U})^{\mathsf{H}}\mathbf{y}. \tag{3.39}$$

The covariance matrix of the estimation error $\boldsymbol{\Delta}\hat{\mathbf{h}}_{\mathsf{LS}} = \hat{\mathbf{h}}_{\mathsf{LS}} - \mathbf{h}_{\mathsf{LS}}$ is given by

$$\mathbf{C}_{\boldsymbol{\Delta}\hat{\mathbf{h}}_{\mathsf{LS}}} = \mathrm{E}\left[\boldsymbol{\Delta}\hat{\mathbf{h}}_{\mathsf{LS}}\boldsymbol{\Delta}\hat{\mathbf{h}}_{\mathsf{LS}}^{\mathsf{H}}\right] = [(\mathbf{S}+\mathbf{U})^{\mathsf{H}}(\mathbf{S}+\mathbf{U})]^{-1} \tag{3.40}$$

The theoretical MSE of the broadband LS estimator, which is equal to the Cramér-Rao Lower Bound (CRLB) in this case [38], is given by

$$\epsilon_{\mathsf{LS}} = \frac{\sigma^2 M_{\mathsf{u}}}{M}\,\mathrm{tr}\left\{\mathbf{C}_{\boldsymbol{\Delta}\hat{\mathbf{h}}_{\mathsf{LS}}}\right\} = \frac{\sigma^2 M_{\mathsf{u}}}{M}\,\mathrm{tr}\left\{[(\mathbf{S}+\mathbf{U})^{\mathsf{H}}(\mathbf{S}+\mathbf{U})]^{-1}\right\}, \tag{3.41}$$

where M_{u} is the total number of subcarriers occupied with either data or training. In practical implementations, $M_{\mathsf{u}} < M$ to take advantage of the spectral containment of the prototype filter. In this case, $\mathbf{C}_{\boldsymbol{\Delta}\hat{\mathbf{h}}_{\mathsf{LS}}}$ is ill conditioned in the sense that the ratio between its largest and smallest eingenvalues is huge. The explanation is that we are not able to estimate the channel in the inactive region of the spectrum. With such an ill conditioning, the inverse of the covariance matrix will numerically explode and hence some measure has to be taken.

To this end, we have decided to utilize a pseudo-inverse instead, computed with the aid of the singular value decomposition (SVD) of $\mathbf{C}_{\boldsymbol{\Delta}\hat{\mathbf{h}}_{\mathsf{LS}}}$. The matrix $\mathbf{C}^{-1}_{\boldsymbol{\Delta}\hat{\mathbf{h}}_{\mathsf{LS}}}$ has L_h singular values but and it can be proven that only $N_{\mathsf{SV}} = \lceil \frac{L_h M_{\mathsf{u}}}{M} \rceil$ of them need to be inverted to obtain the best theoretical MSE performance in (3.41). Hence, we use only those N_{SV} inverted singular values when computing the trace above. In the simulation results, we will show the effect of using this pseudo-inverse in the measured MSE.

3.2.2 Broadband ML

The ML estimate of $\mathbf{h}$ is given by

$$\hat{\mathbf{h}}_{\mathsf{ML}} = [(\mathbf{S}+\mathbf{U})^{\mathsf{H}}\mathbf{C}_{\eta}^{-1}(\mathbf{S}+\mathbf{U})]^{-1}(\mathbf{S}+\mathbf{U})^{\mathsf{H}}\mathbf{C}_{\eta}^{-1}\mathbf{y} \tag{3.42}$$

The associated theoretical MSE is given by

$$\epsilon_{\mathsf{ML}} = \frac{\sigma^2 M_{\mathsf{u}}}{M}\,\mathrm{tr}\left\{\mathbf{C}_{\boldsymbol{\Delta}\hat{\mathbf{h}}_{\mathsf{ML}}}\right\} = \frac{\sigma^2 M_{\mathsf{u}}}{M}\,\mathrm{tr}\left\{[(\mathbf{S}+\mathbf{U})^{\mathsf{H}}\mathbf{C}_{\eta}^{-1}(\mathbf{S}+\mathbf{U})]^{-1}\right\} \tag{3.43}$$

Similarly to the broadband LS estimator, the ML one has also conditioning problems with the inverse covariance matrix. We will also employ here a pseudo-inverse based on SVD.

3.2.3 Broadband MMSE

Similarly with the sub-channel estimation problem, the MMSE estimator is expressed as

$$\hat{\mathbf{h}}_{\mathsf{MMSE}} = \mathbf{C}_{\mathbf{h}}\,(\mathbf{S}+\mathbf{U})^{\mathsf{H}}\left[(\mathbf{S}+\mathbf{U})\,\mathbf{C}_{\mathbf{h}}\,(\mathbf{S}+\mathbf{U})^{\mathsf{H}} + \mathbf{C}_{\eta}\right]^{-1}\mathbf{y} \tag{3.44}$$

The MSE of the broadband MMSE estimator is given by

$$\begin{aligned}\epsilon_{\mathsf{MMSE}} &= \mathrm{tr}\left\{\mathbf{C}_{\boldsymbol{\Delta}\hat{\mathbf{h}}_{\mathsf{MMSE}}}\right\} \\ &= \mathrm{tr}\left\{\left[\mathbf{I}_{L_h} - \mathbf{C}_{\mathbf{h}}\,(\mathbf{S}+\mathbf{U})^{\mathsf{H}}\left[(\mathbf{S}+\mathbf{U})\,\mathbf{C}_{\mathbf{h}}\,(\mathbf{S}+\mathbf{U})^{\mathsf{H}} + \frac{\sigma^2 M_{\mathsf{u}}}{M}\mathbf{C}_{\eta}\right]^{-1}(\mathbf{S}+\mathbf{U})\right]\mathbf{C}_{\mathbf{h}}\right\}\end{aligned} \tag{3.45}$$

In this case, there is no ill-conditioning problem for typical E_{b}/N_0 values. Only for very high E_{b}/N_0 values the SVD needs to be used.

3.2.4 Simulation Results

For the simulations, the same scenario is considered as previously, where the length of $\mathbf{h}$ is $L_h = 36$. Of the $M = 256$ subcarriers, either all or only 111 were carrying training signals. As previously, QPSK pseudo-random training sequences of length $L_{\mathsf{t}} = L_{\mathsf{o}} + 19$ symbols were employed. The parameter M_{e} gives the distance (in frequency) between neighboring pilot subcarriers. It thus denotes how densely or sparsely were the subcarriers occupied with training sequences. Thus, $M_{\mathsf{e}} = 1$ means that all subcarriers are used for the estimation while $M_{\mathsf{e}} = 7$ implies that only 37 subcarriers were used as pilot tones.

In Fig. 3-6, the MSE for the different estimators and various lengths of observation sequences is plotted.

We show some simulation results for $M_{\mathsf{u}} = 210$ in Fig. 3-7. In this case, only $N_{\mathsf{SV}} = \lceil \frac{L_h M_{\mathsf{u}}}{M} \rceil = 30$ singular values are inverted. One can see the error floor because of the bad approximation of the inverse.

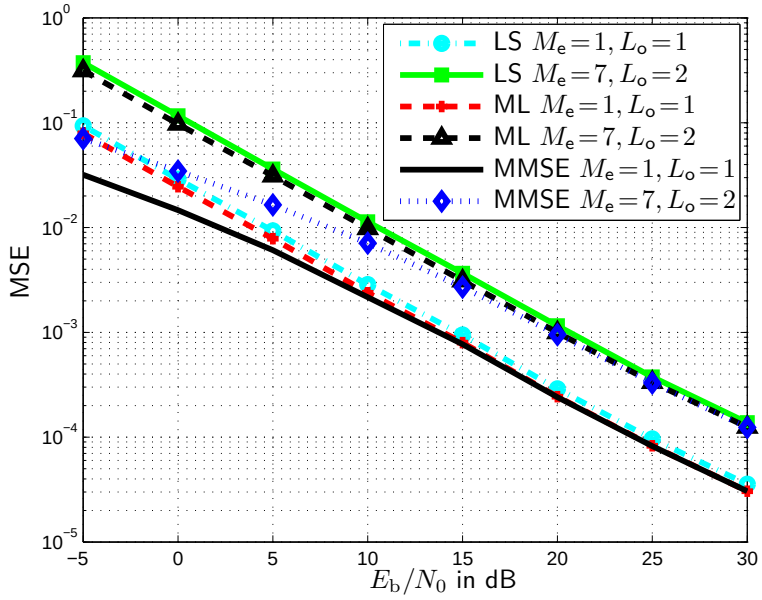

Figure 3-6: MSE as a function of E_b/N_0 for different estimators and training parameters.

Again, for $M_u = 210$ in 3-8, we have employed the pseudo-inverse, but now $N_{SV} = 32$. We can see there that the simulated MSE is closer to the CRLB for a wider range of E_b/N_0 values.

In Fig. 3-9, the result of equalizing these channels with the WL MMSE equalizer of [66, 65] of length 5 and with 16-QAM data is shown. Again, the PCSI case is included for the sake of the comparison.

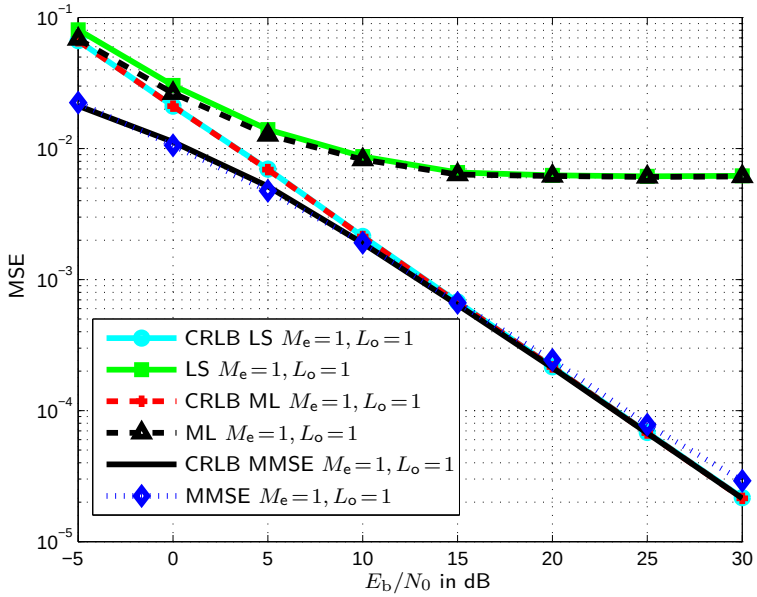

Figure 3-7: MSE as a function of E_b/N_0 for $M_u = 210$ and $N_{SV} = 30$.

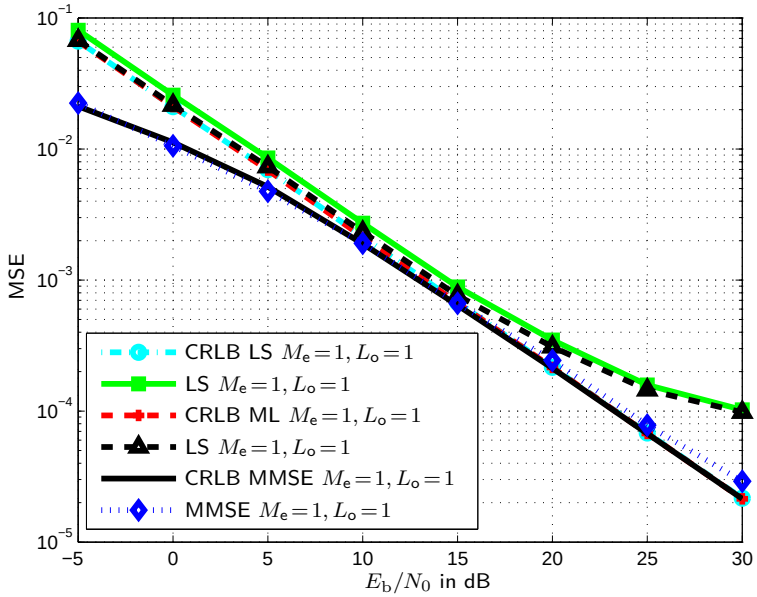

Figure 3-8: MSE as a function of E_b/N_0 for $M_u = 210$ and $N_{SV} = 32$.

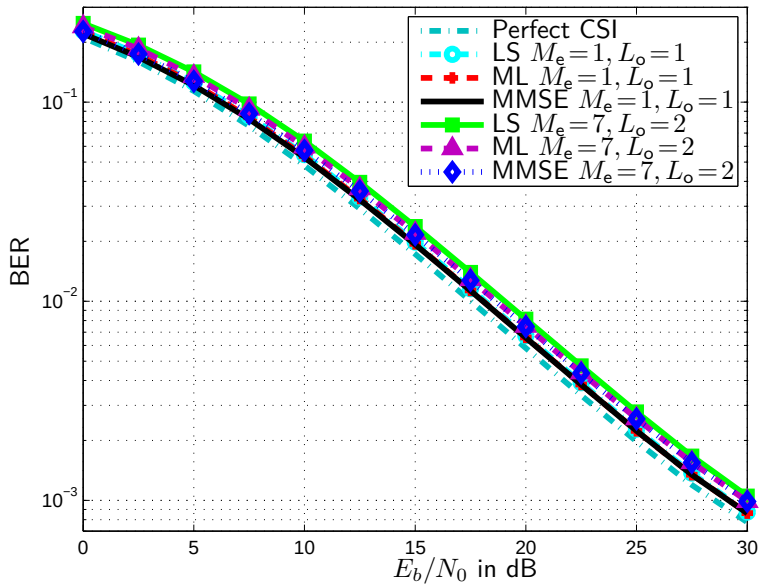

Figure 3-9: BER as a function of E_b/N_0 for different estimators and parameters.

3.3 Impulse Response Estimation – Optimal Preamble Design and Sparsity-aware Techniques

The problem of CIR estimation in FBMC/OQAM is revisited in this section. As previously, no assumptions on the subchannel frequency selectivity are made. The focus here is on the design of *optimal* (in the MSE sense) *short* preambles, of both the full and sparse types [41], consisting of *only one* pilot FBMC symbol, accompanied by one (or more) guards. Existing preamble designs for flat subchannels [36, 41] can be shown to result as special cases. Simulation results are presented, for both mildly and highly frequency selective channels, that demonstrate the significant improvements in performance and robustness to channel dispersion offered by the proposed approach over both CP-OFDM and the optimal flat subchannel-based FBMC/OQAM method. Most notably, no error floors appear anymore over a quite wide range of SNR values, especially when care is taken to protect the preamble from getting interfered by the payload.

The AFB output at the (p,q) FT point is given as

$$\begin{aligned} y_{p,q} &= \sum_l y(l) g_{p,q}^*(l) = \sum_{k=0}^{L_h-1} h(k) \sum_{m=0}^{M-1} e^{-\jmath \frac{2\pi}{M} mk} \sum_n d_{m,n} \jmath^{m+n-p-q} (-1)^{mn-pq} \times \\ &\quad \sum_l g\left(l-k-n\frac{M}{2}\right) g\left(l-q\frac{M}{2}\right) e^{\jmath \frac{2\pi}{M}(m-p)\left(l-\frac{L_g-1}{2}\right)} + \eta_{p,q} \end{aligned} \tag{3.46}$$

with $\eta_{p,q}$ denoting the corresponding noise component. The latter equation describes the AFB output samples in terms of the channel impulse response, that is, in a *time domain (TD)* formulation. Its value is found in the fact that it is *exact* regardless of the relative channel delay spread (only assumed not to exceed M). Recall that the usual frequency-domain input/output description [43]

$$y_{p,q} = H_{p,q} d_{p,q} + \text{interference} + \eta_{p,q}$$

is only valid (to an approximation) for short enough (relative to the extent of g) channels. Eq. (3.46) is thus a good candidate in providing a way to address canne for the general case, namely when the subchannels are not well approximated by the frequency flat model.

3.3.1 TD Channel Estimator

Assume that the preamble is constructed in the usual manner [41], namely consisting of 2 FBMC symbols, with the second consisting of all zeros. This is to protect the pilots from being interfered by the unknown data (or control) samples of the current frame.[1] Then, $d_{m,n}$ is nonzero only for $n=0$. Also, only the case of $q=0$ is of interest. Rewriting eq. (3.46) with these assumptions yields

$$y_{p,0} = \sum_{k=0}^{L_h-1} \Gamma_{p,k} h(k) + \eta_{p,0} \tag{3.47}$$

where

$$\Gamma_{p,k} = \sum_{m=0}^{M-1} e^{-\jmath \frac{2\pi}{M} mk} d_{m,0} \jmath^{m-p} e^{-\jmath \frac{2\pi}{M}(m-p)\left(\frac{L_g-1}{2}\right)} \sum_{l=k}^{L_g-1} g(l-k) g(l) e^{\jmath \frac{2\pi}{M}(m-p)l} \tag{3.48}$$

can be seen to be *the response of the transmultiplexer to this particular input for a channel equal to a k-samples delay*, i.e., $h(l) = \delta(l-k)$, and can be *easily computed*. The AFB output

[1] One guard FBMC symbol is not always sufficient and non-negligible interference may still exist, as it will be seen later on.

sample is the sum of those responses, multiplied with the channel gains. In matrix-vector notation:

$$\boldsymbol{y} = \boldsymbol{\Gamma h} + \boldsymbol{\eta}, \tag{3.49}$$

with

$$\boldsymbol{y} = \begin{bmatrix} y_{0,0} & y_{1,0} & \cdots & y_{M-1,0} \end{bmatrix}^{\mathrm{T}}$$

and similarly for $\boldsymbol{\eta}$, while $[\boldsymbol{\Gamma}]_{p+1,k+1} = \Gamma_{p,k}$. The matrix $\boldsymbol{\Gamma}$ is of dimensions $M \times L_h$, i.e., tall, and hence the equation above can be solved for the channel impulse response $\boldsymbol{h}$ using, for example, least squares (LS).

It must be emphasized here that the noise η is known to be zero mean Gaussian with the same variance as w, however it is not uncorrelated among subcarriers [41]. Its $M \times M$ covariance matrix is known to be given by

$$\boldsymbol{C_\eta} = \sigma^2 \begin{bmatrix} 1 & \jmath\beta & 0 & \cdots & 0 & \jmath\beta \\ -\jmath\beta & 1 & \jmath\beta & \cdots & 0 & 0 \\ \vdots & \ddots & \ddots & \ddots & \ddots & \vdots \\ -\jmath\beta & 0 & 0 & \cdots & -\jmath\beta & 1 \end{bmatrix} \equiv \sigma^2 \boldsymbol{B}, \tag{3.50}$$

with $\pm j\beta$ being the correlation of $g_{m,1}$ with $g_{m\pm1,1}$, *a priori* computable based on the knowledge of g [41]. $\boldsymbol{C_\eta}$ is (almost) *tridiagonal* and *circulant* (and hence diagonalizable via DFT [31]). The invertibility of this matrix is verified in [35].

In view of the color of the noise component in (3.49), Gauss-Markov estimation is better suited here than LS, resulting in the following estimate for $\boldsymbol{h}$ [38]

$$\hat{\boldsymbol{h}} = (\boldsymbol{\Gamma}^{\mathsf{H}} \boldsymbol{C_\eta}^{-1} \boldsymbol{\Gamma})^{-1} \boldsymbol{\Gamma}^{\mathsf{H}} \boldsymbol{C_\eta}^{-1} \boldsymbol{y}$$

or equivalently

$$\hat{\boldsymbol{h}} = (\boldsymbol{\Gamma}^{\mathsf{H}} \boldsymbol{B}^{-1} \boldsymbol{\Gamma})^{-1} \boldsymbol{\Gamma}^{\mathsf{H}} \boldsymbol{B}^{-1} \boldsymbol{y} \tag{3.51}$$

Note that the estimator matrix is independent of the noise power, and hence we do not have to know (or have estimated) σ^2. Because of the Gaussianity of the noise, this can be seen to be also the maximum likelihood (ML) estimate [38]. Since this estimation technique stems from expressing the problem in terms of the time-domain channel (i.e., CIR), it will henceforth be referred to simply as the *TD method*.

3.3.2 Optimal Preamble Design

The goal here is to design the nonzero FBMC symbol in the 2-symbol preamble so as to minimize the mean squared error (MSE) of the channel estimate, subject to a constraint on the transmit energy. This problem can be stated as follows [38, 36]

$$\min_{\boldsymbol{d}} \ \mathrm{tr}\left\{ (\boldsymbol{\Gamma}^{\mathsf{H}} \boldsymbol{B}^{-1} \boldsymbol{\Gamma})^{-1} \right\} \tag{3.52}$$

$$\text{such that} \quad \boldsymbol{d}^{\mathsf{H}} \boldsymbol{B} \boldsymbol{d} \leq \mathcal{E}, \tag{3.53}$$

where the energy is considered at the SFB output (i.e., channel input). For the case of a *full* preamble, namely with all subcarriers carrying pilots,[2] the latter is not trivially related to the energy at the SFB input. The results of this optimization are outlined in the sequel, for both full and sparse (where only isolated pilot tones are used) preambles. Details can be found in [40, 39].

[2] This preamble type is known as *block-type* or *long symbol* in the OFDM literature.

3.3.2.1 Full preamble

Rewrite (3.48) as $\Gamma_{p,k} = \boldsymbol{\mathcal{G}}_{p,k}^{\mathsf{H}} \boldsymbol{d}$, with the obvious definition for the $M \times 1$ vectors $\boldsymbol{\mathcal{G}}_{p,k}$ and $\boldsymbol{d}$. One can then express the matrix $\boldsymbol{\Gamma}$ in the form:

$$\boldsymbol{\Gamma} = \boldsymbol{\mathcal{G}} \boldsymbol{D}, \tag{3.54}$$

where

$$\boldsymbol{\mathcal{G}} = \begin{bmatrix} \boldsymbol{\mathcal{G}}_{0,0}^{\mathsf{H}} & \boldsymbol{\mathcal{G}}_{0,1}^{\mathsf{H}} & \cdots & \boldsymbol{\mathcal{G}}_{0,L_h-1}^{\mathsf{H}} \\ \boldsymbol{\mathcal{G}}_{1,0}^{\mathsf{H}} & \boldsymbol{\mathcal{G}}_{1,1}^{\mathsf{H}} & \cdots & \boldsymbol{\mathcal{G}}_{1,L_h-1}^{\mathsf{H}} \\ \vdots & \vdots & \ddots & \vdots \\ \boldsymbol{\mathcal{G}}_{M-1,0}^{\mathsf{H}} & \boldsymbol{\mathcal{G}}_{M-1,1}^{\mathsf{H}} & \cdots & \boldsymbol{\mathcal{G}}_{M-1,L_h-1}^{\mathsf{H}} \end{bmatrix}$$

and

$$\boldsymbol{D} = \boldsymbol{I}_{L_h} \otimes \boldsymbol{d},$$

The matrix $\boldsymbol{\mathcal{G}}$ has a special structure. Indeed,

$$\boldsymbol{\mathcal{G}} = \begin{bmatrix} \boldsymbol{\mathcal{G}}_0 & \boldsymbol{\mathcal{G}}_1 & \cdots & \boldsymbol{\mathcal{G}}_{L_h-1} \end{bmatrix}, \tag{3.55}$$

where, for $k = 0, 1, \ldots, L_h - 1$, $\boldsymbol{\mathcal{G}}_k = \begin{bmatrix} \boldsymbol{\mathcal{G}}_{0,k} & \boldsymbol{\mathcal{G}}_{1,k} & \cdots & \boldsymbol{\mathcal{G}}_{M-1,k} \end{bmatrix}^{\mathsf{H}}$ is an $M \times M$ matrix. Moreover, it is not hard to show that

$$\boldsymbol{\mathcal{G}}_k = \boldsymbol{W}^k \boldsymbol{G}_k, \quad k = 0, 1, 2, \ldots, L_h - 1 \tag{3.56}$$

where

$$\boldsymbol{W} = \mathrm{diag}(1, e^{-\jmath \frac{2\pi}{M}}, e^{-\jmath 2\frac{2\pi}{M}}, \ldots, e^{-\jmath (M-1)\frac{2\pi}{M}})$$

and $\boldsymbol{G}_k$ is a Hermitian (almost) tridiagonal circulant matrix. In fact, one can readily verify that $\boldsymbol{\mathcal{G}}_0 = \boldsymbol{B}$. Moreover, $\boldsymbol{G}_k$ is diagonalized with the DFT matrix [31], that is,

$$\boldsymbol{G}_k = \boldsymbol{F} \boldsymbol{\Lambda}_k \boldsymbol{F}^{\mathsf{H}}, \tag{3.57}$$

where $\boldsymbol{F}$ is the *unitary* M-point DFT matrix and $\boldsymbol{\Lambda}_k$ is diagonal with the (real) eigenvalues of $\boldsymbol{G}_k$ on its main diagonal.[3] It must be emphasized that $\boldsymbol{\Lambda}_k$ can be easily computed *a priori*, as they only depend on the employed filter bank.

The solution for the pilot FBMC vector is

$$\boldsymbol{d} = \sqrt{\frac{\mathcal{E}}{\lambda_{0,i_{\mathrm{opt}}}}} \boldsymbol{F}(:, i_{\mathrm{opt}}), \tag{3.58}$$

where i can be determined as

$$i_{\mathrm{opt}} = \arg\min_i \lambda_{0,i} \sum_{k=1}^{L_h-1} \frac{\lambda_{0,((k+i))_M}}{\lambda_{k,i}^2}, \tag{3.59}$$

with $((\cdot))_M$ denoting that the argument is circularly shifted back to the set $\{1, 2, \ldots, M\}$ if it exceeds M. This (offline) search can be facilitated if the symmetries of the $\boldsymbol{\Lambda}$ matrices described above are utilized [40].

[3] For a closed form expression of the eigenvalues of $\boldsymbol{G}_0 = \boldsymbol{B}$, see [35].

Real-valued optimal pilots
The pilot symbol above is complex valued in general. Constraining $\boldsymbol{d}$ to be *real-valued* can be seen to correspond to all equal $d_{m,0}$'s or equal with alternating signs. The former choice turns out to be the best. That is:

$$\boldsymbol{d} = \sqrt{\frac{\mathcal{E}}{M}}\mathbf{1}_M \tag{3.60}$$

Remarks

1. The estimator can also be written as

$$\hat{\boldsymbol{h}} = (\tilde{\boldsymbol{\Gamma}}^{\mathsf{H}}\tilde{\boldsymbol{\Gamma}})^{-1}\tilde{\boldsymbol{\Gamma}}^{\mathsf{H}}\tilde{\boldsymbol{y}} \tag{3.61}$$
$$= \tilde{\boldsymbol{\Gamma}}^{\dagger}\tilde{\boldsymbol{y}}, \tag{3.62}$$

   where

$$\tilde{\boldsymbol{\Gamma}} = \boldsymbol{\Lambda}_0^{-1/2}\boldsymbol{F}^{\mathsf{H}}\boldsymbol{\Gamma}, \tag{3.63}$$
$$\tilde{\boldsymbol{y}} = \boldsymbol{\Lambda}_0^{-1/2}\boldsymbol{F}^{\mathsf{H}}\boldsymbol{y}, \tag{3.64}$$

   with $\boldsymbol{\Lambda}_0^{-1/2}\boldsymbol{F}^{\mathsf{H}}$ being a (a-priori known) square root of the matrix $\boldsymbol{B}$, and $\tilde{\boldsymbol{\Gamma}}^{\dagger}$ is the Moore-Penrose pseudo-inverse of $\tilde{\boldsymbol{\Gamma}}$. It must be emphasized that, with the preamble chosen as above, the matrix $\tilde{\boldsymbol{\Gamma}}^{\mathsf{H}}\tilde{\boldsymbol{\Gamma}}$ is diagonal and hence computing its inverse is straightforward. Eq. (3.61) can then be implemented as a matrix multiplication (requiring M^2 complex multiplications) with the matrix being *a-priori* known. Nevertheless, as shown below, when using the optimal preamble the estimator is amenable to considerable simplifications.

2. Observe that $\boldsymbol{d}$ in (3.60) is a multiple of the first column of the $\boldsymbol{F}$ matrix. Hence it is an eigenvector of all $\boldsymbol{G}_k$ matrices:

$$\boldsymbol{G}_k\boldsymbol{d} = \lambda_{k,1}\boldsymbol{d}$$

   where $\lambda_{0,1} = 1$. It then turns out that

$$\tilde{\boldsymbol{\Gamma}} = \sqrt{\mathcal{E}}\boldsymbol{\Lambda}_0^{-1/2}\begin{bmatrix}\boldsymbol{L}_1\\ \mathbf{0}\end{bmatrix}$$

   where $\boldsymbol{L}_1 = \mathrm{diag}(\lambda_{0,1}, \lambda_{1,1}, \ldots, \lambda_{L_h-1,1})$. Finally, the estimator in (3.61) becomes

$$\hat{\boldsymbol{h}} = \frac{1}{\sqrt{\mathcal{E}}}\boldsymbol{L}_1^{-1}\begin{bmatrix}\boldsymbol{I}_{L_h} & \mathbf{0}\end{bmatrix}\boldsymbol{F}^{\mathsf{H}}\boldsymbol{y} \tag{3.65}$$

   The latter expression leads us to the following simple computational procedure for implementing the estimator:

   i) Take the *first* L_h terms of $\mathrm{IDFT}(\boldsymbol{y})$:[4]

$$\boldsymbol{x} = \begin{bmatrix}\boldsymbol{I}_{L_h} & \mathbf{0}\end{bmatrix}\boldsymbol{F}^{\mathsf{H}}\boldsymbol{y}$$

[4] Could be implemented via *partial IFFT*.

ii) Divide by the diagonal entries of $\boldsymbol{L}_1$ and normalize:

$$\hat{\boldsymbol{h}} = \frac{1}{\sqrt{\mathcal{E}}}\boldsymbol{x} \oslash \mathrm{diag}(\boldsymbol{L}_1)$$

In its straightforward implementation, the above procedure requires around $\frac{M}{2}\log_M + L_h$ multiplications. It is of interest to observe that $\mathrm{IDFT}(\boldsymbol{y})$ may also be directly found from the (polyphase) filter bank structure (see, e.g., [56, Fig. 4]) and hence its first L_h entries can be made available at no cost. The computational cost of the estimator is then proportional to L_h.

3. Observe that $\left[\begin{array}{cc} \boldsymbol{I}_{L_h} & \boldsymbol{0} \end{array}\right] \boldsymbol{F}^{\mathsf{H}} = \boldsymbol{F}(:, 1:L_h)^{\mathsf{H}}$ and note that the M-point CFR is related to $\boldsymbol{h}$ as

$$\boldsymbol{H} = \sqrt{M}\boldsymbol{F}(:, 1:L_h)\boldsymbol{h}$$

4. One can come up with a procedure analogous to the above for the general (possibly complex valued) optimal preamble in (3.58). Then instead of the eigenvalues $\lambda_{k,1}$, the ith eigenvalues of the $\boldsymbol{G}_k$ matrices would be involved.

3.3.2.2 Sparse preamble

In a sparse preamble, only the symbols loaded on a set of isolated (surrounded by nulls) subcarriers are nonzeros. Clearly, to estimate L_h parameters, at least an equal number of equations are needed. Hence, for economy and to simplify the presentation, it will be assumed that there are no more than L_h pilot tones, indexed as $\mathcal{P} = \{p_1, p_2, \ldots, p_{L_h}\} \subset \{0, 1, \ldots, M-1\}$. L_h is either the channel length or an upper bound thereof. Moreover, for the sake of the simplicity and without loss of generality, it will be assumed that $\frac{M}{L_h}$ is an integer. The preamble design problem then consists of

(a) finding the right places for the pilot tones, and

(b) choosing the values for the pilot symbols.

Let $\boldsymbol{d}_{\mathcal{P}} = \left[\begin{array}{cccc} d_{p_1} & d_{p_2} & \cdots & d_{p_{L_h}} \end{array}\right]^{\mathrm{T}}$ be the vector of pilots loaded on the pilot subcarriers. The optimal solution is given by *equipowered and equispaced* pilot tones, with

$$|d_{p_i}| = \sqrt{\frac{\mathcal{E}}{L_h}}, \quad i = 1, 2, \ldots, L_h \tag{3.66}$$

and

$$p_i = p_0 + (i-1)\frac{M}{L_h}, \quad i = 1, 2, \ldots, L_h \tag{3.67}$$

with p_0 freely chosen. For example, $p_0 = 0$ if subcarrier no. 0 is to be a pilot tone. The resulting MSE is given by

$$\mathrm{MSE} = \sigma^2 \sum_{k=0}^{L_h-1} \frac{1}{\alpha_k^2 \mathcal{E}} = \frac{\frac{1}{L_h}\left(1 + \sum_{k=1}^{L_h-1} \frac{1}{\alpha_k^2}\right)}{\mathrm{SNR}_{\mathrm{sbc}}} \tag{3.68}$$

with

$$\alpha_k = \sum_{l=k}^{L_g-1} g(l-k)g(l), \quad \text{for } k = 0, 1, \ldots, L_h - 1 \tag{3.69}$$

being the lag-k autocorrelation of g (decreasing with k) and $\alpha_0 = 1$, while $\mathrm{SNR}_{\mathrm{sbc}} = \frac{\mathcal{E}/L_h}{\sigma^2}$ denotes the per-subcarrier SNR.

Remarks.

1. Eq. (3.51) is now written as

$$\hat{\boldsymbol{h}} = \left(\boldsymbol{\Gamma}_{\mathcal{P}}^{\mathsf{H}}\boldsymbol{\Gamma}_{\mathcal{P}}\right)^{-1}\boldsymbol{\Gamma}_{\mathcal{P}}^{\mathsf{H}}\boldsymbol{y}_{\mathcal{P}} = \boldsymbol{\Gamma}_{\mathcal{P}}^{-1}\boldsymbol{y}_{\mathcal{P}} \tag{3.70}$$

   where $\boldsymbol{\Gamma}_{\mathcal{P}}$ is the $L_h \times L_h$ matrix resulting if we keep from $\boldsymbol{\Gamma}$ only its rows and columns corresponding to the pilot subcarrier indexes, and similarly for $\boldsymbol{y}_{\mathcal{P}}$. Obviously, its inverse, $\boldsymbol{\Gamma}_{\mathcal{P}}^{-1}$, can be computed *offline*. The above computation then requires L_h^2 complex multiplications. More on this will be presented in the next section, where sparse solutions for the CIR will be sought.

2. An alternative computational procedure, which resembles more the one usually employed in CP-OFDM, is described below. For the sake of the simplicity and without loss of generality, let $p_1 = 0$. Then $p_i = (i-1)\frac{M}{L_h}$, $i = 1, 2, \ldots, L_h$. Define $\boldsymbol{H}_{\boldsymbol{\alpha}} = \left[\begin{array}{cccc} H_{\boldsymbol{\alpha}}(0) & H_{\boldsymbol{\alpha}}(1) & \cdots & H_{\boldsymbol{\alpha}}(L_h-1)\end{array}\right]^{\mathrm{T}}$ as the L_h-point DFT of the impulse response weighted (or windowed) by the α_k's:

$$H_{\boldsymbol{\alpha}}(l) = \sum_{k=0}^{L_h-1} \alpha_k h(k) e^{-\jmath k l \frac{2\pi}{L_h}}, \quad l = 0, 1, \ldots, L_h - 1$$

   with $\boldsymbol{\alpha} = \left[\begin{array}{cccc} \alpha_0 & \alpha_1 & \cdots & \alpha_{L_h-1}\end{array}\right]^{\mathrm{T}}$ (cf. (3.69)). Then one can also implement (3.70) as follows:

   (a) Compute the "windowed" CFR vector first:

$$\hat{\boldsymbol{H}}_{\boldsymbol{\alpha}} = \boldsymbol{y}_{\mathcal{P}} \oslash \boldsymbol{d}_{\mathcal{P}} \tag{3.71}$$

   (b) Compute the "windowed" impulse response via IFFT and divide by the weights α_k's to arrive at the CIR estimate:

$$\hat{\boldsymbol{h}} = \mathrm{IDFT}(\hat{\boldsymbol{H}}_{\boldsymbol{\alpha}}) \oslash \boldsymbol{\alpha} \tag{3.72}$$

   This alternative procedure costs $\frac{L_h}{2}\log_2 L_h$ multiplications for the IFFT, L_h complex divisions (nevertheless amenable to simplification) for (3.71), and $2(L_h - 1)$ real divisions for (3.72).

3.3.3 Simulation Results

3.3.3.1 Full Preambles

Examples of the performance of the TD method with full preambles are shown in Fig. 3-10. Real pilots are employed for the proposed estimator and, in addition to the optimal ones derived above, pseudorandom (equipowered) pilots are also tested for the sake of comparison. Filter banks designed as in [8] were employed. A subcarrier spacing of 15 kHz (as is a common choice in LTE) was considered. Two examples corresponding to channels with relatively low and high frequency selectivity are provided. The normalized MSE (NMSE), $E(\|\boldsymbol{H} - \hat{\boldsymbol{H}}\|^2/\|\boldsymbol{H}\|^2)$, is

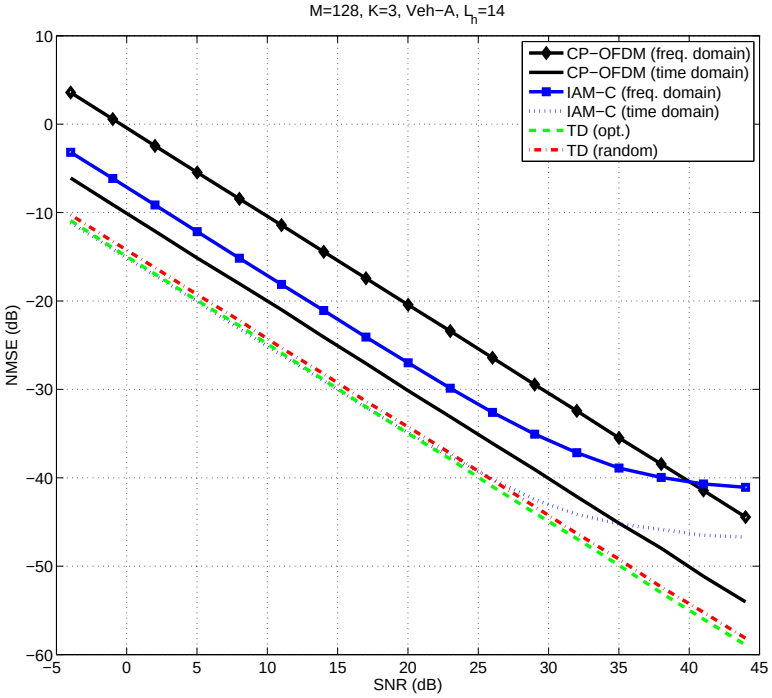

(a)

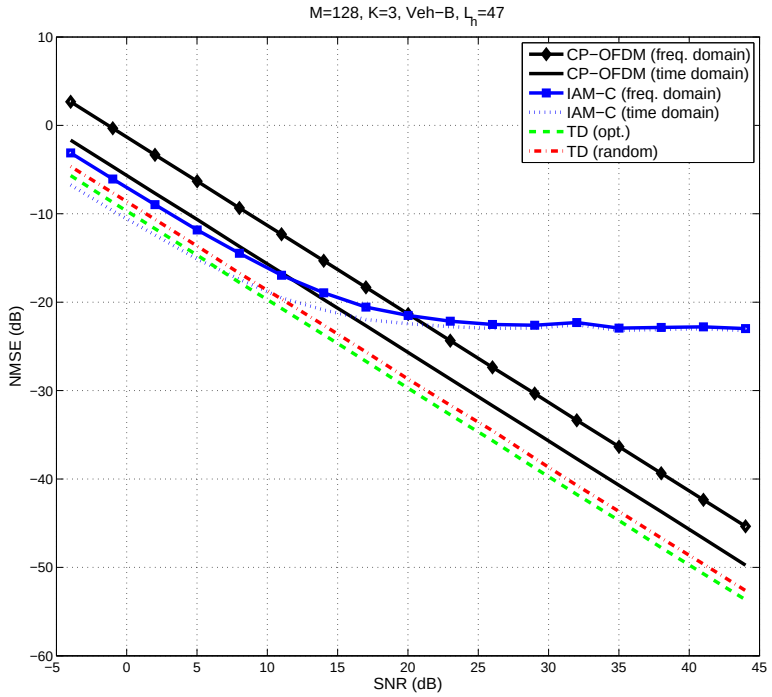

(b)

Figure 3-10: MSE performance of the methods under study for channels of (a) medium and (b) high frequency selectivity.

plotted versus the SNR. Due to its optimality among the preambles of the given structure for channels of low delay spread, the IAM-C method is employed as a benchmark representative of

the methods assuming flat subchannels [41]. CP-OFDM is also included in the comparison. The CP used was the shortest possible that ensures zero ICI and ISI, namely equal to the channel order. For CP-OFDM, the full preamble is optimally chosen as one of the columns of the DFT matrix, as suggested by [36]. For IAM-C, the preamble is as recalled above and explained in [35]. For a fair comparison, the SFB output training signals for the FBMC/OQAM methods were scaled so as to have the same power with that of CP-OFDM. For the sake of the completeness of the comparison, and to demonstrate the effect of the channel length knowledge, the frequency-domain methods (i.e., IAM-C and CP-OFDM) are also enriched with a DFT-interpolation step. This consists of filtering the CFR estimates through taking the inverse DFT and truncating it to the assumed known length L_h (see [13, 18, 37]). These variations will be henceforth called "time domain", to distinguish them from the "frequency domain" estimation methods.

The method developed above is seen to outperform IAM-C in both cases and as expected does not exhibit the well known error floors at high SNR values. The gain from the use of the proposed preamble design over a pseudorandom one is evident, though not considerable in these examples. Nevertheless, a pseudo-random preamble was seen to be useless with very long channels ($L_h \approx M$) in [40] as it then induces ill conditioning for the matrix of (3.51), in contrast to the optimal preamble that still yields a good performance. A more carefull look however shows that the method performs slightly worse than IAM-C at low SNRs, especially in Fig. 3-10(b). Notice that IAM-C has already shown advantage at low SNRs over methods relying on less inaccurate assumptions than itself [35]. This is due to the strong noise attenuation achieved by its maximized "pseudo-pilots" in noise-(not interfence-) limited regimes. Concluding, it must be emphasized that the good performance attained by the proposed method is achieved with only *one* pilot (nonzero) FBMC symbol (accompanied by 2–3 guards as shown in the sequel), implying considerable savings in bandwidth and computational cost as well as increased robustness to channel time variations compared to the estimators that rely on much longer training sequences.

Remarks

1. Note that the improvement from following a time-domain approach over a frequency domain approach is diminishing as the channel length increases with respect to M. This should be expected in view of results reported in [21, 13] on the MSEs for CFR estimation achieved through time-domain and frequency domain approaches in CP-OFDM.[5] Namely, the time domain approach is better by a factor of $\frac{L_h}{M}$ (i.e., MSE lower by $10\log_{10}\frac{M}{L_h}$ dB). This can be verified in the above figures. The two approaches result in the same MSE at the extreme case $L_h = M$. Similar results are seen to hold for IAM-C. Specifically, as shown in [36], the DFT interpolation (i.e., projection onto the space of L_h-long channels), referred to as "time domain" approach, improves the MSE of IAM by $10\log_{10}\left(\frac{M}{L_h}\frac{1}{1+2\beta}\right)$ dB. This improvement can be observed in the figures, particularly in the medium frequency selective channel case (a) (where the assumptions leading to the results of [36] are not too far from reality). However, in the high frequency selective case, the "frequency domain" and "time domain" curves almost coincide, as expected. Most importantly, the IAM-C method fails and starts to floor at SNRs above 10 dB. In contrast, the TD method works as before, still completely avoiding the error floor effect.

2. Another way to *smooth* the obtained CFR values estimates besides the DFT interpolation tested above is suggested in [37] and relies again on the assumption of the CFR being locally constant, i.e., that $H(m)$ is (almost) invariant over a certain interval around the

[5] In fact, what we call here "time domain" approach is the estimator C studied in [21].

mth subcarrier frequency. This is the basic assumption underlying IAM methods and is another way to say that the channel coherence bandwidth is large compared to the subcarrier spacing. The shortest such interval, namely the one covering the immediate neighbors in the subcarrier domain, will be assumed here. One can then write, for the mth subcarrier,

$$\hat{H}(p) = H(m) + \frac{\eta_{p,0}}{c_p}, \quad \text{for } p \in \{m-1, m, m+1\}$$

or

$$\hat{\boldsymbol{H}}_m = H(m)\mathbf{1}_3 + \boldsymbol{T}_m^{-1}\boldsymbol{\eta}_m \tag{3.73}$$

with

$$\hat{\boldsymbol{H}}_m = \begin{bmatrix} \hat{H}(m-1) & \hat{H}(m) & \hat{H}(m+1) \end{bmatrix}^{\mathrm{T}}$$

and

$$\boldsymbol{T}_m = \mathrm{diag}(\boldsymbol{c}_m)$$

where

$$\boldsymbol{c}_m = \begin{bmatrix} c_{m-1} & c_m & c_{m+1} \end{bmatrix}^{\mathrm{T}},$$

c_p being the pseudo-pilot at subcarrier p. The *best linear unbiased estimate (BLUE)* of $H(m)$ based on these "data" is then given by [38]

$$\hat{\hat{H}}(m) = \frac{\mathbf{1}_3^{\mathrm{T}}\boldsymbol{C}_m^{-1}\hat{\boldsymbol{H}}_m}{\mathbf{1}_3^{\mathrm{T}}\boldsymbol{C}_m^{-1}\mathbf{1}_3}$$

with

$$\boldsymbol{C}_m = \boldsymbol{T}_m^{-1}\boldsymbol{C}_{\boldsymbol{\eta}_m}\boldsymbol{T}_m^{-\mathsf{H}}$$

being the covariance of the estimation error in (3.73). Clearly,

$$\boldsymbol{C}_m^{-1} = \frac{1}{\sigma^2}\boldsymbol{T}_m^{\mathsf{H}}\boldsymbol{B}^{-1}(m-1:m+1, m-1:m+1)\boldsymbol{T}_m$$

where

$$\boldsymbol{B}(m-1:m+1, m-1:m+1) = \begin{bmatrix} 1 & \jmath\beta & 0 \\ -\jmath\beta & 1 & \jmath\beta \\ 0 & -\jmath\beta & 1 \end{bmatrix} \equiv \boldsymbol{B}_3$$

Finally:

$$\hat{\hat{H}}(m) = \frac{\boldsymbol{c}_m^{\mathsf{H}}\boldsymbol{B}_3^{-1}(\boldsymbol{c}_m \odot \hat{\boldsymbol{H}}_m)}{\boldsymbol{c}_m^{\mathsf{H}}\boldsymbol{B}_3^{-1}\boldsymbol{c}_m} \tag{3.74}$$

This estimator is also derived in [37], yet without the correlation of the noise components among subcarriers taken into account. The result is (3.74) with $\boldsymbol{B}_3^{-1}$ replaced by the identity matrix and is given by [37, eq. (5)]

$$\hat{\hat{H}}(m) = \frac{\sum_{p=m-1}^{m+1}|c_p|^2\hat{H}(p)}{\sum_{p=m-1}^{m+1}|c_p|^2} \tag{3.75}$$

The filtering defined in (3.74) was applied in a low dispersion scenario and the result is shown in Fig. 3-11. The filter of (3.75) was also tested and gave similar results. Observe

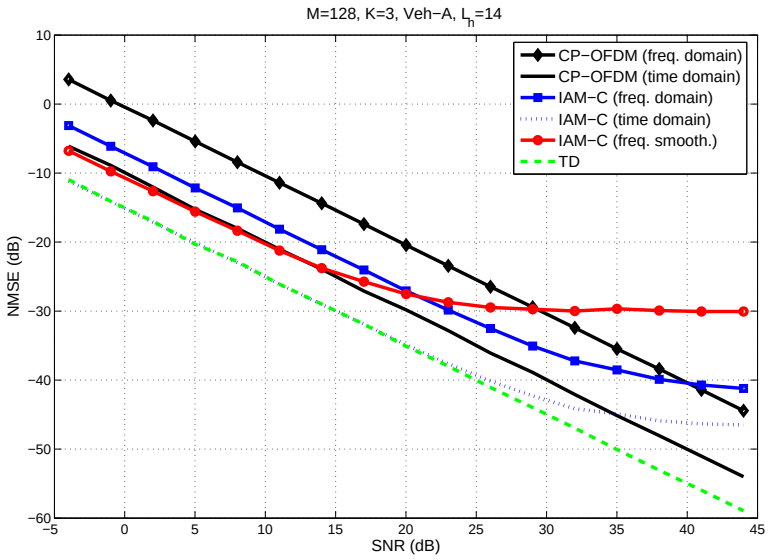

Figure 3-11: MSE performance of the studied methods including IAM-C with BLUE frequency smoothing (see eq. (3.74)).

that frequency smoothing offers a significant improvement in estimation accuracy at low to medium SNRs. However, at higher SNRs, the error floor is now more severe than before, due to the failure of the assumption of equal $H(p)$ for $p = m - 1$ to $m + 1$. To cope with this, a windowing that weighs more the central frequency of the frequencies involved can be applied here as well, in accordance to [37, eq. (8)]. This modification can provide more accurate estimates, particularly if the unbiasedness constraint is relaxed [37].

3. It is of interest to have a look at the shape of the modulated preambles used above. These are shown in Fig. 3-12, where a scaling as described previously has been incorporated. It should not be surprising that all signals have an impulse-like appearance (cf. [41]). Simple modifications to these optimal preambles that could mitigate a possibly high peak to average power ratio (PAPR) problem can be envisaged, e.g., in line with [34].

3.3.3.2 Sparse Preambles

Two illustrative examples of the MSE performance of the above method are given in Fig. 3-13, for channels of low and high frequency selectivity. Again, the NMSE is shown as a function of SNR. $N_p = 16$ and 64 pilot tones were used, respectively. IAM employed equispaced and equipowered pilots as suggested in [36]. The knowledge of the channel length was made use of via a DFT interpolation of the estimated CFR values. For CP-OFDM, equispaced and equal pilots were used in the preamble, in accordance with the results of [36]. Again, appropriate scaling was applied to ensure the transmit powers are the same for all methods. Observe how the TD method developed here is freed of the error floor effect present in the IAM method. The latter is more severe for more frequency selective channels (where the flat subchannels assumption is far from being met) as seen in Fig. 3-13(b). Notice, however, that, for low to medium SNR values and in Fig. 3-13(b), TD is slightly outperformed by IAM.

To show the effect of underestimating the length of the CIR (and hence the number of subcarriers that need to carry pilots), an example is provided in Fig. 3-14. Comparing with Fig. 3-13(b), one can observe that under these conditions TD performs quite similarly with

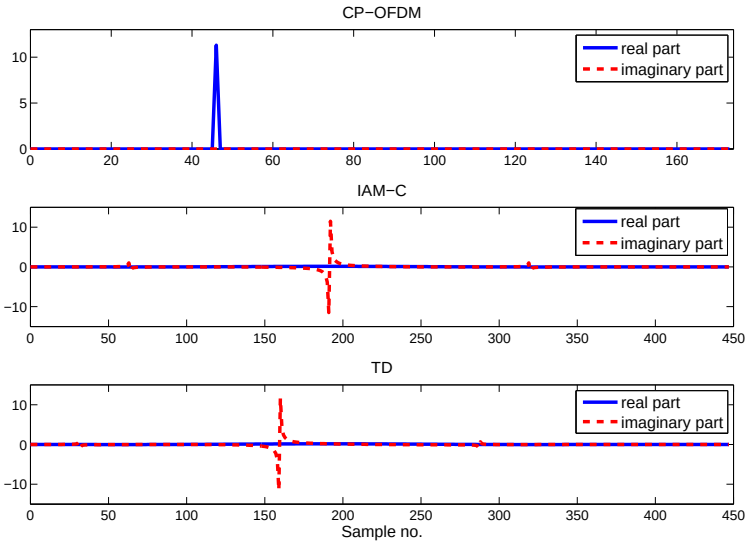

Figure 3-12: SFB outputs for the optimal preambles in (a) CP-OFDM, (b) IAM-C, and (c) TD. Filter bank parameters are as in Fig. 3-10.

IAM while it outperforms both IAM and CP-OFDM at higher SNR values. One can conclude from this example that, although TD's performance is degraded in the presence of channel undermodeling, it generally gets no worse than that of the other methods, particularly at low to medium SNRs. More about this question will be discussed in the next subsection, on sparsity awareness.

3.3.3.3 What about interference from data symbols?

The previous results assume that the zero FBMC symbol following the pilots is sufficient to protect them from the interference of the data[6] symbols following the preamble in the transmitted frame. However, as also seen elsewhere (e.g., [41]), this is not exactly true and some nonnegligible interference from the data is suffered. A way to overcome this is to boost the pilots over the data. Nevertheless, to come up with an efficient transmission scheme, special care is needed to be taken to cope with this undesired interference. This may involve some more guard FBMC symbols, more than one. To have an idea of the effect the data may have on the estimation performance of the methods considered above, a related example is shown in Fig. 3-15(a), where a single guard is used. Observe that even though TD suffers a considerable performance deterioration under these conditions, it still performs much better than the time-domain IAM-C. The performance gain is higher at the weak noise (hence interference-limited) regime. Nevertheless, as it was also observed in the previous sections, the corresponding differences in BER are not that significant. This can be seen in Fig. 3-15(b), where the performances of per-subchannel zero forcing (ZF) equalizers with QPSK data are shown. The frequency sampling-based 3-taps ZF equalizers of [32] were employed for FBMC. To verify the close to optimal BER performance for the TD-based equalizer, the case of perfect channel information (PCI) was also included.

Adding more guard symbols can considerably ameliorate the results. With these filter bank parameters, Fig. 3-16 shows that three guard FBMC symbols are sufficient for an interference-free result. This amounts to a preamble of length equal to two OFDM symbols. To be

[6] In fact, they may be control information.

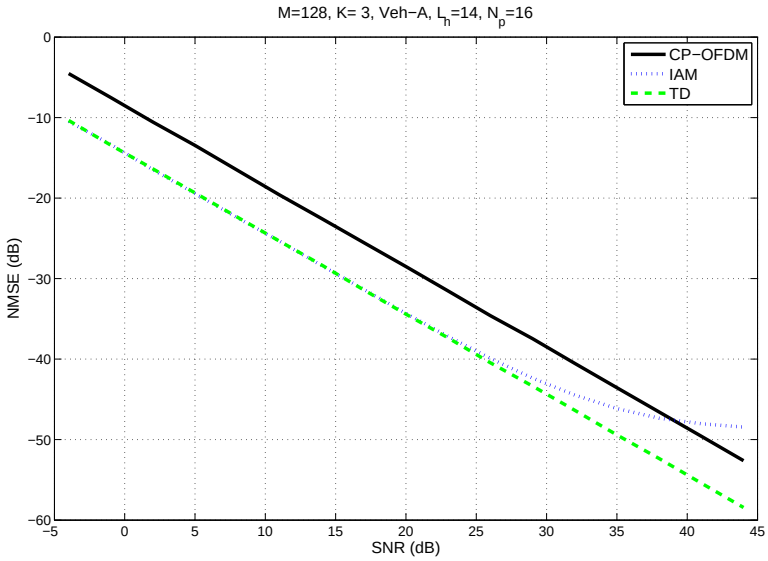

(a)

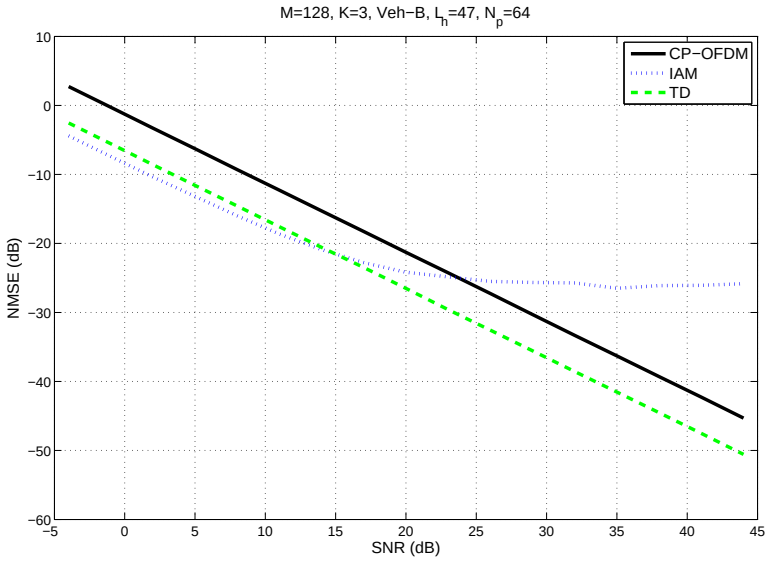

(b)

Figure 3-13: MSE performance of the methods under study, with optimal sparse preambles, for channels of (a) low and (b) high frequency selectivity.

fair in comparing the methods, an equally long preamble was used in IAM-C and CP-OFDM, with the channel estimate in CP-OFDM computed as an average of the estimates yielded by the two symbols [60]. The error floor in BER observed in this and the previous example for FBMC/OQAM and at high E_{b}/N_0 values can be attributed first to the residual intercarrier interference (due to performing equalization per subcarrier only) and second to the limited length of the equalizer. More complex equalizers could be used, however the aim here was to illustrate the detection performance obtained in a simple setup.

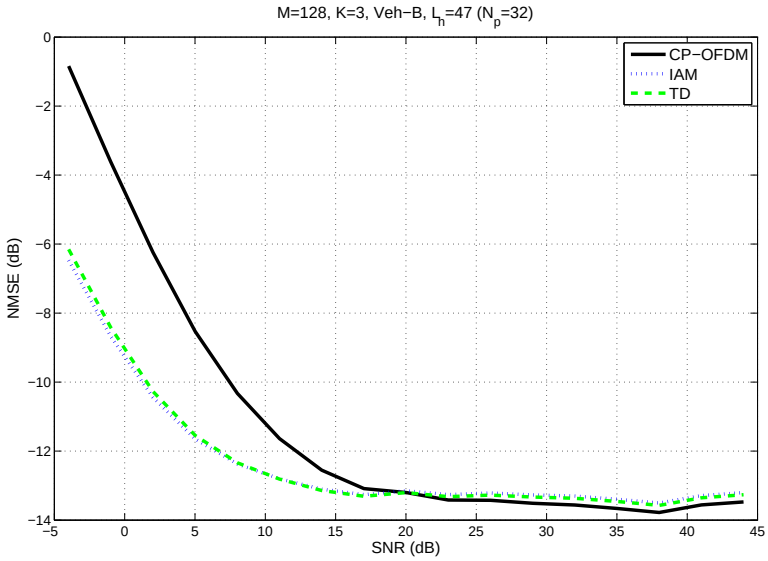

Figure 3-14: As in Fig. 3-13(b), with underestimated channel length.

3.3.4 Sparsity-Aware Techniques

Wireless channels tend to exhibit a *sparse* multipath structure in practice, particularly in high data rate transmissions [2]. Thus, their CIRs tend to be dominated by a relatively small number of clusters of significant paths. Moreover, sparsity can be in both the delay and the Doppler dimension [58]. An example of delay sparsity is depicted in Fig. 3-17. Only six of its 47 taps are nonnegligible. This is *not* a strictly sparse CIR. This is the case in practice for *non-sample spaced* channels (due to inter-path interference). In the sparse signals terminology, these CIRs are known as *compressible*. This special structure of the channel can be exploited in developing channel estimation techniques with improved performance and/or reducing the training resources required, such as bandwidth (number of pilots and/or observations) and power. A large number of algorithms for sparse/compressible channels can be found in the literature referring to a general or a multicarrier context (e.g., [14, 51, 73, 9, 58, 67, 45, 50, 19] to name but a few). More recent ones typically rely on the so-called *Compressive Sensing (CS)* idea [17]. Put in simple terms, and in the context of interest here, CS aims at recovering the unknown $\boldsymbol{h}$ based on a limited (*compressive*) number of *appropriately* taken measurements (*sensing*) of the channel [16]. The central assumption that permits this is that the channel is (sufficiently) sparse (or compressible) (plus, of course, some requirements on the sensing matrix, that are often too hard to check). CS-induced guidelines for pilot selection and placement in OFDM systems are quite simple and generally comprise pseudo-random selection of both their values and places [2]. Recently, analogous results were reported for filter bank-based multicarrier (not of the FBMC/OQAM type) systems as well [58].

3.3.4.1 Sparsity-aware TD

In this subsection, sparsity-aware techniques will first be studied for preamble-based channel estimation of the sparse type and consist of simple modifications of schemes presented above for time domain channel estimation. The number of pilot tones will be assumed to be not smaller than the length of the channel. An illustrative example of the gains achievable when CIR sparsity is exploited is shown in Fig. 3-18. The experiments were for VehB channels. The

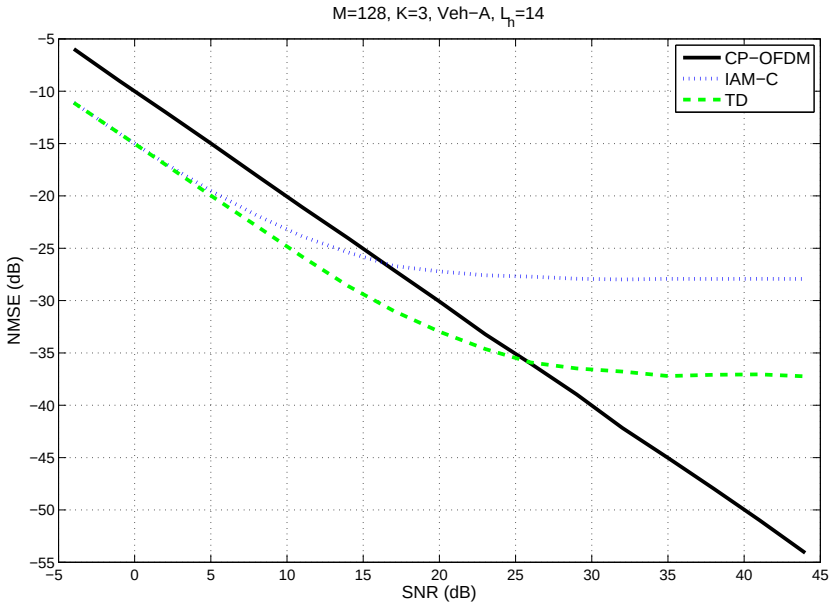

(a)

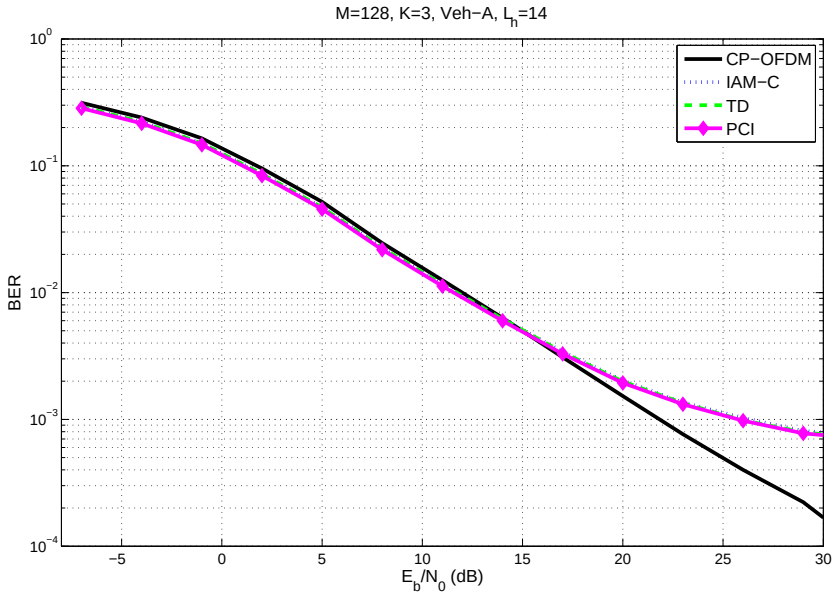

(b)

Figure 3-15: As in Fig. 3-10(a), but with the preamble followed by data symbols. (a) NMSE; (b) BER.

sparse preambles for CP-OFDM and TD are built in the corresponding optimal ways as above. Half of the subcarriers carry pilots. (This is a quite dense "sparse" preamble.) Both CP-OFDM and TD assume this (=64) to be the length of the channel. In addition to the (time domain) CP-OFDM and FBMC *unstructured* [12] channel estimation techniques described previously, we consider two modified versions in which sparsity plays a role. The first one, called *sparse LS (SpLS)* [14, 12], assumes a certain number, L, of nonzero taps ($= 64/2 = 32$ in this example) for the CIR and, after detecting their position in its LS estimate, it re-solves the LS problem for these particular coefficients. Variations of this approach exist that, instead of assuming a

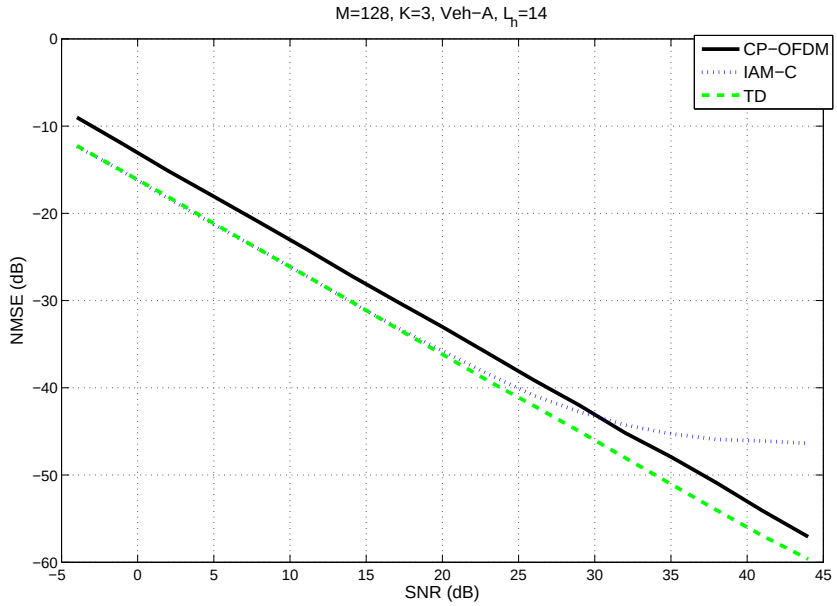

(a)

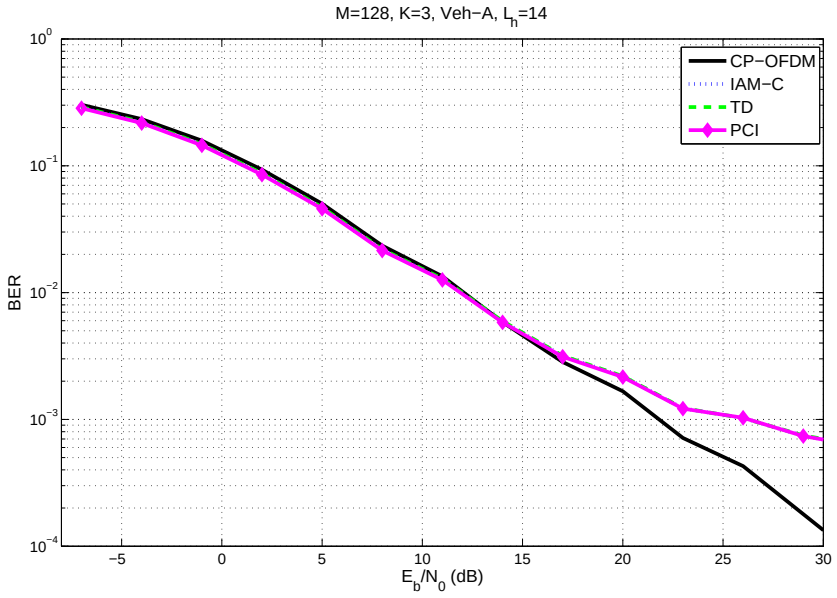

(b)

Figure 3-16: As in Fig. 3-15, but with 3 guard FBMC symbols. (a) NMSE; (b) BER.

sparsity level for $\boldsymbol{h}$, focus on those taps whose coefficients exceed a certain (pre-set) threshold. Alternatively, L is first estimated through some order selection criterion (e.g., [51]).

The second modification consists of applying some existing algorithm from the CS set of tools to recover the sparse CIR. In view of their (conceptual and implementation) simplicity, the so-called *greedy* algorithms were adopted in our experiments. A high performance yet simple member of this class, the *Orthogonal Matching Pursuit (OMP)* [61, 59], was used in the experiment of Fig. 3-18. Being a greedy algorithm, OMP gradually determines the *support* of $\boldsymbol{h}$, that is, the taps that deserve to be kept as nonzero. It must be emphasized that the OMP employed here does *not* assume any estimate for L and it only relies on an upper bound on the

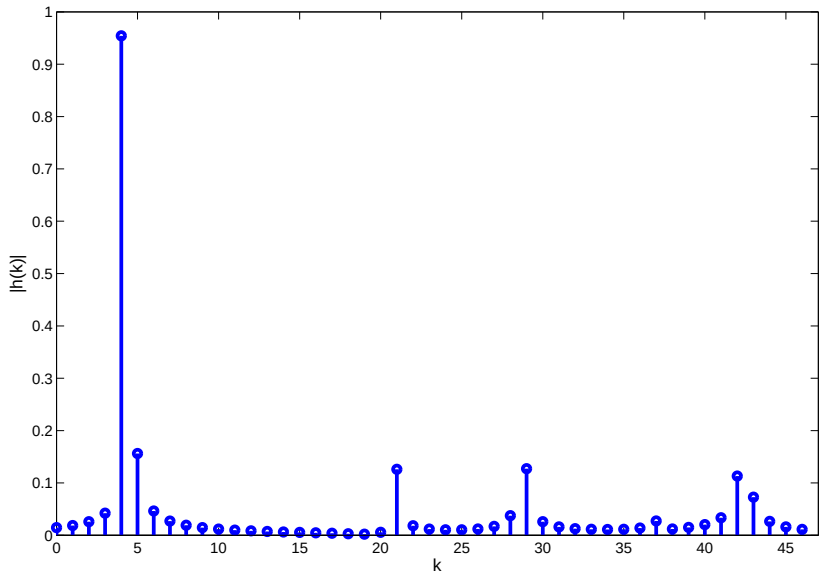

Figure 3-17: Impulse response of a sparse channel (magnitude).

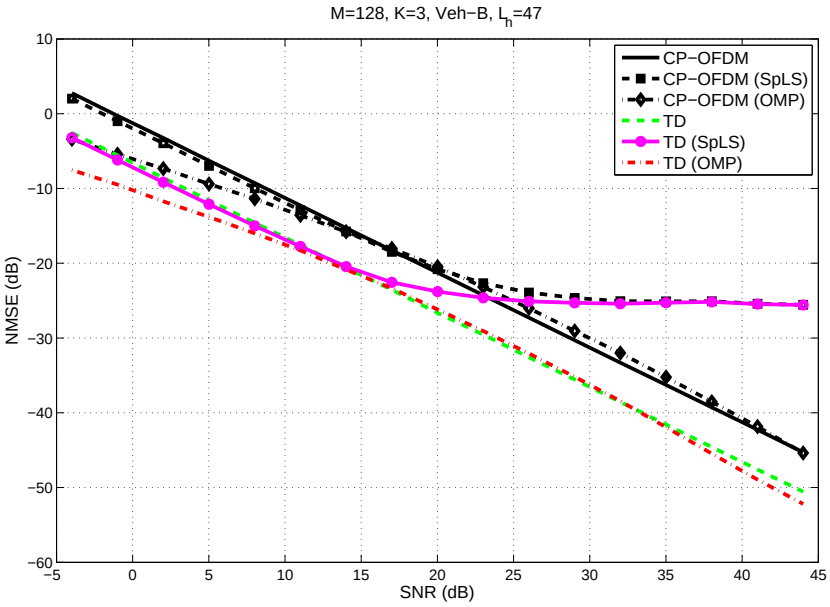

Figure 3-18: Comparison of time-domain methods, for sparse channel impulse responses.

magnitude of the MSE for its convergence. The latter was set based on a-priori knowledge of the noise power. Other, more sophisticated versions, requiring even less information from the user could also be employed.

Fig. 3-18 shows a considerable gain in MSE performance from the use of the OMP-based techniques but only at sufficiently low SNRs. Thus, TD with OMP is better than simple TD by about 4 dBs at an SNR of 0 dB. Much more significant improvements and over the whole range of SNRs have been observed for strictly sparse (*sample spaced*) channels. It is of interest to also see the results from the sparsity-aware techniques when nonnegligible interference from

data is present. Such an example is depicted in Fig. 3-19, whose experimental setup is otherwise as in the previous figure. Notice how the OMP-based TD method is now offering noticeable

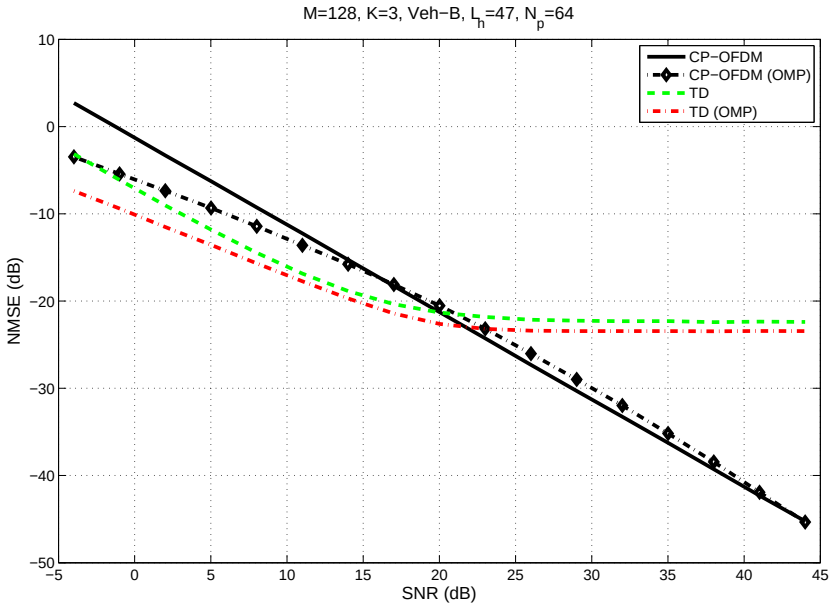

Figure 3-19: As in Fig. 3-18, with interference from data.

improvement (again, considerable at low SNRs) over the entire SNR range considered. These examples confirm that the sparsity of the CIR is worth being considered in its estimation, and demonstrates that simple sparsity-aware modifications to the existing algorithms can bring significant performance improvement.

3.3.5 Parametric channel estimation: A MUSIC-LS approach

Another class of channel estimation techniques of interest that have been applied in OFDM and take the CIR sparsity into account are those relying on the path-delay parametrization of the channel. Their value is found at the explicit incorporation of the channel parameterization in the estimation algorithm and can be referred with the name of *parametric* methods (e.g., [69]). One technique of this kind was studied in this project and presented here. It will be shown to be well suited for the highly frequency selective scenarios considered.

First, the subchannel frequency selectivity is described by a polynomial (Taylor) model. This, along with the standard path-delay model for the channel, results in a formulation of the problem that is reminiscent of an array processing problem, with the delays playing the roles of directions of arrivals. A subspace-based algorithm, based on MUSIC, is then developed for estimating the delays. The estimation of the path gains is then made easy and can be performed either in the LS or (if statistical information is available) the MMSE sense. The simulation results demonstrate a very important performance improvement over both IAM-based methods and corresponding CP-OFDM schemes. Estimating the number of paths is an important problem in this type of algorithms. A recently reported criterion will be shown to yield quite satisfying results in this respect.

The (continuous-time) channel $h(t)$ is assumed to follow the model

$$h(t) = \sum_{l=1}^{L} \rho_l \, \delta(t - \tau_l), \tag{3.76}$$

involving L paths, whose complex gains are ρ_l and whose associated (relative) delays are τ_l, $l = 1, 2, \ldots, L$. In frequency, the channel is then described by

$$H(f) = \sum_{l=1}^{L} \rho_l \, e^{-\jmath 2\pi f \tau_l} \tag{3.77}$$

Approximating $H(f)$ by a Taylor polynomial of order R around the frequency of the pth subcarrier, f_p, the output of the AFB at the FT point (p, q) can be written as

$$y_{p,q} = \sum_{r=0}^{R} H_p^{(r)} \, m_{p,q}^{(r)} + \eta_{p,q} \tag{3.78}$$

with the quantities $m_{p,q}$ only depending on the prototype filter used and the transmitted data around the considered FT point. By $H_p^{(r)}$, we denote the rth-order derivative of $H(f)$ at f_p. In view of (3.77), this equation can be employed for estimating the channel parameters. For a more compact expression:

$$y_{p,q} = \boldsymbol{M}_{p,q}^{\mathrm{T}} \cdot \boldsymbol{H}_p(\boldsymbol{\tau}, \boldsymbol{\rho}) + \eta_{p,q} \tag{3.79}$$

where

$$\boldsymbol{M}_{p,q} = \left[\begin{array}{cccc} m_{p,q}^{(0)} & m_{p,q}^{(1)} & \ldots & m_{p,q}^{(R)} \end{array} \right]^{\mathrm{T}} \tag{3.80}$$

$$\boldsymbol{H}_p(\boldsymbol{\tau}, \boldsymbol{\rho}) = \left[\begin{array}{cccc} H_p^{(0)} & H_p^{(1)} & \ldots & H_p^{(R)} \end{array} \right]^{\mathrm{T}} \tag{3.81}$$

$$\tag{3.82}$$

and

$$\boldsymbol{\tau} = \left[\begin{array}{cccc} \tau_1 & \tau_2 & \ldots & \tau_L \end{array} \right]^{\mathrm{T}},$$

$$\boldsymbol{\rho} = \left[\begin{array}{cccc} \rho_1 & \rho_2 & \ldots & \rho_L \end{array} \right]^{\mathrm{T}}$$

Let us consider the following sequence of observation vectors

$$\boldsymbol{y}_p(l) = \left[\begin{array}{c} y_{p+2(l-1),q} \\ y_{p+2(l-1)+1,q} \\ \vdots \\ y_{p+2(l-1)+(N_c-1),q} \end{array} \right], \quad l = 1, 2, \ldots \tag{3.83}$$

Each one of them consists of the AFB outputs at N_c consecutive subcarriers at a given time instant q. The sequence (3.83) is built by sliding a conceptual rectangular window at the output of the AFB in "steps" of two subcarriers per slide. In other words, the first vector encompasses the outputs $y_{p,q}, y_{p+1,q}, \ldots, y_{p+(N_c-1),q}$, the second vector the outputs

$y_{p+2,q}, y_{p+3,q}, \ldots, y_{p+2+(N_c-1),q}$ and so on (p is the subcarrier index where the sliding process begins). It is straightforward to notice that vectors $\boldsymbol{y}_p(l)$ share elements with each other and that the sliding window approach is a means to augment the number of observations given the finite number of subcarriers M. This augmentation strategy is associated to *frequency smoothing*. Note that N_c should be chosen large enough so as to exceed L.

Each vector in the sequence can be written as

$$\boldsymbol{y}_p(l) = \boldsymbol{\mathcal{A}}_p \boldsymbol{\mathcal{D}}^{p+2(l-1)} \boldsymbol{\rho} + \boldsymbol{\eta}_p(l) \tag{3.84}$$

where $\boldsymbol{\eta}_p(l)$ is defined similarly with $\boldsymbol{y}_p(l)$. The involved quantities are defined as follows:

$$\begin{aligned} \boldsymbol{\mathcal{A}}_p &= \begin{bmatrix} \boldsymbol{M}^{\mathrm{T}}_{p+2(l-1),q} \boldsymbol{A}(\boldsymbol{\tau}) \\ \boldsymbol{M}^{\mathrm{T}}_{p+2(l-1)+1,q} \boldsymbol{A}(\boldsymbol{\tau}) \boldsymbol{D} \\ \vdots \\ \boldsymbol{M}^{\mathrm{T}}_{p+2(l-1)+(N_c-1),q} \boldsymbol{A}(\boldsymbol{\tau}) \boldsymbol{D}^{N_c-1} \end{bmatrix} \\ \boldsymbol{\mathcal{D}}^{p+2(l-1)} &= \mathrm{diag}(e^{-\jmath 2\pi f_{p+2(l-1)}\tau_1}, e^{-\jmath 2\pi f_{p+2(l-1)}\tau_2}, \ldots, e^{-\jmath 2\pi f_{p+2(l-1)}\tau_L}) \end{aligned}$$

with

$$\begin{aligned} \boldsymbol{D} &= \mathrm{diag}(e^{-\jmath 2\pi \Delta f \tau_1}, e^{-\jmath 2\pi \Delta f \tau_2}, \ldots, e^{-\jmath 2\pi \Delta f \tau_L}) \\ \boldsymbol{A}(\boldsymbol{\tau}) &= \begin{bmatrix} 1 & 1 & \ldots & 1 \\ -\tau_1 & -\tau_2 & \ldots & -\tau_L \\ \vdots & \vdots & \vdots & \vdots \\ \frac{(-\tau_1)^r}{r!} & \frac{(-\tau_2)^r}{r!} & \ldots & \frac{(-\tau_L)^r}{r!} \\ \vdots & \vdots & \vdots & \vdots \\ \frac{(-\tau_1)^R}{R!} & \frac{(-\tau_2)^R}{R!} & \ldots & \frac{(-\tau_L)^R}{R!} \end{bmatrix} \end{aligned}$$

Also, $f_{p+2(l-1)} = (p+2(l-1))\,\Delta f$, and Δf is the subcarrier spacing. The components of $\boldsymbol{\eta}_p(l)$ are typically correlated as we saw previously. However, since its statistics are *a priori* known, a noise pre-whitening can be performed to the above data in order to come up with .

Eq. (3.84) has the form of the input/output equations that describe direction of arrival estimation problems in the array processing literature [44]. The well known MUSIC algorithm [44] can thus be applied to estimate $\boldsymbol{\tau}$ provided the matrix $\boldsymbol{\mathcal{A}}_p$ does *not* depend on the observation index l. By revisiting the structure of the matrices constituent to this matrix, one concludes that a sufficient condition to achieve the sought after independence is the formation of $\boldsymbol{y}_p(l)$ by use of a window sliding at steps of 2 subcarriers, in conjunction with choosing the pilot FBMC symbol judiciously. Such a symbol could be, for example, one consisting of *all equal* pilots. First, a sample estimate of the data covariance, $\boldsymbol{C}_{\boldsymbol{y}} = E(\boldsymbol{y}_p(l)\boldsymbol{y}_p^{\mathsf{H}}(l))$, is needed. This can be computed as

$$\hat{\boldsymbol{C}}_{\boldsymbol{y}} = \frac{1}{l_{\max}} \sum_{l=1}^{l_{\max}} \boldsymbol{y}_p(l)\boldsymbol{y}_p^{\mathsf{H}}(l),$$

where $l_{\max}$ is the maximum value l can assume, given the finite number of available subcarriers M. Subsequently, the MUSIC spectrum is constructed and its peaks detected. The delays corresponding to the MUSIC spectrum peaks make up the estimated vector $\hat{\boldsymbol{\tau}}$.

Once the delays have been estimated, a LS estimator can be applied in (3.84) to compute $\hat{\boldsymbol{\rho}}$. It is worth noting that one could solve *multiple* LS problems, one for each of the available $\boldsymbol{y}_p(l)$, $l = 1, 2, \ldots, l_{\max}$ and then average over those findings (again a frequency smoothing). It is this way that we ran our experiments. The resulting algorithm, consisting of a MUSIC step to compute $\hat{\boldsymbol{\tau}}$ and LS to find $\hat{\boldsymbol{\rho}}$, will be referred to hereafter as the MUSIC-LS algorithm [26, 27, 29, 30].

An experimental validation of the MUSIC-LS performance is given in Fig. 3-20. The comparison includes the IAM-C method as well as its time-domain ("Smoothing") and frequency smoothed ("Averaging") variants. Most importantly, a MUSIC-LS algorithm for CP-OFDM is also tested, which was built following similar arguments and along the lines found in [69]. Classical LS for CP-OFDM is also included. The subcarrier spacing was again chosen in accordance with the common LTE recommendation, $\Delta f = 15$ kHz while sample spaced channels are assumed for illustration purposes. The Taylor expansion order is $R = 4$. It is also assumed that the number of channel paths is known. This assumption will be waived shortly. For a more

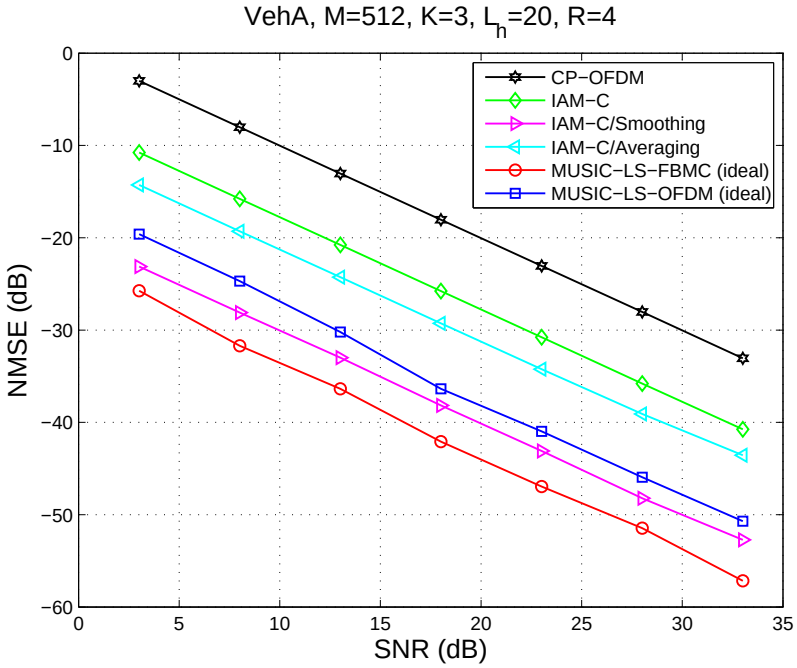

Figure 3-20: MSE performance of the methods under study for a VehA channel. Subchannel CFRs were approximated as polynomials of order $R = 4$.

frequency selective channel (VehB), the results are given in Fig. 3-21. In both cases, it is seen that MUSIC-LS for FBMC/OQAM outperforms all other methods. Among others, it performs better than its OFDM counterpart, showing the potential of the FBMC/OQAM paradigm. It is also observed that its gains over the IAM-C methods are greater, the higher the channel selectivity.

MUSIC-LS performance naturally depends on the order of the Taylor expansion employed. Fig. 3-22 exemplifies the effect of Taylor order R on algorithm performance. The results pertain to Veh-B derived channel realizations.

In a realistic scenario, the number of channel paths, $\hat{L}$, will be typically unknown and it will have to be estimated. This problem has been extensively studied in the literature and there are plenty of solution approaches reported. We here chose to follow a simple approach, namely

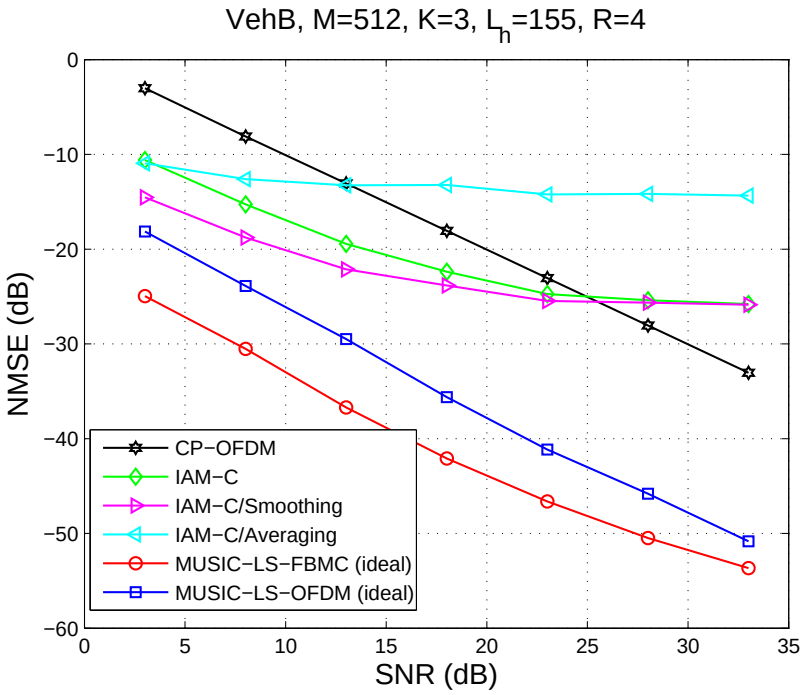

Figure 3-21: As in Fig. 3-20, with VehB channels.

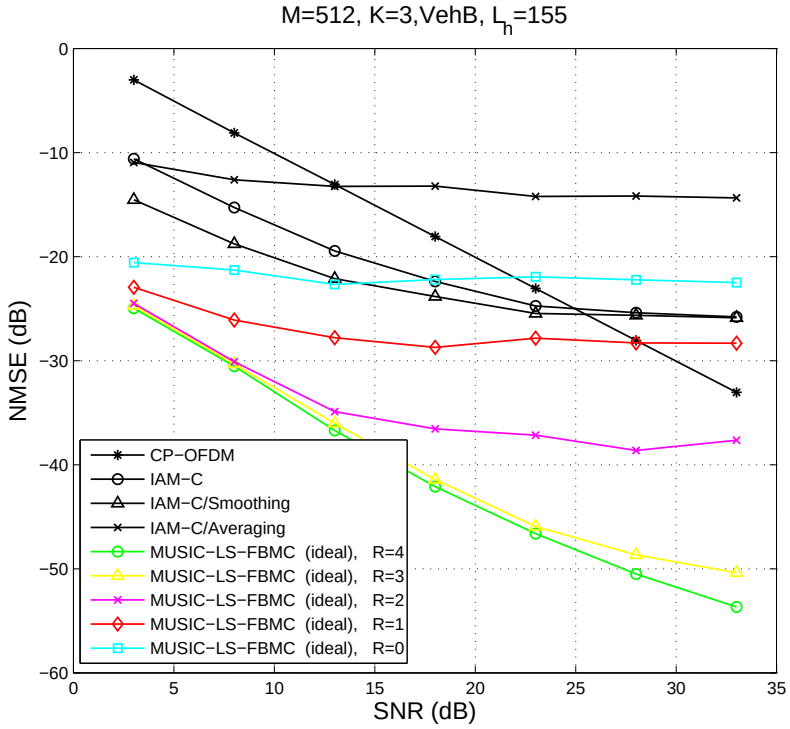

Figure 3-22: Effect of Taylor approximation order R.

estimating $\hat{L}$ as the rank of the covariance matrix of observations, $\hat{\boldsymbol{C}}_y$. This is convenient in our context since an eigenvalue decomposition of this matrix is needed anyway for the MUSIC

step. To this end, a rank detection criterion suggested in [42] was found useful. Some of its qualities that guided our selection is that it is based on minimal hypotheses (in contrast to e.g. information theoretic criteria [68]), works even with a small data set, and it offers a class of cost functions suitable for the purpose of rank detection. Following this criterion, if $\hat{\lambda}_i$, $i = 1, 2, \ldots, N_c$, are the eigenvalues of the sample covariance matrix, then its rank can be estimated as

$$\hat{L} = \arg \min_{0 \le k \le N_c - 1} \mathrm{IC}(k, C_{l_{\max}})$$

where

$$\mathrm{IC}(k, C_{l_{\max}}) = \hat{\lambda}_{k+1} + k C_{l_{\max}}, \quad k = 0, 1, \ldots, N_c - 1$$

and the function C_N satisfies the following: $C_N > 0$, $C_N \to 0$, and $(\sqrt{N} C_N)/\sqrt{\log \log N} \to \infty$ with increasing N. It has been found by experimentation that a suitable choice of C_N for the task at hand is $C_N = \left(\frac{1}{\log N}\right)^{0.9}$, termed as $C_N(9)$ in [42]. In Fig. 3-23, the results of Fig. 3-21 are repeated together with the curves that corresponds to the estimated number of paths. It is

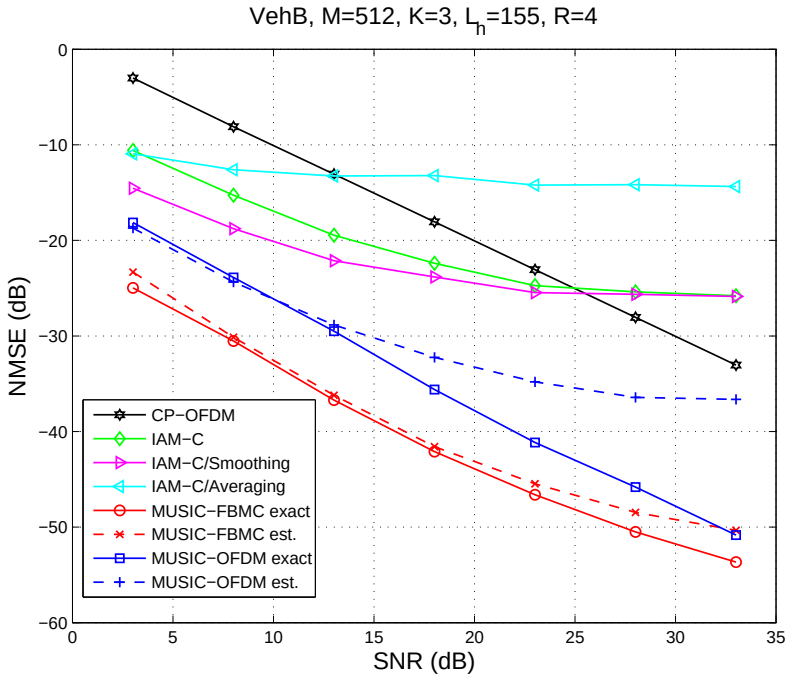

Figure 3-23: As in Fig. 3-21, but with estimated number of paths.

seen that the FBMC/OQAM estimation-based curve remains close to the ideal one and retains the merits of very good performance. It is noteworthy to remark that IAM-C/Smoothing was given *perfect* knowledge of L_h.

A word on complexity

From the computational complexity standpoint, the basic IAM-C method outperforms all other FBMC methods, as it only requires a complex division per subchannel. The other IAM-C variants add complexity to these basic scheme trading complexity deterioration for better performance. The MUSIC-LS method is the least favourable in terms of complexity. However, fast MUSIC schemes, such as [52, 72], could be applied to offer complexity savings.

MUSIC-MMSE

A means of improving the end result at low SNRs would be to use MMSE estimation instead of

LS. The estimator is easily built [38] on the basis of (3.84). Such an example is depicted in Fig. 3-24, where all required quantities are assumed perfectly known. Of course, such an improvement

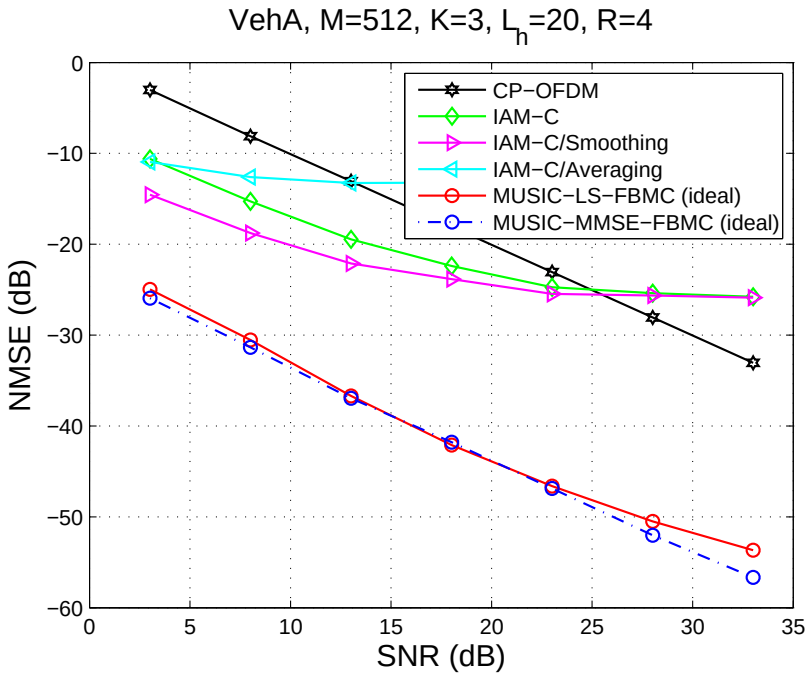

Figure 3-24: Same scenario with Fig. 3-20, with MMSE estimation performance included.

would only be possible in practice if we had estimates for the required statistics,namely the noise variance and the covariance of the path gains. A common way to estimate the noise variance is as the average of the eigenvalues of $\hat{\boldsymbol{C}}_{\boldsymbol{y}}$ which are associated with its null space. The latter is known once the rank has been computed. The covariance matrix of $\boldsymbol{\rho}$ is harder to estimate, particularly if no other a priori knowledge (for example, the channel power delay profile) is available. Nevertheless, and in the light of the commonly made assumption of uncorrelated paths, a rough choice of $\hat{\boldsymbol{C}}_{\boldsymbol{\rho}} = \mathrm{diag}(\frac{1}{L}, \frac{1}{L}, \ldots, \frac{1}{L})$ has been seen to be sufficient to get reasonable results (e.g., [69]).

3.4 Concluding Remarks

Having a good estimate of the channel in the beginning of a (sub-)frame can be quite useful in processing the data payload in cases where the channel is (almost) constant in time or slowly varying. Tracking fast varying channels, either in a pilot- or a decision-aided fashion, can also benefit from an initial good estimate. It is thus important to study the problem of channel estimation based on a known preamble. This is the subject of this chapter, where FBMC/OQAM modulation was considered, in view of its numerous advantages and the interesting challenges it implies to the channel estimator design. The study was divided into two parts, namely estimation of the impulse responses of the subchannels and that of the broadband channel. The CIR estimate can be used in the design of equalizers, with the former category of methods being directly applicable when equalization is performed on a per-subcarrier basis. For multi-band equalizer design, the broadband CIR estimate would be more useful.

Channel estimators were developed for all the common optimality criteria, including LS, ML, and MMSE. The more challenging scenario of exploiting the non-pilot subcarriers to also

transmit data while training the estimator was given special attention, in view of the possibility it offers to decrease the loss in training bandwidth. To cope with this problem, an iterative scheme based on the EM algorithm was developed and extensively tested. Simulation results were reported that confirm a good performance for the estimators derived, with the MMSE one being the best performing one, as expected. Results from applying per-subcarrier equalizers based on the obtained channel estimates showed MSE differences not to correspond to equally important BER reduction, leading to the conclusion that more sophisticated equalizers are needed to fully exploit the gains in MSE. The practical scenario of having inactive (null) subcarriers at the edges of the spectrum was also investigated and shown to result in ill conditioning for the estimation error covariance matrix. A simple, yet effective solution was proposed, based on replacing the matrix inverse by its SVD-based pseudo-inverse.

The first part of the chapter was concerned with estimators that rely on training sequences of any given length, and numerical results were presented to show the effect of the preamble duration on the estimation accuracy obtained. In a fast fading environment, and in order not to spend too much bandwidth for training, one would go for as short preambles as possible, while still attaining a good enough estimation performance. To meet this requirement, broadband CIR estimation was re-visited in the second part of the chapter, with the focus being on the design of short preambles (of one FBMC pilot symbol accompanied by 1–3 zero guards) that are optimal in terms of the channel MSE and subject to a limit on the training energy. Solutions were derived for both the cases of preambles that are fully- and partially-occupied by nonzero pilots and simple and efficient algorithms were outlined for their implementation. These results extend earlier preamble designs to the more realistic setup of highly frequency selective channels of interest in this WP. Extensive comparisons with a number of IAM variants as well as corresponding CP-OFDM estimators demonstrated a superior performance of the estimators developed here at an SNR range much wider than the one usually covered by IAM schemes. Inaccuracies such as CIR length over- and under-estimation were discussed. The BER results lead to a conclusion similar to that drawn in the first part of the chapter.

Possible improvements in the estimation performance of these methods were sought in the exploitation of the sparse/compressible nature of wireless CIRs. The means employed were the application of existing ideas from sparse channel estimation and compressive sensing (CS) in developing simple sparsity-aware variants that have the potential to provide a lower MSE with a small size of training data. Extensive simulations showed the well known in CS orthogonal matching pursuit (OMP) algorithm to be a simple, fast, and effective solution to the above requirement. Finally, again in a sparse channel context, a parametric method was presented that relies on a path-delay description of the channel. It comprises two distinct steps, a MUSIC-based procedure to estimate the delays and a linear LS or MMSE estimator for the path gains estimation. The underlying idea is to model the frequency selective subchannel responses as Taylor polynomials around the central subcarrier frequencies. Varying the order of the polynomials provides a more or less good approximation of the subchannels and allows very important gains over IAM variants and MUSIC-based CP-OFDM. The number of paths is first estimated with the aid of a model order selection criterion, which is free of assumptions on either the problem statistics or the data set size.

The value of the results reported in this chapter is mainly found in their fundamental nature, which stems from the variety of criteria and associated techniques and provides a palette of options with varying performance, complexity, information requirements, and bandwidth overhead. They can thus prove to be useful in other WPs, including WP4 (MIMO case) and WP9 (demonstrator), as a complement to scattered pilot assisted channel estimation as well as equalization. Nevertheless, there remain some important questions which, if answered, would

greatly increase the applicability of the techniques and designs presented here. These were already mentioned at several points throughout this presentation, directly or indirectly. It is useful to summarize some of them here:

- Application of these estimation techniques in tracking fast varying channels. This issue is further discussed in the next chapter and emphasized in Chapter 6.
- Extending the optimal design to preambles of any given length. Preliminary results in this direction have already appeared in [48].
- Exploiting the MSE performance gains through more sophisticated (e.g., multi-band) equalizers. This is a topic for D3.2.
- A better understanding of workings of the estimators and the possibilities for their improvement in the presence of practical constrains such as the over- or under-estimation of the (sub-)channel length.

4. Channel Estimation, Equalization, and Synchronization in Fast-Convolution based Receivers

Fragmented spectrum use scenarios, like the heterogenous PMR case, impose new challenges due to the existence of strong interfering unwanted spectral components between the used spectral slots. In this work, the target is to exploit the new opportunities provided by the flexible fast-convolution filter bank (FC-FB) signal processing, introduced in the EMPhAtiC deliverable D2.1, for effectively suppressing the unwanted spectral components from the channel estimation/equalization and synchronization processes. One urgent need is also to develop reliable channel equalization and synchronization schemes for the demonstrator. The embedded equalization and synchronization concept under development utilizes the FFT weights of the FC-FB structure also for channel equalization, timing and frequency offset compensation, and for timing and frequency offset estimation.

Integrating the synchronization and channel equalization functions with the FC-FB processing structure leads to efficient overall implementation. Even more importantly, the target is to move these functions from the time-domain processing side to frequency domain, to be implemented through subcarrier processing. This is important in fragmented spectrum use scenarions, i.e., non-contiguous multicarrier systems, because otherwise it is difficult to manage the strong interfering spectral components which may be dynamically allocated between the used portions of the received spectrum. Furthermore, the FC-FB processing structure is able to support simultaneous processing of non-synchronized signals from different users. In this respect, our goal is to support asynchronous operation in cellular uplink or ad-hoc scenarios, such that only coarse frequency synchronization is required.

The embedded equalization scheme implements optimal fractionally-spaced multi-tap linear subchannel equalizers by modifying the FFT weights, without additional coefficients, and provides good performance also in case of significant frequency selectivity of subchannels. Timing offset compensation is implemented through linearly frequency-dependent phase shift of the FFT bins, and operates well beyond the target range of $\pm$ half of subcarrier sampling interval. Frequency offset compensation with the resolution of $\pm$half of the FFT bin spacing can be reached through right choice of the FFT bins. For timing offset estimation, the idea is to use the FC-FB structure for implementing correlation between the received signal and a preamble effectively in FFT-domain. Subchannel filtering is in use and it helps to suppress strong interferences in the unused spectral slots.

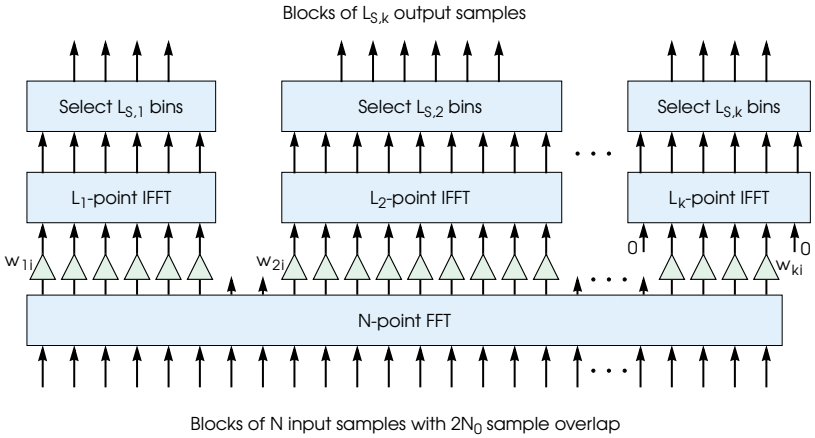

Figure 4-1: Fast convolution based flexible analysis filter bank using overlap-save processing.

4.1 Fast-Convolution Filter Banks

This section focuses on a special implementation scheme for multirate filter banks which is based on fast-convolution (FC) processing. The basic idea of fast convolution is that a high-order filter can be implemented effectively through multiplication in frequency domain, after taking DFT's of the input sequence and the filter impulse response. Eventually, the time domain output is obtained by IDFT. Commonly, efficient implementation techniques, like FFT/IFFT, are used for the transforms, and overlap-save processing is adopted for processing long sequences. The general structure is represented in Figure 4-1. The application of FC to multirate filters has been presented in [10], and FC implementations of channelization filters have been considered in [11, 71, 49]. The authors have introduced in [53] the idea of FC-implementation of nearly perfect-reconstruction filter bank systems and detailed analysis and FC-FB optimization methods are developed in [54]. These papers demonstrate the greatly increased flexibility and efficiency of FC-FB in communication signal processing, in comparison with the commonly used polyphase implementation structure.

There are two key parameters which have an effect on the spectral characteristics of the FC-FB scheme:

- The IFFT size L is defining how well the filter frequency response can be optimized. In general, increasing the value of L helps to improve the stopband attenuation.

- The overlap factor $1-L_S/L$: In FC based multirate signal processing there is an inevitable cyclic distortion effect because the overlapping part of the processing block cannot be made big enough to absorb the tails of the filter impulse response. Naturally, this effect can be reduced by increasing the overlap factor.

In [54] these effects were analyzed using a periodically time variant model for FC processing and effective tools for frequency response analysis and FC filter optimization were developed.

In FC processing, the subchannel bandwidths and center frequencies can be independently tuned, with the resolution of the FFT bin spacing. Different types of multiplexes can be combined in a single FC-FB structure. It is also possible to use different transition band shapes for different multiplexes, if so desired. The flexibility of the scheme can be used also for coarse frequency offset compensation by shifting the set of frequency bins connected to the subchannel processing functions.

4.2 The LTE-like Broadband PMR Scheme

We focus here on a 5 MHz LTE-like multicarrier system utilizing the FBMC/OQAM waveform and using FC-FB based receiver implementation. The 5 MHz bandwidth case is suitable for broadband PMR, and the LTE system is a good candidate for possible broadband PMR system deployment in new frequency bands. As the dominating broadband cellular network standard, LTE is a natural reference for advanced multicarrier system development for PMR, and a high level of commonality with LTE is expected from the new system. The 5 MHz LTE uses the sampling rate of $f_s = 7.68$ MHz with $M = 512$ subcarriers (out of which 300 active subcarriers are used) and 15 kHz subcarrier spacing [15]. The 300 active subcarriers are scheduled in resource blocks of 12 subcarriers, i.e., there are 25 resource blocks (RBs). Also LTE variants with lower bandwidth are interesting for broadband PMR, depending on the available bandwidth. Especially, the 1.4 MHz version has been selected the reference basis for the EMPhAtiC demonstrator development. It uses 1.92 MHz sampling rate, 128 subcarriers, and $6 \times 12 = 72$ active subcarriers. Most of the other parameters, like subcarrier spacing and frame structure are the same for different LTE bandwidths.

To accommodate non-synchronized usage of the subcarriers, for example, the highest subcarrier of each contiguous set of resource blocks allocated to a user should be left unused, as a guardband. FBMC/OQAM allows to transmit 15 multicarrier symbols in a subframe of two slots (1 ms), instead of 14 in basic LTE, which compensates the additional overhead in data transmission capacity due to the guardbands. The performance of the equalization and synchronization offset compensation is evaluated with *Vehicular A* and *3GPP Hilly Terrain* channel models for the static and mobile users. Since the broadband PMR system is expected to be used also in large macrocells, channel models with relatively wide delay spreads, like the *Hilly Terrain*, are important to be take into consideration in the system development. For such channels, the LTE version with extended cyclic prefix (CP) should be considered as the reference. This variant of LTE transmits 6+6 multicarrier symbols per subframe, but otherwise the main parameters are the same as described above.

The following two filter bank configurations are under consideration:

a) Polyphase filter bank: PHYDYAS prototype [64] with $K = 4$, 3-tap frequency-sampling based equalizer with MSE criterion [32].

b) FC filter bank: In the 5 MHz case the long transform length of $N = 4096$, short transform length of $L = 16$, and $L_s = 10$ useful subcarrier samples (5 OQAM symbols) per processing block. In the 1.4 MHz case, the long transform length is 1024 but the other parameters are the same. The weights of the FC-FB structure were optimized using the methods presented in [54] and EMPhAtiC deliverable D2.1.

4.3 Channel Equalization

Here we consider a subcarrier-wise channel equalization structure which is using the channelization weights of the fast-convolution filter banks structure also for channel equalization purposes. This is referred to as embedded equalizer. It approximates a linear fractionally-spaced equalizer and the conceptual model of the receiver front-end includes the following elements [7, 70]:

- Pulse-shape matched filter: This comes from the the RRC-type FC-FB design through the weights w_{ki}.

- Channel matched filter H_{ki}^*, where H_{ki} is the channel frequency response at corresponding FFT bin.
- Folding effect due to resampling at symbol rate.
- Linear equalizer with MSE criterion.

The resulting weighting coefficients can be expressed as [70]:

$$\hat{w}_{ki} = \frac{H_{ki}^* w_{ki}^*}{|H_{ki} w_{ki}|^2 + |H_{k\tilde{i}} w_{k\tilde{i}}|^2 + 1/\gamma} \tag{4.1}$$

where γ is the signal to noise ratio and $\tilde{i}$ is the FFT bin index folding on top of FFT bin i in subchannel k.

In order to construct the embedded equalizer, the channel estimate should be available at all the FFT bins of the active subchannels. Naturally, piecewise constant or piecewise linear approximations can be used to simplify the calculations if the channel is not highly frequency selective within the subbands. The same embedded equalizer model can be used for FBMC/OQAM, FMT, and single carrier waveforms.

The weights of the FC-FB structure must be constant over each processing block of $L_s/2$ OQAM symbols, i.e., 5 symbols with the used parametrization. The coefficients can be updated for each processing block.

As a benchmark for the comparisons, we consider the polyphase filter bank structure, using the PHYDYAS prototype [64] with overlapping factor of $K = 4$, together with 3-tap frequency-sampling based subcarrier equalizers with MSE criterion [57].

Numerical results: The examples here are for the 5 MHz LTE-like case with 300 active subchannels, assuming perfect channel knowledge. In the FC-FB case, the instantaneous channel response in the middle of each 5-symbol FFT processing block is used. In the polyphase case, the channel is updated for each OQAM half-symbol. Figures 4-2 and 4-3, show the performance of both configurations for QPSK modulation in the case of *Hilly Terrain* and *Vehicular A* channel models for both the static user and the user with 200 km/h mobility. As can be seen from these figures, the embedded FC-FB equalizer works well even in the case of high mobility with the used parameters and PMR frequency band ($f_c = 400$ MHz). In the 2.5 GHz frequency band, the limitations due to the increased block length of FC-FB are visible with high mobility, but the effect is not severe. Figure 4-4 shows, the simulation results also for the case where the subcarrier width has been increased by a factor of four. It can be seen that the embedded equalizer is able to handle high frequency selectivity better than the 3-tap equalizer used in PHYDYAS.

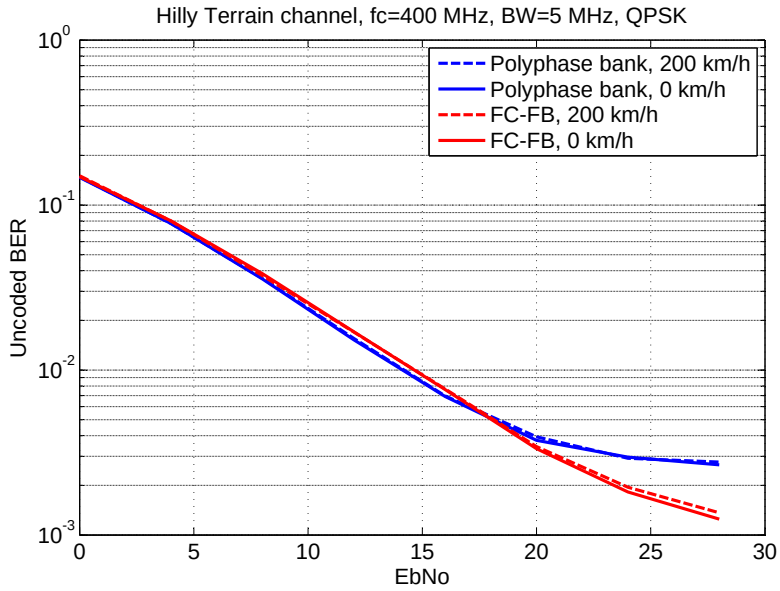

Figure 4-2: Performance of the polyphase and fast-convolution filter banks in the case of *Hilly Terrain* channel model for a static user and a user with 200 km/h mobility. QPSK modulation and perfect channel knowledge assumed.

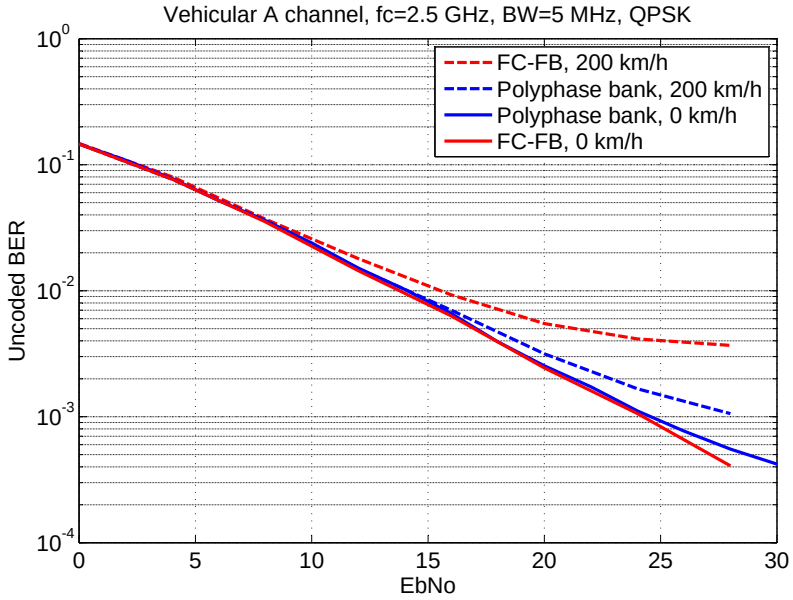

Figure 4-3: Performance of the polyphase and fast-convolution filter banks in the case of *Vehicular A* channel model for a static user and a user with 200 km/h mobility. QPSK modulation and perfect channel knowledge assumed.

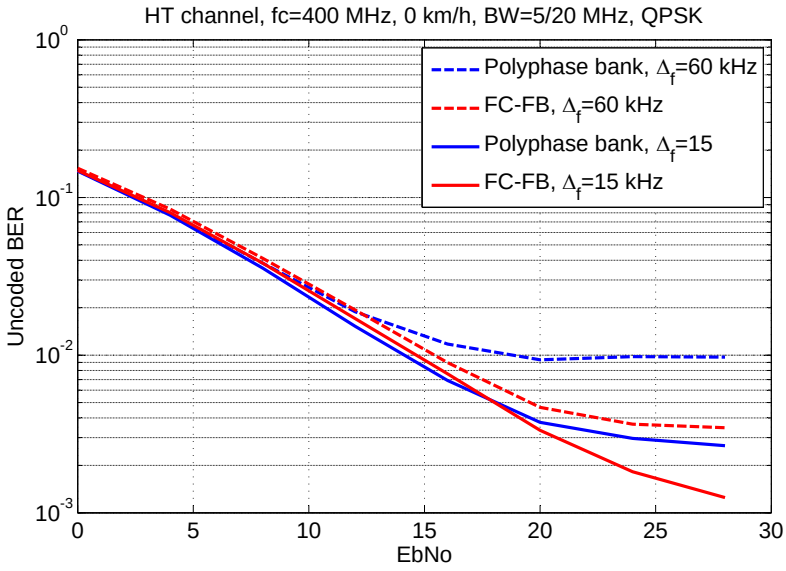

Figure 4-4: Performance of the polyphase and fast-convolution filter banks in the case of *Hilly Terrain* channel model for subcarrier spacing of $\Delta_f = 15$ kHz and $\Delta_f = 60$ kHz. QPSK modulation and perfect channel knowledge assumed.

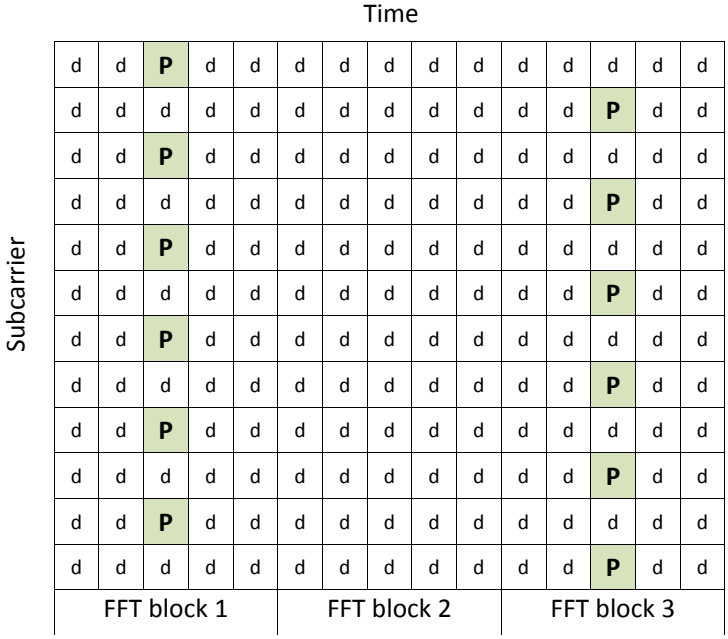

Figure 4-5: MBSFN pilot structure.

4.4 Equalization with Channel Estimation

Here we consider only basic scattered pilot based channel estimation methods. We assume that 1 ms subframes of 15 multicarrier symbols are used. Consequently, with the demonstrator parameters, each subframe is composed of exactly 3 FFT processing blocks, which is a benefit from the practical implementation point of view. One considered pilot structure is the DM-RS downlink pilot structure associated with the PDSCH transmission mode of LTE. This model has been implemented in the FIBAsim link-level simulator of the EMPhAtiC project for polyphase filter banks. Also preliminary results for an FC-FB implementation with channel estimation and embedded equalization are included. In this model, pilots are included in every subcarrier within each subframe, as illustrated in Figure 4-5. This pilot structure resembles the MBSFN pilot structure of LTE, and this acronym is used later on to identify it. Here, pilots are included in odd subcarriers in the middle of the first FFT processing block and in even subcarriers in the middle of the last processing block of each transmission slot of 15 multicarrier symbols. The channel estimates are first smoothed by using a moving average of length two over each subcarrier. Then linear interpolation in the time direction is used to get the channel estimates for each processing block. Filtering/smoothing in the frequency direction doesn't seem to improve the performance. Due to the OQAM signal structure, the auxiliary pilot model [57] is used for scattered pilots in both cases.

Numerical results: The WiMAX pilot boost of 2.5 dB is assumed and the simulation uses the 5 MHz LTE-like case (300 active subcarriers) with a block length of 10 subframes, i.e., 150 subcarrier symbols. Consequently, the overhead in EbNo due to the pilots is 0.6 dB with DM-RS pilot structure (4 pilots per resource block) and 0.8 dB with the denser MBSFN pilot structure (6 pilots per resource block).

Figure 4-6 shows the simulated bit error rate for the polyphase case with DM-RS in the case of *Vehicular A* channel, in comparison with perfect channel information (PCI) case. It can be seen that the resulting performance is reasonably close to the case of perfect channel

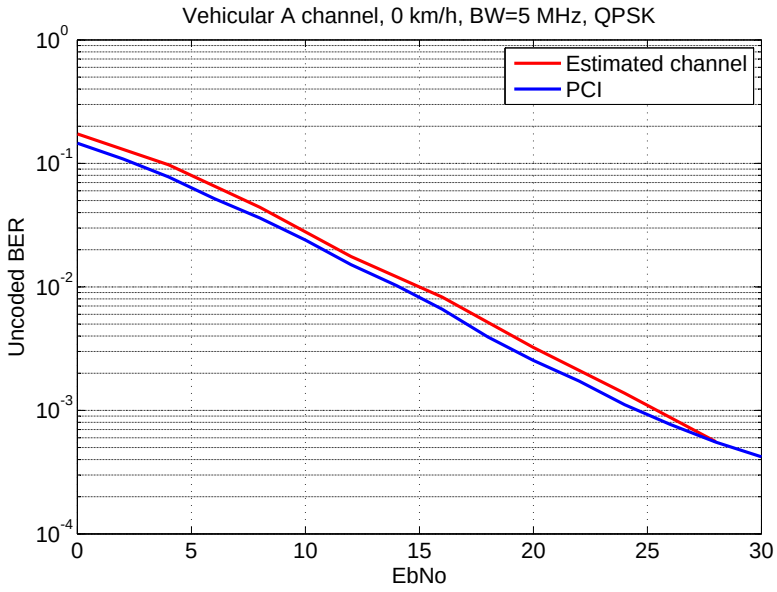

Figure 4-6: Simulated bit error rate in the case of *Vehicular A* channel. QPSK transmission with perfect channel information (PCI) and pilot-based estimation in a quasistatic channel.

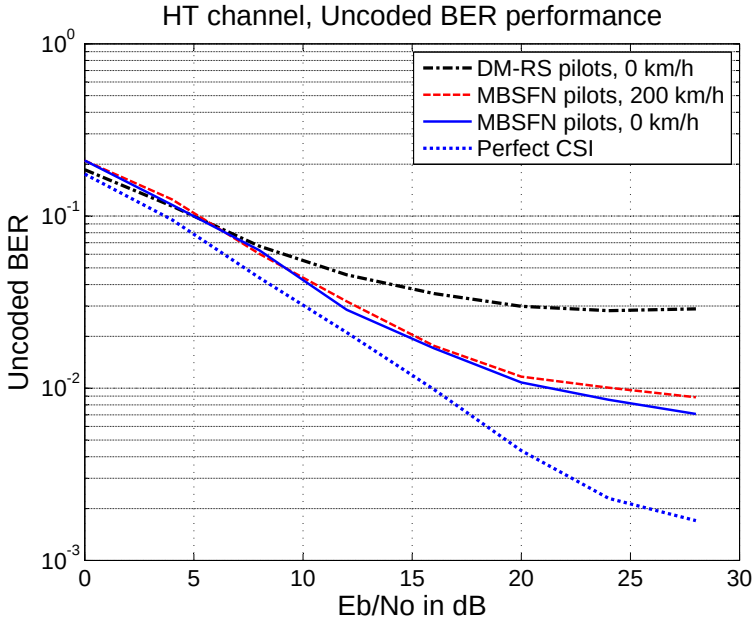

Figure 4-7: Simulated uncoded bit error rate in the case of *Hilly Terrain* channel with perfect channel state information (CSI) and pilot based estimation. QPSK modulation is used.

knowledge. Figure 4-7 shows the results in the case of *Hilly Terrain* channel. It is quite clear that the DM-RS pilot structure is not dense enough in the frequency direction for the *Hilly Terrain* channel. While the MBSFN pilot structure provides clearly better performance, the performance still suffers from insufficient frequency resolution in channel estimation. This can be expected to be more critical in case of high-order modulations. Therefore, scattered-pilot based estimation of highly frequency selective channels should be further studied in the future

work of EMPhAtiC WP3.

4.5 Synchronization

Here we consider the problems of carrier frequency offset estimation and timing offset estimation in the context of fragmented spectrum use with FB-MC waveforms. In timing offset estimation, the idea is to use the FC-FB structure for implementing correlation between the received signal and the known preamble effectively in FFT-domain. The scheme is illustrated in Fig. 4-8. We consider a frame structure which includes two consecutive OQAM symbols for synchronization purposes. In the initial model, pilots are loaded in active subcarrier of the first and last subsymbol, and the two half-symbols in the center contain zeros.

On the receiver side, subchannel filtering is in use and it helps to suppress strong interferences in the unused spectral slots. The idea is to use this synchronization scheme independently for each multiplex of subchannels which are not synchronized with each other. The scheme can be used for FBMC/OQAM, FMT, and SC waveforms, but we focus here on the FBMC/OQAM case.

The timing estimation process includes the following steps:

- Long FFT of the analysis FC-FB of the receiver, jointly for all received multiplexes. The same FFT output is used later for data detection within the processing block containing the synchronization symbol.
- Subcarrier channelization for active subchannels through the weights.
- Long IFFT which combines the active subcarriers with each multiplex. This is repeated for the two half-symbols used in synchronization. The overlapping odd and even subcarriers can be combined in the IFFT input, so two IFFT's of the same length as the FFT are needed. The IFFT outputs are combined non-coherently (squared magnitude sum), taking into account the delay difference of the half-symbols.
- Finding the peak of the combined IFFT output. Figure 4-9 shows an example of a resulting correlation peak.

Coarse carrier frequency offset (CFO) estimation is combined with this structure. The CFO can be estimated from the phase rotation between the two half-symbols at the correlation peak. For the used pilot structure, a CFO of 1 FFT bin (subcarrier spacing $/8$) corresponds to a phase rotation of $3\pi/8$, or a rotation of π corresponds to 2.67 FFT bins. Due to phase ambiguity, the CFO estimation range is thus around ± 2.67 FFT bins.

Numerical results: We consider here the EMPhAtiC demonstrator case, using 1.4 MHz bandwidth and 72 active subcarriers, but otherwise the same parameters as earlier. For higher number of subcarriers in the multiplex, the performance is expected to be better. Offset-QPSK model is used for the pilot symbols, and their power level is the same as that of the offset-QPSK data symbols. Figures 4-10 and 4-11 show the correct timing offset detection probability for different SNRs as a function of CFO for *AWGN* and *Hilly Terrain* channels. For the *AWGN* channel, the criterion for correct timing offset is that the delay exactly matches the channel time delay in high-rate samples, whereas in the *Hilly Terrain* case, ± 2 sample offsets are tolerated. This is because the *Hilly Terrain* channel exhibits such variations in the effective delays in time domain. Over 95 % detection probability is reached with *AWGN* channel for SNRs above -3 dB within the CFO range of ± 3 FFT bins corresponding to ± 5.6 kHz with the considered

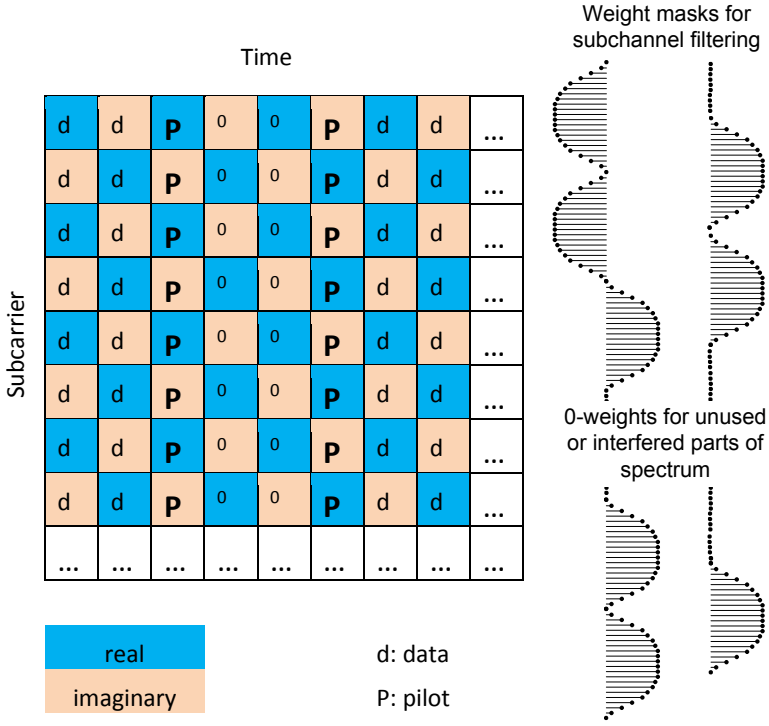

Figure 4-8: Pilot and data allocations for LTE-like pilot structure.

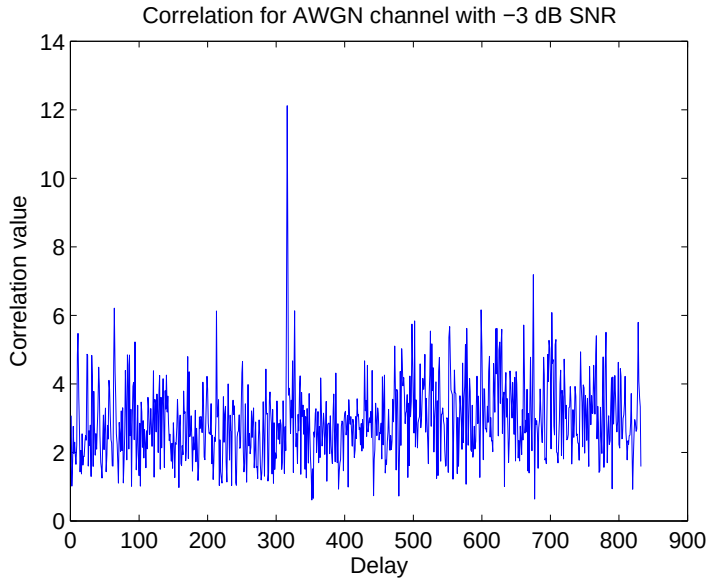

Figure 4-9: Correlation for the *AWGN* channel with -3 dB SNR.

parameters. With *Hilly Terrain* channel, the same is reached with SNRs above 3 dB, and 92 % detection probability is reached with 0 dB SNR for the CFO range of $\pm$ 2 FFT bins. It can be noted that the timing offset estimation range exceeds the range of reliable CFO estimation.

Figures 4-12 and 4-13 show CFO estimation results for both channels. These results include only the cases where the correct timing estimate was found. It can be seen that the bias of the estimate is very small. The RMS error is $0.2 \ldots 0.3$ times the FFT bin spacing for small CFOs and $0.3 \ldots 0.6$ times the FFT bin spacing for CFOs approaching 2 FFT bins. When

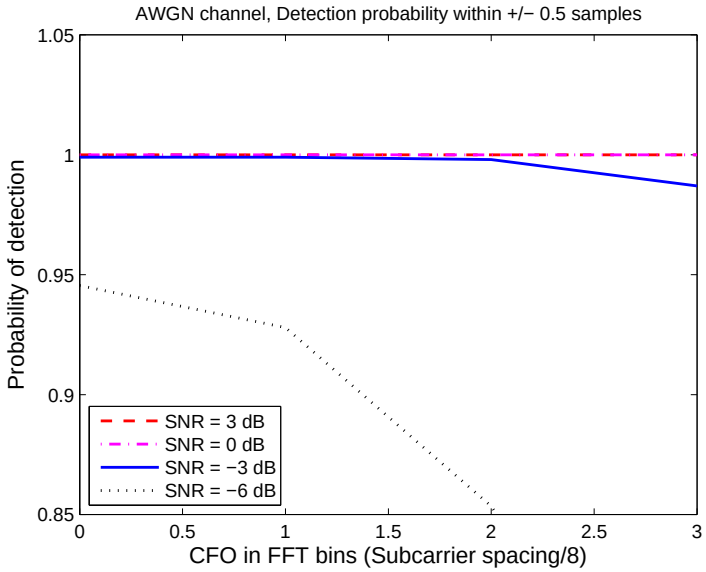

Figure 4-10: Probability of correct timing estimation for the *AWGN* channel.

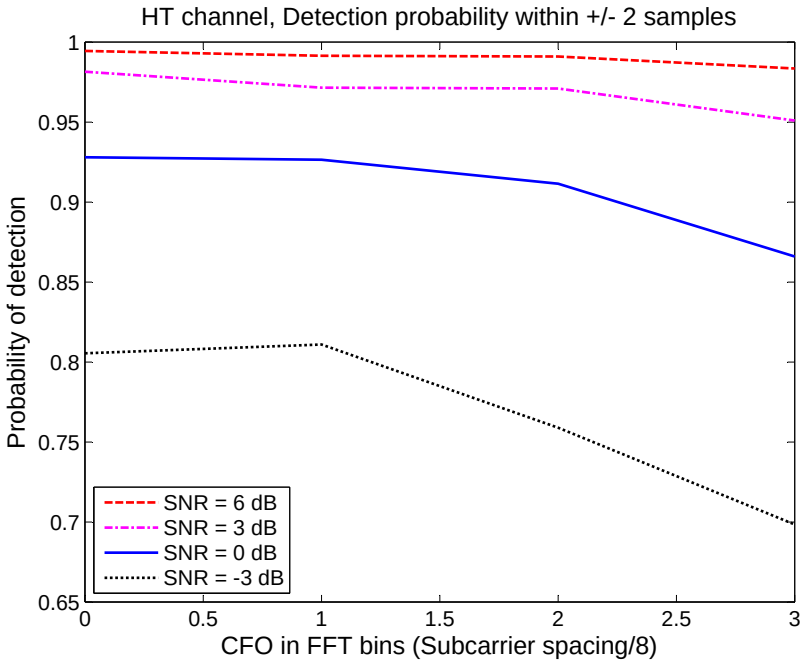

Figure 4-11: Probability of correct timing estimation within ± 2 samples for the *Hilly Terrain* channel.

the CFO exceeds ± 2 FFT bins, the CFO estimation performance degrades rapidly.

Regarding the demonstrator implementation, the specified local oscillator accuracy is ± 2.5 ppm, i.e., about ± 1 kHz in the PMR frequency band around 400 MHz. In this range, reliable timing offset estimation can be reached and the performance of CFO estimation is sufficient such that the residual frequency offsets can be handled through subcarrier processing, e.g., using the ideas of [57].

As mentioned, the initial idea was to include zero values between the two half-symbols used as the synchronization preamble. However, it turned out that the performance loss when inserting data symbols in this region is relatively small.

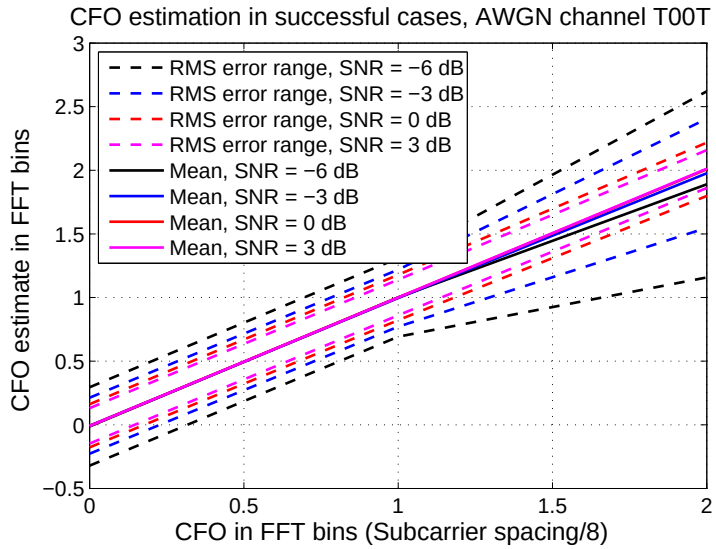

Figure 4-12: RMS and mean errors of CFO in FFT bins for the *AWGN* channel.

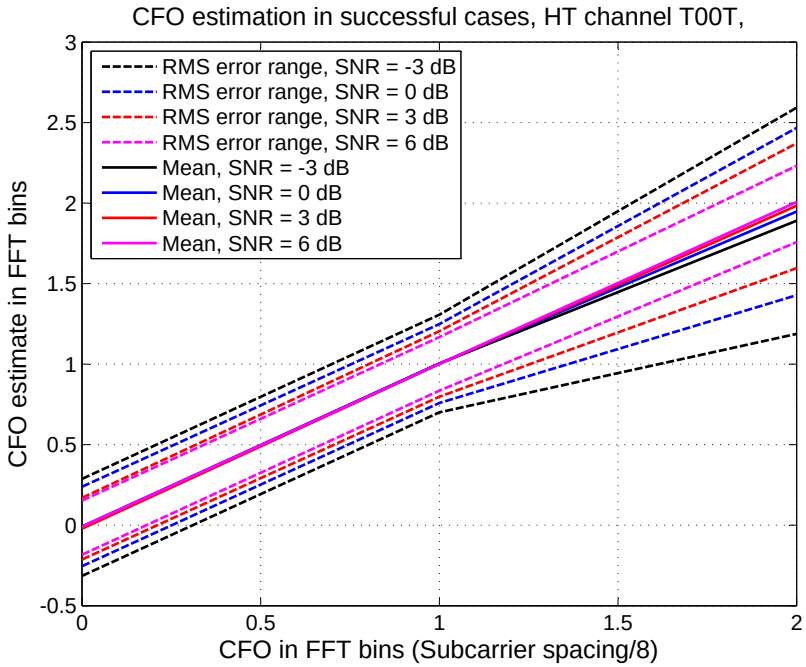

Figure 4-13: RMS and mean errors of CFO in FFT bins for the *Hilly Terrain* channel.

It was found out that increasing the distance of the two half-symbols improves the CFO estimation accuracy with small CFOs, while it reduces the estimation range. The proposed preamble design is considered to make a feasible trade-off between CFO estimation range and accuracy for the PMR case.

For these numeric results, a single pair of random pilot sequences was used. It was selected based on a few experiments. In the future work, optimization of the preamble to maximize the synchronization performance and optimize the waveform characteristics (like PAPR) is needed.

4.6 Frequency Offset Compensation

Two alternatives can be considered for frequency offset compensation in FC processing. The first one is based on shifting the set of weights corresponding to subcarrier to proper FFT bins. The residual CFO after this is within ± 0.5 FFT bins, which can be handled well in subcarrier processing, e.g., using the ideas of [57]. It is also possible to fine-tune this frequency shifting process, basically by resampling the RRC-type weight mask corresponding to the fractional frequency shift. The first approach is conceptually quite straightforward, whereas the evaluation of the latter approach remains as a topic for future studies.

4.7 Timing Offset Compensation

The considered filter bank processing approach is particularly important for the base station transmitters and receivers, in which case there is a need to process simultaneously different non-synchronized FB-MC waveforms, and possibly also legacy signals. On the terminal side and in the ad-hoc context, a down-scaled version of the filter bank can be used, supporting a limited set of waveforms with reduced complexity.

Considering effective implementation of the base station receiver, it would be desirable to use a single FC-FB engine to process multiple uplink signals emerging from different non-synchronized mobiles. These signals may use different types of waveforms but they are assumed to be non-overlapping, i.e., a narrow guardband is inserted between different signal spectra. The relative frequency offsets are assumed to be small enough such that sufficient spectral isolation is maintained. As an example, with the 15 kHz subcarrier spacing of LTE, a few kHz frequency offsets can be tolerated without introducing significant cross-talk even with a single subcarrier guardband. Naturally, this depends on the filter bank design and expected power level differences between different uplink signals. Our focus here is on the relative timing offsets. The target is to compensate arbitrary fractional timing offsets in the range of $[-T/2, T/2] = [-T_s/4, T_s/4]$, where T is subchannel sample interval and T_s is the symbol interval.

In the FC-FB structure, the timing offset compensation can be implemented by adjusting the filtering delay through the phase response of each subchannel filter. A fractional timing offset (delay) of τ_k in subchannel k can be compensated by introducing an additional linear phase response to the FFT-domain weights:

$$\hat{W}_{k\ell} = W_{k\ell} e^{j2\pi\ell\tau_k/L_k} \tag{4.2}$$

where $W_{k\ell}$, $\ell = -L_k/2, -L_k/2+1, \ldots, L_k/2-1$ are the original FFT-domain weights for subchannel k. The filter phase slope can be used for controlling the timing offset.

The basic FC-FB system can be designed for real FFT-domain weights, in which case the timing offset compensation would slightly increase the overall implementation complexity [54]. However, there are various reasons for considering complex weights, including (i) increased possibilities for the frequency response optimization and (ii) use of complex weights also used for subcarrier-wise channel equalization, as discussed above. All in all, the additional complexity due to the timing offset compensation in the FC-FB structure is relatively small.

Numerical Results: Here, we consider only the FC-FB system parameterized as above in the 1.4 MHz LTE-like case with 72 active subcarriers. An important consideration in the proposed way of timing offset compensation utilizing the FC-FB structure is the inevitable cyclic distortion in the FC implementation of multirate filters. In optimized design, the effect is symmetric within the processing block. With timing offset compensation, the cyclic truncation effect becomes

more severe on one side of the effective linear impulse response [54]. This appears as reduced attenuation of out-of-band spectral components and increased inband interference. The latter effect is partly due to the nearly perfect-reconstruction nature of the filter bank and partly due to the cyclic distortion due to FC-FB implementation.

The inband and out-of-band effects can be seen in Figure 4-14. The inband interference is just the mean-squared error in the subcarrier symbols, after timing offset compensation, as a function of the original timing offset. The out-of-band test situation includes just one active subcarrier, which is not synchronized to the receiver processing. This is basically modeling a narrowband legacy communication signal. Then we measure the interference power level at 2nd, 3rd, 5th, 10th, and 20th subcarrier (SC) from the active one, at the distances of 30 kHz, 45 kHz, 75 kHz, 150 kHz, and 300 kHz away from the active SC.

Figure 4-14 shows first the inband interference for the optimized design with complex weights. In this case, the performance as a function of the timing offset is symmetric and inband performance variations are very small within the target range of timing offset control, ± 0.25 OQAM symbol intervals, and well beyond it. The figure shows also the results with real weights. In this case there is asymmetry in the characteristics, but the inband performance is good enough anyway. Even though the real weights have some benefits from the basic FC-FB implementation point of view, the use of complex weights becomes necessary if timing offset compensation is implemented using the proposed approach.

It can be seen that the variations in the out-of-band performance are also relatively small within the target range of timing offset control, and the out-of-band interference attenuation is not severely compromised even in much wide tuning range.

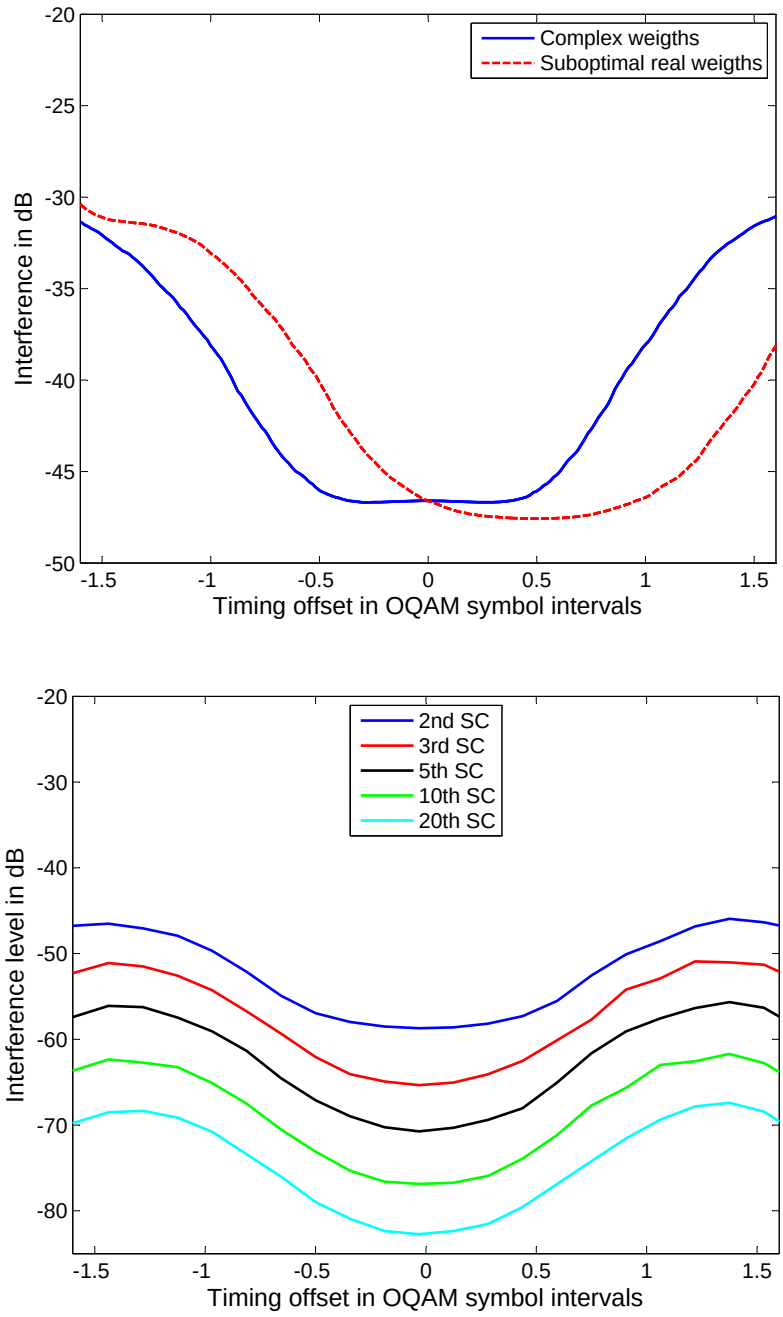

(b)

Figure 4-14: Inband and out-of-band effects of timing offset control in the FC-FB implementation of FBMC/OQAM. 1.4 MHz case with 72 active subcarriers. (a) Inband effects. (b) Out-of-band effects.

4.8 Concluding Remarks

We have demonstrated the feasibility of the embedded equalization concept, which is integrated with the fast-convolution filter bank processing structure. It shows good equalization performance in channels which exhibit high level of frequency selectivity at the subcarrier level. The extended length of processing blocks turned out not to be a serious problem even with relatively high mobility. In contrast, the channel estimation for highly frequency selective subchannels is a

critical issue. Since the PMR system is expected to operate in large macrocells, it should be able to operate with long delay spread channels, like the *Hilly Terrain* channel model. However, the commonly used LTE-like pilot structures do not have sufficient resolution in frequency direction for channel estimation. Using a pilot structure containing pilots in all subcarriers, promising results were obtained in the QPSK modulation case with the *Hilly Terrain* channel. Anyway, pilot assisted channel estimation for such channel models remains as an important item for future studies.

A joint scheme for precise timing estimation and coarse frequency offset estimation was proposed. This scheme is based on FFT-domain processing and can be integrated effectively with the FC-FB structure and it shows promising performance, considering also the requirements for the demonstrator development.

Timing offset compensation by adjusting the FFT domain weights performs well in a much wider range of timing offsets than what is actually needed for processing non-synchronized waveforms in an FC-FB engine. Certain loss (typically well below 10 dB) in the suppression of out-of-band interferences is observed, but proper design of the FC-FB weights results in very good performance. In comparison, with low-complexity subband processing after polyphase AFB, the demonstrated feasible timing offset compensation range is no more than $\pm 10\%$ of the symbol interval [57]. Further improvement can be expected by modifying the FC-FB optimization algorithm to maximize the attenuation for worst-case timing offset, instead of the 0 timing offset case.

The combination of presented algorithms allows to implement the synchronization and channel equalization related functions in frequency domain, through subchannel processing. This is an important feature for fragmented spectrum use scenarios, since it would be very difficult to reach the needed flexibility for interference avoidance through time-domain techniques. The methods are also able to support asynchronous FDMA operation in spectrally efficient manner, with minimized guardbands between non-synchronized subband signals.

For example, in cellular uplink transmission, the FC-FB based transmission modes allow fully asynchronous operation regarding timing offsets between transmissions and relatively coarse mutual frequency synchronization is sufficient. This allows the transmission of short data packets without initial synchronization, and maintaining the synchronization of idle stations is not critical. Also the latency due to initial synchronization can be minimized. However, in case of continuous transmission in cell-based systems, there are good reasons for establishing synchronism between the uplink signals. These reasons include reduced signal processing complexity and maximization of the overheads in TDD and TDMA operation modes due to time-domain guard intervals between transmission bursts, which have to be able to absorb the timing uncertainties.

5. Channel Estimation for FMT Systems – A Two-Dimensional MAP Approach

The purpose of this chapter is to present a (sub-optimal) *Maximum A Posteriori (MAP)* channel estimation technique, useful for single-tap equalization. It can be used for both classical OFDM and for FMT schemes such as the ones described in WP 2.

The idea stems from the observation that the fast fading channel of broadband systems can be viewed as a two-dimensional (2-D) signal (time and frequency). The algorithm is a block by block pilot-based channel estimator, based exclusively on the received samples corresponding to pilot symbols that are distributed in both time and frequency domains. In order to estimate the channel as accurately as possible, all correlations between channel coefficients in time and frequency are taken into account. The main benefit of this algorithm is that we apply channel estimation directly in frequency and time-domains at pilots and data positions, thus obtaining a 2-D channel estimate; the algorithm does not need any supplementary interpolation step.

5.1 System Model

The transmitted frame is composed of symbols distributed regularly in both the time and frequency planes (temporal division and sub-carriers). Any symbol located in the time-frequency plane is uniquely identified by its temporal position and sub-carrier position. The data are

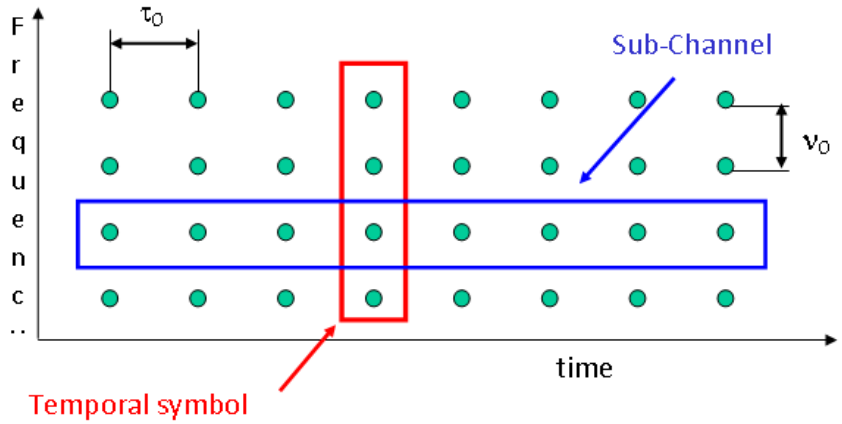

organized in frames, in which some specific symbols, the pilots, distributed along both time and frequency axes are inserted inside the transmitted data. The aim is to estimate the propagation channel for those specific positions and then be able to "interpolate" in both time and frequency domains throughout the entire frame for data positions. For this, we will use *Basis Expansion Models (BEM)* in order to perform the interpolation jointly within the channel estimation phase in one step only.

First, let us calculate the covariance matrix of the channel limited by the physical constraints of the realistic propagation channel variations, namely maximum Doppler frequency shift and maximum delay spread in time.

- On the frequency axis:

- Fading variation is defined by the temporal profile of the channel: Delay spread $= (0, \tau_{\max})$. For example, for a Hilly Terrain (HT) profile in the UHF band: $\tau_{\max} \approx 17\mu$s.
- So frequency components in the FFT of the channel taken along the time axis (Doppler spectrum of the channel) that lie beyond these limits are physically impossible.

- Similarly, on the time axis:
  - Fading variation is defined by the Doppler spectrum of the channel: Doppler shifts: $(-f_D, f_D)$, i.e. for 400 MHz band and maximum mobile speed 200 km/h: $f_D \approx 80$ Hz.
  - So delay components in the IFFT of the channel taken along the frequency axis (temporal profile of the channel) that lie outside these limits are physically impossible.

Given these physical propagation channel variation limitations, we are able to define dedicated projection basis to represent possible channel variations. To this end, we have considered the following:

- Uniform Doppler power spectrum, with maximum Doppler shift depending on selected maximum mobile speed and RF carrier
- Uniform multipath intensity profile, with maximum delay spread depending on envisaged environment conditions and RF carrier propagation characteristics.

The temporal covariance matrix of the channel is the auto-correlation matrix of the channel in the temporal domain. Hence it is obtained by an IDFT of the **frequency channel power distribution**. The corresponding frequency domain covariance matrix is obtained by a DFT of

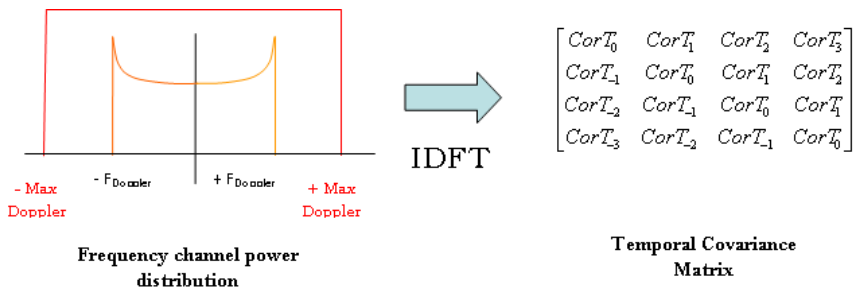

the **temporal channel power distribution**. The **global covariance matrix of the channel** is the Kronecker product of the frequency and temporal covariance matrices

The problem is to estimate the channel response at all FT points (m, n) in a frame of size $M \times N$. Let us now denote by:

1. $\boldsymbol{y}$ the received vector (received signal),
2. $\boldsymbol{\mathcal{H}}$ the $MN \times 1$ channel vector to estimate,
3. $\boldsymbol{\eta}$ the noise,

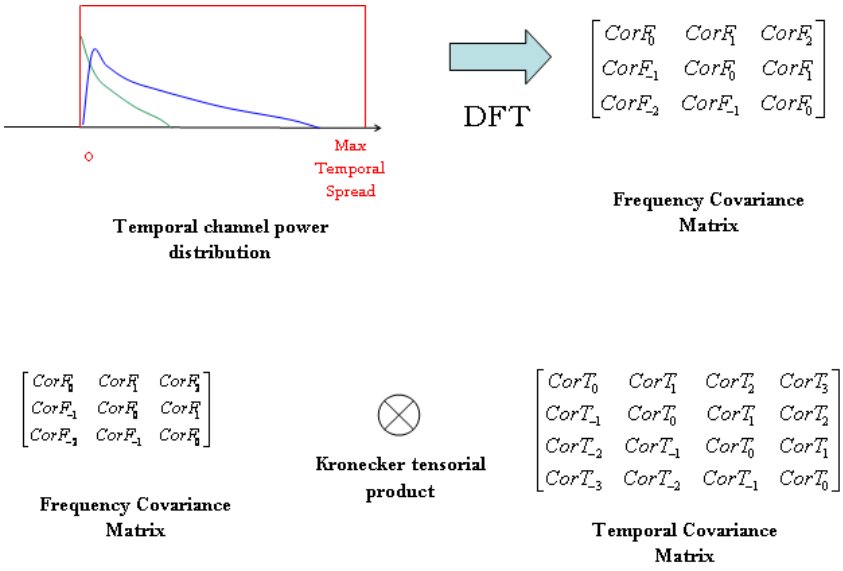

4. σ^2 the noise variance,
5. $\boldsymbol{R}$ the covariance matrix of the channel calculated in this way (see above). We denote its eigenvalue decomposition as follows

$$\boldsymbol{R} = \boldsymbol{Q}\boldsymbol{N}\boldsymbol{Q}^{\mathsf{H}} \tag{5.1}$$

Clearly:

$$\boldsymbol{y} = \boldsymbol{E}\,\boldsymbol{\mathcal{H}} + \boldsymbol{\eta}$$

where $\boldsymbol{E}$ is the data matrix (to be detailed later on).

5.2 2-D MAP Channel Estimation Approach

The MAP (Maximum A Posteriori) criterion can be stated as

$$\max_{\boldsymbol{\mathcal{H}}} \{p(\boldsymbol{\mathcal{H}}|\boldsymbol{y})\}$$

with $p(\cdot)$ denoting the probability density function (pdf). Applying the Bayes' formula results in

$$p(\boldsymbol{\mathcal{H}}|\boldsymbol{y}) = p(\boldsymbol{y}|\boldsymbol{\mathcal{H}})p(\boldsymbol{\mathcal{H}})$$

In the presence of additive white Gaussian noise with zero mean and variance σ^2:

$$p(\boldsymbol{y}|\boldsymbol{\mathcal{H}}) \propto e^{-\frac{\|\boldsymbol{y}-\boldsymbol{E}\boldsymbol{\mathcal{H}}\|^2}{2\sigma^2}}$$

But the propagation channel is not totally unknown. It follows physical constraints as described previously. Indeed, the frequency spreading is limited to maximum Doppler shift. It lies between $-f_D$ and f_D, where $f_D = \frac{v}{c} f_c$, with v being the mobile speed, c the light speed, and f_c the carrier frequency. Thus, the spectral components of the propagation channel along the frequency axis are limited by those bounds. Similarly, the temporal spread of the propagation channel is limited. It depends on the RF frequency bands and the surrounding environment. For

example, in the 400 MHz frequency band, for a Typical Urban (TU) environment, the maximum temporal spread is about 5μs, whereas for a Hilly Terrain (HT) environment, it is about 17μs. Thus, the temporal components of the impulse response of the channel are limited by those bounds.

All these constraints are clearly set in the global covariance matrix of the propagation channel. For a Rayleigh mobile radio channel,

$$p(\boldsymbol{\mathcal{H}}) \propto e^{-\frac{\boldsymbol{\mathcal{H}}^{\mathsf{H}}\boldsymbol{R}^{-1}\boldsymbol{\mathcal{H}}}{2}}$$

Hence:

$$p(\boldsymbol{\mathcal{H}}|\boldsymbol{y}) \propto e^{-\frac{\|\boldsymbol{y}-\boldsymbol{E}\boldsymbol{\mathcal{H}}\|^2}{2\sigma^2}} e^{-\frac{\boldsymbol{\mathcal{H}}^{\mathsf{H}}\boldsymbol{R}^{-1}\boldsymbol{\mathcal{H}}}{2}}$$

Maximizing it is equivalent to minimizing

$$\frac{\|\boldsymbol{y}-\boldsymbol{E}\boldsymbol{\mathcal{H}}\|^2}{\sigma^2} + \boldsymbol{\mathcal{H}}^{\mathsf{H}}\boldsymbol{R}^{-1}\boldsymbol{\mathcal{H}},$$

which results in

$$(\boldsymbol{E}^{\mathsf{H}}\boldsymbol{E} + \sigma^2\boldsymbol{R}^{-1})\boldsymbol{\mathcal{H}} = \boldsymbol{E}^{\mathsf{H}}\boldsymbol{y} \tag{5.2}$$

Not surprisingly, this is also the linear MMSE (Wiener) estimator [38].

5.3 The Algorithm

In practice, only certain symbols (i.e., the pilots) are known at the receiver. Hence, let us set in the matrix $\boldsymbol{E}$ the entries corresponding to pilots equal to their (known) values and put zeros elsewhere. Using (5.1) in (5.2) yields (after some algebra):

$$(\boldsymbol{P} + \sigma^2\boldsymbol{I})\tilde{\boldsymbol{\mathcal{H}}} = \boldsymbol{N}^{1/2}\boldsymbol{Q}^{\mathsf{H}}\boldsymbol{E}^{\mathsf{H}}\boldsymbol{y}$$

where

$$\boldsymbol{P} = \boldsymbol{N}^{1/2}\boldsymbol{Q}^{\mathsf{H}}\boldsymbol{E}^{\mathsf{H}}\boldsymbol{E}\boldsymbol{Q}\boldsymbol{N}^{1/2}$$

and

$$\tilde{\boldsymbol{\mathcal{H}}} = \boldsymbol{N}^{-1/2}\boldsymbol{Q}^{\mathsf{H}}\boldsymbol{\mathcal{H}}$$

Considering further the eigenvalue decomposition of the (Hermitian) matrix $\boldsymbol{P}$, say

$$\boldsymbol{P} = \boldsymbol{X}\boldsymbol{K}\boldsymbol{X}^{\mathsf{H}},$$

we finally arrive at

$$\hat{\boldsymbol{\mathcal{H}}} = \boldsymbol{Q}\boldsymbol{N}^{1/2}\boldsymbol{X}(\boldsymbol{K} + \sigma^2\boldsymbol{I})^{-1}\boldsymbol{X}^{\mathsf{H}}\boldsymbol{N}^{1/2}\boldsymbol{Q}^{\mathsf{H}}\boldsymbol{E}^{\mathsf{H}}\boldsymbol{y} \tag{5.3}$$

The complexity of the above MAP channel estimator can be significantly reduced through a low rank approximation approach [20]. The idea is to represent the channel using only a subset of the eigenvector basis, namely keeping only eigenvectors associated to the highest eigenvalues, that is to say the most representative ones. Thus, let $\boldsymbol{Q}'$ denote the $L \times L'$ matrix whose columns are the L' principal eigenvectors in $\boldsymbol{Q}$ and $\boldsymbol{N}'$ the corresponding $L' \times L'$ diagonal matrix of principal eigenvalues. Then

$$\boldsymbol{\mathcal{H}} = (\boldsymbol{N}')^{1/2}\boldsymbol{Q}'\tilde{\boldsymbol{\mathcal{H}}}$$

Notice that, in this way, we depart from optimality because we are losing some information, but in practice this is negligible due to the fact that the part of neglected energy corresponding to dismissed eigenvectors is really very low. Some comments about this step:

- Optimality is only slightly degraded;
- L' is preferably chosen equal to or smaller than the number of pilots;
- If $\boldsymbol{R}$ is separable in time and frequency, then the same holds for $\boldsymbol{Q}$. This comes from the relation connecting the eigenvalue decomposition of a Kronecker product to those of its factors.
- $\boldsymbol{Q}'$ is then separable in time and frequency if the matrix of remaining eigenvectors is obtained by the Kronecker product of remaining eigenvectors in the frequency domain by eigenvectors in the temporal domain.
- $\boldsymbol{N}'$ is the matrix of corresponding remaining eigenvalues (product of corresponding eigenvalues in the frequency domain and of corresponding eigenvalues in the temporal domain).

The corresponding solution for the channel is again given by (5.3), where only the principal eigenpairs of $\boldsymbol{R}$ are kept.

5.4 Implementation Considerations

The practical MAP channel estimator implementation takes into account the fact that the constraints that apply to the propagation channel are split between temporal domain on the one hand and frequency domain on the other. The two domains are separable. It means that the covariance matrix is a Kronecker product of two matrices, one expressing the constraint in the temporal domain, the other one the constraint in the frequency domain. Then it is possible to select the principal eigenvalues in each of the temporal and the frequency domains. This further simplifies the implementation of the algorithm, especially memory needs, as we will see below.

First, write $\boldsymbol{Q}'$ as the Kronecker product of two matrices: $\boldsymbol{V}$, expressing a constraint on the Doppler power spectrum of the channel, and $\boldsymbol{U}$, which expresses a constraint on the delay power spectrum of the channel. Thus:

$$\boldsymbol{Q}' = \boldsymbol{V} \otimes \boldsymbol{U}$$

This time-frequency separability is crucial for a low complexity implementation. For the number of columns of $\boldsymbol{Q}'$, we have

$$L' = (2F+1)(2T+1),$$

where F is (approximately) the number of positive frequency components up to maximum Doppler shift and T the number of positive time samples up to maximum delay spread. This is to be compared with $L = MN$.

Let us first construct $\boldsymbol{V}$. Consider an $N \times Q$ matrix $\boldsymbol{S}$, whose columns are complex exponentials (with N components) with frequencies that lie in the interval $[-f_D, f_D]$, with f_D being the maximum Doppler shift. Then $\boldsymbol{V}$ is built as

$$\boldsymbol{V} = \arg\max_{\boldsymbol{X}} \|\boldsymbol{X}^{\mathsf{H}}\boldsymbol{S}\|^2$$

This leads to the conclusion that $\boldsymbol{V}$ should be chosen as the matrix of the $2F+1$ principar left singular vectors of $\boldsymbol{S}$. We note that in practice the spectrum of $\boldsymbol{S}\boldsymbol{S}^{\mathsf{H}}$ decreases very rapidly, hence the approximation will be both economic and accurate. An $M \times (2T+1)$ matrix $\boldsymbol{U}$ can be found in an analogous manner.

5.5 Digression

It must be noted that a similar approach can be found in the following patent: FR 2814011 from France Télécom, inventors: Siala and Jaffrot. They also described a channel estimator based on a MAP approach, but using a different implementation processing. They focus on building covariance matrices but for pilot symbols only (instead of the whole frame as in our case). Then they solve for the MMSE estimate and at the end they are forced to extend the channel estimates obtained on pilot positions to the rest of the frame for data positions. As a result, they are obliged to implement an additional interpolation step to finally achieve the entire channel estimation at all symbol positions.

Using our approach and implementation, we are able to skip this interpolation phase and perform the channel estimation in one single step. This is one of the great advantages of our approach. Moreover, we are able to simplify the calculations and reduce memory consumption using additional properties such as time-frequency separability and basis reduction (low rank approximation) while achieving a performance close to optimal.

5.6 Simulation results

We consider the FMT scheme described in the corresponding part of D2.1. We adopted values for the parameters from the 3GPP LTE standard, and we added two additional parameters (temporal pulse shaping filter support and roll-off factor) as shown in Table 5.6. As described in detail in D2.1, the pulse shaping filter used in this FMT scheme is a classical square root raised cosine (SRRC) filter applied in the frequency domain.

In addition, the frame structure and frame formatting from the 3GPP LTE standard release 8 were adopted. The various physical channels and pilots (Reference Signals) configurations implemented in the simulation are compliant with the standard. In particular, for channel estimation purpose, we used the CRS (Common Reference Signals) scheme: the positions and RS sequence and values are then obtained following the corresponding specifications.

The experiments were performed by introducing this FMT scheme into an existing 3GPP LTE Physical Link Layer simulator. The latter implements the whole radio communications emission/reception chain, including channel propagation modeling. We simply replaced the OFDM (IFFT + CP insertion) modulation block by the FMT modulation one at the emitter side and, in the same way, replaced the OFDM demodulation block by the FMT demodulation processing at the receiver side. Schematically, the simulated system is depicted in Fig. 5-1. Simulation results are reported for both the AWGN case and the 3GPP EVA channel propagation model in Figs. 5-2(a) and (b), respectively. A mobile speed of 50 km/h was assumed. In both cases, the BER performance of a single tap (per FT point) equalizer is shown. For comparison purposes, the perfect CSI case is also included. Moreover, different modulation and coding schemes were tested, namely several QAM modulation constellations (QPSK, 16QAM, 64QAM) and different channel coding ratios (1/3 and 1/2). We observed that under all simulation conditions the SNR loss over the perfect CSI case is around 1 dB, and in no case higher than 1.5 dB.

Configuration parameters	**FMT derived from LTE**
Basic modulation access mode (LTE)	OFDMA (downlink mode)
Frequency carrier (PMR case)	450 MHz
Bandwidth (LTE)	1.4 MHz
FFT size (LTE)	128
Sampling frequency (LTE)	1.92 MHz
Sub-carrier spacing (LTE)	15 kHz
CP (LTE)	512/2048*NFFT=1/4
Symbol duration (LTE)	160 samples: NFFT+CP
Number of used sub-carriers (LTE)	72 (6 RBs)
Pulse shaping filter size** in samples **(FMT)	***12*(NFFT+CP))***
Roll-off factor (FMT)	α ***= 0.22***

Table 5-1: Simulation parameters

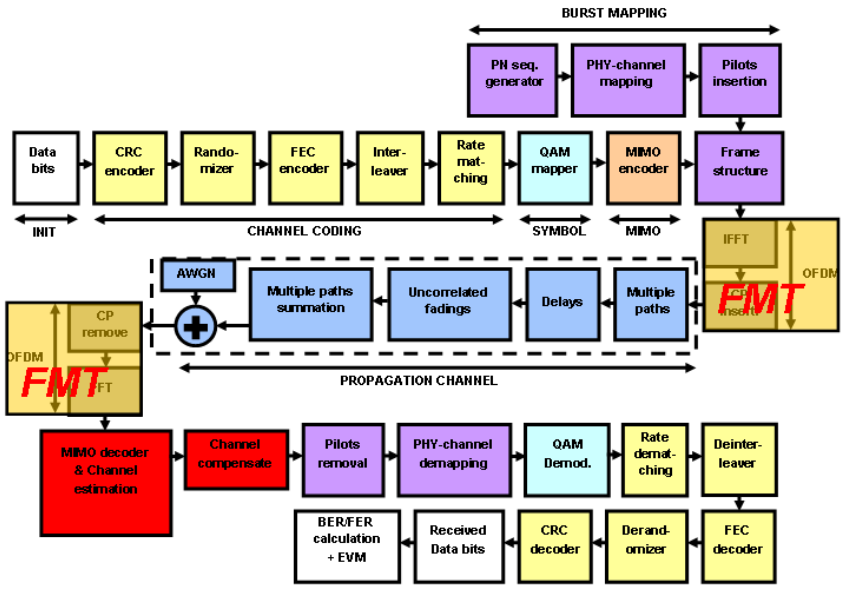

Figure 5-1: Schematic diagram of the simulator employed.

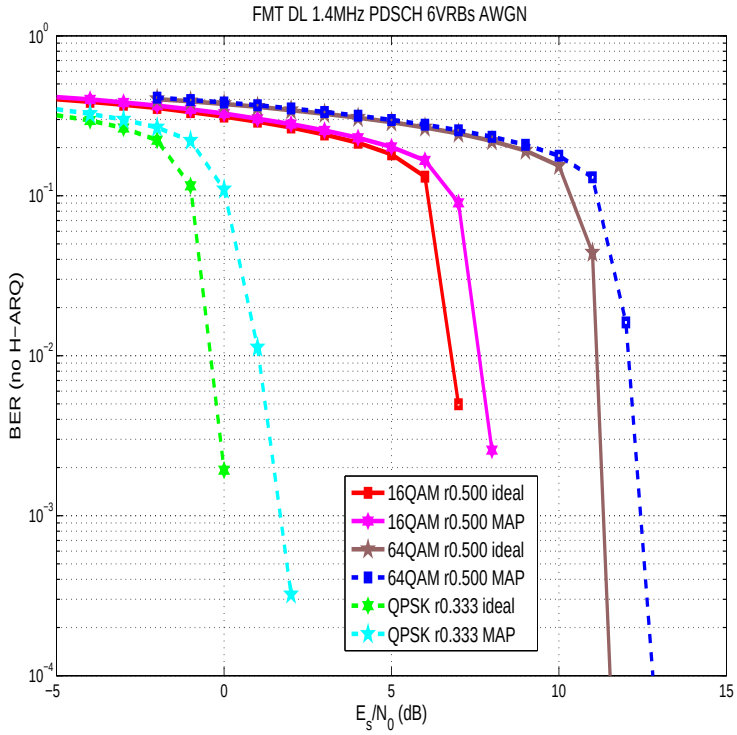

(a)

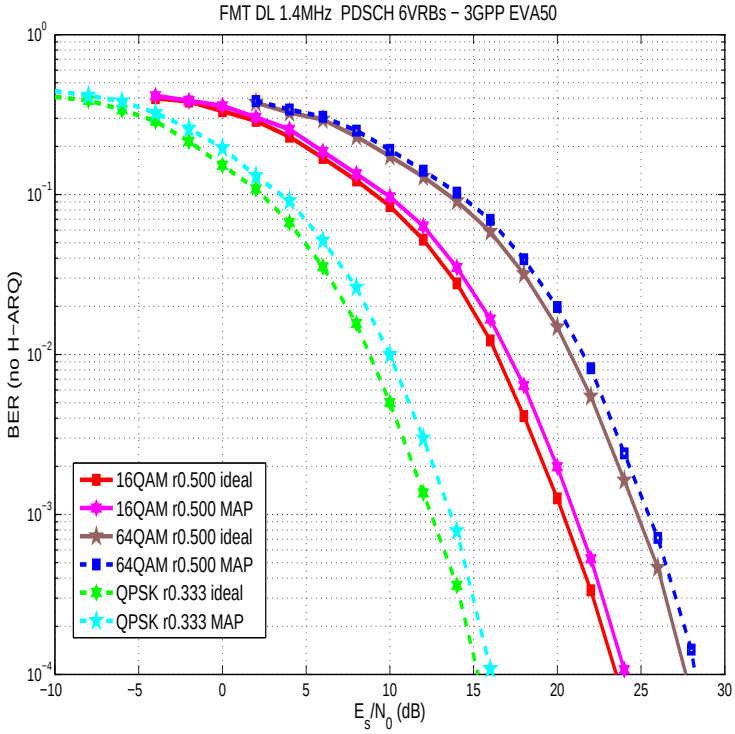

(b)

Figure 5-2: BER performance of the proposed algorithm for (a) an AWGN and (b) a 3GPP EVA channel.

5.7 Concluding Remarks

The proposed two-dimensional channel estimation algorithm has several good features:

- As the auto covariance matrix is built for the whole frame (instead of taking into account pilots only), we are able to assume the separability between time and frequency domains. Thus, we can consider the two dimensions separately in order to build their respective bases, and the overall global basis is then a simple Kronecker product. This allows us to simplify the calculations and reduce complexity.
- As we do not consider specific pilot schemes, such as their positions and values when building the BEM, the algorithm is applicable to any possible pilot configuration.
- Since the channel covariance matrix is separable, eigenvectors and eigenvalues issued from decomposition are also separable. As a consequence, our global basis could be computed using Kronecker product of temporal eigenvectors basis and frequency eigenvectors basis, and the same way for eigenvalues. This separability is quite favourable in terms of complexity, because we only have to memorize eigenvectors and eigenvalues for both dimensions separately instead of the whole Kronecker product basis (and this is significantly lower as far as memory consumption is concerned).
- The low rank approximation also leads to computational savings.

6. Conclusions and Future Research

This report summarized the principal results of research efforts aimed at developing channel estimation and synchronization algorithms that can cope with propagating conditions of high frequency and/or time selectivity. Emphasis was put on FBMC/OQAM modulation, in view of its high spectrum efficiency.

For channel estimation, both preamble-based and scattered pilot-based methods were studied. In the first case, the estimation problem was considered at both the subchannel and the broadband channel level, proposing impulse response estimators designed with a number of optimality criteria and varying performances. The estimators were developed for any given training sequence of any length, relying on the assumption that the channel is time invariant in the preamble duration. Special care was taken for coping with the realistic case of having null subcarriers at the edges of the spectrum. The effect of the sequence length on the estimation and equalization performance was assessed via simulations. The more interesting case of short sequences, which would be more practical in a fading environment, was also tested, with satisfactory results. Notably, the shortest possible preamble case (of one pilot FBMC symbol accompanied by a few guard ones) was given special attention and optimal (in the MSE sense) designs were derived, for both the block- and comb-type preamble structures. Efficient and simple algorithms were described for implementing the associated estimators. The effect of the interference from the payload was studied and shown that no more than 3 guard FBMC symbols are needed in order to yield an interference-free result. The possible gains in estimation performance from taking the (time domain) channel sparsity into account were evaluated through simple modifications to the previously developed estimation schemes. It was seen that the improvement in the MSE is more apparent at low SNRs and most importantly when there is significant interference to the preamble by the data surrounding it. A parametric method was also presented, that exploits the path-delay description of the channel to explicitly estimate the number of paths, their delays and their gains. The basic idea is that a frequency selective subchannel response can be modeled as a polynomial of an order that depends on the degree of its selectivity. Very important performance gains were observed compared to classical (IAM) methods and corresponding estimators for CP-OFDM.

The assumption of a time invariant channel is far from being met in the scenarios of interest for this project. Hence the preamble-based methods reported here should be complemented with a tracking ability, as pointed out in the sequel. In this respect, one should choose the preamble of the shortest possible duration, to make sure that at least the initial, preamble-based estimate is accurate enough. This is one of the next steps to be taken in WP3.

The case of pilots scattered over the frame was also considered. Particularly for the EMPhAtiC demonstrator development, synchronization and channel equalization methods were developed, making effective use of the FC-FB filter bank structure. It was seen that using a synchronization preamble of two FBMC symbols in each transmission frame, sufficient time and frequency offset estimation accuracy can be achieved using the demonstrator parameters. This scheme can tolerate strong interferences in the used frequency band, however, detailed performance evaluation under different interference scenarios remains as a topic for future work. The synchronization module can use a-priori knowledge about the used resource blocks, and/or information obtained from the spectrum sensing function to suppress the interfered/unused parts of the spectrum from the synchronization process.

A channel equalizer, embedded in the FC-FB structure and employing the FFT weight coefficients for performing equalization, was designed and evaluated. It was shown to exceed in performance the 3-tap subcarrier equalization model of PHYDYAS in the case of high frequency

selectivity at the subcarrier level. However, due to the limitations of the currently available pilot-assisted channel estimation methods, it is not easy to make use of this benefit, and hence either of these two approaches can be used in the demonstrator.

Since the PMR system is expected to operate in large macrocells, it should be able to function sufficiently well with long delay spread channels, like those that obey the Hilly Terrain (HT) channel model. However, the commonly used LTE-like pilot structures do not have sufficient resolution in the frequency direction for estimating such channels. Using a pilot structure containing pilots in all subcarriers, improved results were obtained in the QPSK modulation case with the HT channel. In this context, applying the estimators developed previously with comb-type *midambles* deserves to be studied as a possible solution. Anyway, channel estimation based on scattered pilots (probably in addition to a preamble) for such channel models remains as an important item for future studies. Exploiting the sparse/compressible structure of the channel with the aim of reducing the required pilot density could be one of the directions to follow. Again, the preamble-based channel estimation methods developed here are able to overcome the above limitation in case of stationary channels. To cope with practical fading channels, these methods must be complemented with channel tracking. This could be done in a decision directed manner, possibly utilizing scattered pilots. Such a direction was followed in PHYDYAS, based on linear interpolation in time, also applicable in MIMO channels. However, it was only studied for low-order constellations and needs to be extended to more realistic conditions.

It should be noted that, in this document, the preambles for synchronization and channel estimation are developed and evaluated independently. However, it should be possible to use the same preamble for both purposes, and this is one of the next topics to be worked out.

Finally, FMT modulation was also considered, in the context of channel estimation and equalization. A 2-D algorithm was presented, whose main features include: the ability to estimate the channel response in both time and frequency with no constraint on the pilot format employed, and a computationally more attractive version relying on low rank approximation. Its performance was successfully evaluated in LTE-like scenarios for both stationary and fading channels. Nevertheless, the subchannel frequency selectivity, present in highly dispersive channels, was not addressed. This can be a future research direction towards improving the applicability of this approach.

7. References

[1] FP7-ICT Project PHYDYAS – Physical Layer for Dynamic Spectrum Access and Cognitive Radio. http://www.ict-phydyas.org.

[2] W. U. Bajwa, J. Haupt, A. M. Sayeed, and R. Nowak. Compressed channel sensing: A new approach to estimating sparse multipath channels. *Proceedings of the IEEE*, 98(6):1058–1076, June 2010.

[3] K. Balachandran, K. C. Budka, T. P. Chu, T. L. Doumi, and J. H. Kang. Mobile responder communication networks for public safety. *IEEE Commun. Mag.*, 44(1):56–64, January 2006.

[4] L. G. Baltar, M. Newinger, and J. A. Nossek. Structured subchannel impulse response estimation for filter bank based multicarrier systems. In *Proc. ISWCS*, pages 191–195, Aug. 2012.

[5] L. G. Baltar, D. S. Waldhauser, and J. A. Nossek. MMSE subchannel decision feedback equalization for filter bank based multicarrier systems. In *Proc. ISCAS*, pages 2802–2805, 2009.

[6] L.G. Baltar and J.A. Nossek. Multicarrier systems: A comparison between filter bank based and cyclic prefix based OFDM. In *Proc. InOWo*, Aug. 2012.

[7] J. R. Barry, E. A. Lee, and D. G. Messerschmitt. *Digital Communication*. Boston: Kluwer Academic Publishers, third edition edition, 2004.

[8] M. G. Bellanger. Specification and design of a prototype filter for filter bank based multicarrier transmission. In *Proc. ICASSP*, 2001.

[9] C. R. Berger, Z. Wang, J. Huang, and S. Zhou. Application of compressive sensing to sparse channel estimation. *IEEE Communications Magazine*, pages 164–174, Nov. 2010.

[10] M. Borgerding. Turning overlap-save into a multiband mixing, downsampling filter bank. *IEEE Signal Processing Mag.*, pages 158–162, March 2006.

[11] M.-L. Boucheret, I. Mortensen, and H. Favaro. Fast convolution filter banks for satellite payloads with on-board processing. *IEEE J. Select. Areas Commun.*, 17(2):238–248, February 1999.

[12] C. Carbonelli, S. Vedantam, and U. Mitra. Sparse channel estimation with zero tap detection. *IEEE Transactions on Wireless Communications*, 6(5):1743–1753, May 2007.

[13] Z. Cheng and D. Dahlhaus. Time versus frequency domain channel estimation for OFDM systems with antenna arrays. In *Proc. ICSP*, 2002.

[14] S. Cotter and B. D. Rao. Sparse channel estimation via matching pursuit with application to equalization. *IEEE Trans. Commun.*, 50(3):374–377, March 2002.

[15] E. Dahlman, S. Parkvall, and J. Sköld. *4G LTE / LTE-Advanced for Mobile Broadband*. Academic Press, 2011.

[16] M. A. Davenport, M. F. Duarte, Y. C. Eldar, and G. Kutyniok. Introduction to compressed sensing. *chapter 1 in [17]*.

[17] Y. C. Eldar and G. Kutyniok, editors. *Compressed Sensing: Theory and Applications*. Cambridge University Press, New York, 2012.

[18] D. Li *et al.* Single-symbol preamble design and channel estimation for filter bank multicarrier modulations. In *Proc. PIMRC*, 2012.

[19] J. Meng *et al.* Compressive sensing based high-resolution channel estimation for OFDM system. *IEEE Journal of Selected Topics in Signal Processing*, 16(1):15–25, Feb. 2012.

[20] O. Edfors *et al.* OFDM channel estimation by singular value decomposition. In *Proc. VTC*, 1996.

[21] O. Edfors *et al.* Analysis of DFT-based channel estimators for OFDM. *Wireless Personal Communications*, 12:55–70, 2000.

[22] P. Amini *et al.* Filter bank multitone: A physical layer candidate for cognitive radios. In *Proc. SDR*, 2005.

[23] B. Farhang-Boroujeny. OFDM versus filter bank multicarrier. *IEEE Signal Processing Magazine*, 28(3):92–112, May 2011.

[24] B. Farhang-Boroujeny and R. Kempter. Multicarrier communication techniques for spectrum sensing and communication in cognitive radios. *IEEE Commun. Mag., Special Issue on Cognitive Radios for Dynamic Spectrum Access*, 46(4):80–85, April 2008.

[25] G. Garbo, S. Mangione, and V. Maniscalco. MUSIC-based modal channel estimation for wideband ofdm-oqam. In *Proc. WD*, 2008.

[26] G. Garbo, S. Mangione, and V. Maniscalco. MUSIC-based modal channel estimation for wideband OFDM-OQAM. In *Proc. IFIP*, 2008.

[27] G. Garbo, S. Mangione, and V. Maniscalco. MUSIC-LS modal channel estimation for an OFDM-OQAM system. In *Proc. ICSPCS*, 2008.

[28] G. Garbo, S. Mangione, and V. Maniscalco. Wireless OFDM-OQAM with a small number of subcarriers. In *Proc. WCNC*, 2008.

[29] G. Garbo, S. Mangione, and V. Maniscalco. Orthogonal multicarrier transmission with modal channel estimation. In *Proc. ICT*, 2009.

[30] G. Garbo, S. Mangione, and V. Maniscalco. Efficient simulation of orthogonal multicarrier transmission over multipath fading channels. In *Proc. 50th FITCE*, 2011.

[31] R. M. Gray. Toeplitz and Circulant Matrices: A Review. *Foundations and Trends in Communications and Information Theory (now publ.)*, 2(3), 2005.

[32] T. Ihalainen, T. Hidalgo Stitz, M. Rinne, and M. Renfors. Channel equalization in filter bank based multicarrier modulation for wirelesscommunications. *EURASIP Journal on Advances in Signal Processing*, Article ID 49389, 18 pages, 2007.

[33] J. Javaudin, D. Lacroix, and A. Rouxel. Pilot-aided channel estimation for OFDM/OQAM. In *Proc. VTC*, 2003.

[34] D. Katselis. Some preamble design aspects in CP-OFDM systems. *IEEE Communications Letters*, 16(3):356–359, March 2012.

[35] D. Katselis, M. Bengtsson, C. Rojas, H. Hjalmarsson, and E. Kofidis. On preamble-based channel estimation in OFDM/OQAM systems. In *Proc. EUSIPCO*, 2011.

[36] D. Katselis, E. Kofidis, A. Rontogiannis, and S. Theodoridis. Preamble-based channel estimation for CP-OFDM and OFDM/OQAM systems: A comparative study (see arxiv:0910.3928v1 [cs.it] for an extended version). *IEEE Transactions on Signal Processing*, 58(5):2911–2916, May 2010.

[37] D. Katselis, C. R. Rojas, M. Bengtsson, and H. Hjalmarsson. Frequency smoothing gains in preamble-based channel estimation for multicarrier systems. *Signal Processing*, 93(9):2777–2782, Sept. 2013.

[38] S. M. Kay. *Fundamentals of Statistical Signal Processing, Vol. I: Estimation Theory*. Prentice Hall, 1993.

[39] E. Kofidis. Preamble-based channel estimation in OFDM/OQAM systems: A time-domain approach. *arXiv:1306.2581v1 [cs.IT]*, June 2013.

[40] E. Kofidis. Short preamble-based estimation of highly frequency selective channels in FBMC/OQAM. In *ICASSP*, 2014. submitted.

[41] E. Kofidis, D. Katselis, A. Rontogiannis, and S. Theodoridis. Preamble-based channel estimation in OFDM/OQAM systems: A review. *Signal Processing*, 93(7):2038–2054, July 2013.

[42] D. Kundu. Estimating the number of signals in the presence of white noise. *Journal of Statistical Planning and Inference*, 90:57–68, March 2000.

[43] C. Lélé, J.-P. Javaudin, R. Legouable, A. Skrzypczak, and P. Siohan. Channel estimation methods for preamble-based OFDM-OQAM modulations. *European Transactions on Telecommunications*, 19(7):741–750, Nov. 2008.

[44] J. Liberti and T. Rappaport. *Smart Antennas for Wireless Communications*. Prentice Hall, 1999.

[45] P. Maechler, P. Greisen, B. Sporrer, S. Steiner, N. Felber, and A. Burg. Implementation of greedy algorithms for LTE sparse channel estimation. In *Proc. ASILOMAR*, 2010.

[46] X. Mestre, M. Sánchez-Fernández, and A. Pascual-Iserte. Characterization of the distortion of OFDM/OQAM modulations under frequency selective channels. In *Proc. EUSIPCO*, 2012.

[47] T.K. Moon. The expectation-maximization algorithm. *IEEE Signal Processing Magazine*, 13(6):47–60, 1996.

[48] M. Newinger, L. G. Baltar, and J. A. Nossek. MMSE training design for filter bank multicarrier systems with per-subcarrier channel estimation. In *Proc. VTC (Fall)*, 2013.

[49] L. Pucker. Channelization techniques for software defined radio. In *Proc. SDR*, Orlando, FL, USA, November 18–19 2003.

[50] C. Qi and L. Wu. Optimized pilot placement for sparse channel estimation in OFDM systems. *IEEE Signal Processing Letters*, 18(12):749–752, Dec. 2011.

[51] M. R. Raghavendra, S. Bhashyam, and K. Giridhar. Improving channel estimation in OFDM systems for sparse multipath channels. In *Proc. SPAWC*, pages 106–109, 2004.

[52] Q. S. Ren and A. J. Willis. Fast root MUSIC algorithm. *Electronics Letters*, 33(6):450–451, March 1997.

[53] M. Renfors and f. harris. Highly adjustable multirate digital filters based on fast convolution. In *Proc. ECCTD*, pages 9–12, Linköping, Sweden, August 2011.

[54] M. Renfors, J. Yli-Kaakinen, and f. harris. Analysis and design of efficient and flexible fast-convolution based multirate filter banks. submitted to *IEEE Trans. Signal Processing*, 2013.

[55] P. J. Schreier and L. L. Scharf. *Statistical Signal Processing of Complex-Valued Data*. Cambridge University Press, 2010.

[56] P. Siohan, C. Siclet, and N. Lacaille. Analysis and design of ofdm/oqam systems based on filterbank theory. *IEEE Transactions on Signal Processing*, 50(5):1170–1183, May 2002.

[57] T. Hidalgo Stitz, T. Ihalainen, A. Viholainen, and M. Renfors. Pilot-based synchronization and equalization in filter bank multicarrier communications. *EURASIP J. Adv. Signal Process.*, 2010, Article ID 741429.

[58] G. Tauböck, F. Hlawatsch, D. Eiwen, and H. Rauhut. Compressive estimation of doubly selective channels in multicarrier systems: Leakage effects and sparsity-enhancing processing. *IEEE Journal of Selected Topics in Signal Processing*, 4(2):255–271, April 2010.

[59] S. Theodoridis, Y. Kopsinis, and K. Slavakis. Sparsity-aware learning and compressed sensing: An overview. *arXiv:1211.5231v1 [cs.IT]*, Nov. 2012.

[60] A. Tomasoni, D. Gatti, S. Bellini, M. Ferrari, and M. Siti. Efficient OFDM channel estimation via an information criterion. *IEEE Transactions on Wireless Communications*, 12(3):1352–1362, March 2013.

[61] J. A. Tropp and S. J. Wright. Computational methods for sparse solution of linear inverse problems. *Proc. IEEE*, 98(5):948–958, June 2010.

[62] M. Valkama, A. Springer, and G. Hueber. Digital signal processing for reducing the effects of RF imperfections in radio devices – An overview. In *Proc. ISCAS*, pages 813–816, 2010.

[63] R. van Nee and R. Prasad. *OFDM for Wireless Multimedia Communications*. Artech House publ., 2000.

[64] A. Viholainen. Prototype filter and structure optimization. PHYDYAS Project Document, January 2009.

[65] D. S. Waldhauser. *Multicarrier Systems Based on Filter Banks*. Ph.D. thesis (Technische Universität München), Shaker Verlag, Aachen, 2009.

[66] D. S. Waldhauser, L. G. Baltar, and J. A. Nossek. MMSE subcarrier equalization for filter bank based multicarrier systems. In *Proc. SPAWC*, pages 525–529, 2008.

[67] N. Wang, Z. Zhang, G. Gui, and P. Zhang. Improved sparse channel estimation for multicarrier systems with compressive sensing. In *Proc. WPMC*, 2011.

[68] M. Wax and T. Kailath. Detection of signals by information theoretic criteria. *IEEE Transactions on Acoustics, Speech, and Signal Processing*, 33(2):387–392, April 1985.

[69] B. Yang, K. B. Letaief, R. S. Cheng, and Z. Cao. Channel estimation for OFDM transmission in multipath fading channels based on parametric channel modeling. *IEEE Transactions on Communications*, 49(3):467–479, March 2001.

[70] Y. Yang, T. Ihalainen, M. Rinne, and M. Renfors. Frequency-domain equalization in single-carrier transmission: Filter bank approach. *EURASIP Journal on Advances in Signal Processing*, 2007:Article ID 10438, 16 pages, 2007. doi:10.1155/2007/10438.

[71] C. Zhang and Z. Wang. A fast frequency domain filter bank realization algorithm. In *Proc. ICSP*, volume 1, pages 130–132, Beijing, China, August 21–25, 2000.

[72] H. Zhang, H.C. Wu, and S.Y. Chang. Novel fast MUSIC algorithm for spectral estimation with high subspace dimension. In *Proc. ICNC*, 2013.

[73] X. Zhou, Y. Fang, and M. Wang. Compressed sensing based channel estimation for fast fading OFDM channels. *Journal of Systems Engineering and Electronics*, 21(4):550–556, Aug. 2010.

Glossary and Definitions

Acronym	Meaning
AFB	Analysis Filter Bank
AWGN	Additive White Gaussian Noise
CFO	Carrier Frequency Offset
CFR	Channel Frequency Response
CIR	Channel Impulse Response
CP	Cyclic Prefix
CRLB	Cramér-Rao Lower Bound
CSI	Channel State Information
EM	Expectation Maximization
FB	Filter Bank
FB-MC	Filter Bank-based MultiCarrier
FBMC/OQAM	Filter bank-based multicarrier using OQAM
FC	Fast Convolution
FC-FB	Fast Convolution based Filter Bank
FMT	Filtered MultiTone
FT	Frequency-Time
IAM	Interference Approximation Method
(I)FFT	(Inverse) Fast Fourier Transform
LS	Least Squares
LTE	Long Term Evolution
ML	Maximum Likelihood
(M)MSE	(Minimum) Mean Squared Error
MUSIC-LS(MMSE)	MUltiple SIgnal Classification - Least Squares (Minimum Mean Squared Error)
NMSE	Normalized MSE
OFDM	Orthogonal Frequency Division Multiplexing
OMP	Orthogonal Matching Pursuit
PC(S)I	Perfect Channel (State) Information
OQAM	Offset Quadrature Amplitude Modulation
PMR	Professional Mobile Radio
RMS	Root Mean Squared (error)
SC	SubCarrier
SFB	Synthesis Filter Bank
SNR	Signal to Noise Ratio
SVD	Singular Value Decomposition
TD	Time Domain